



---

All Theses and Dissertations

---

2015-10-01

# Image-Charge Detection Novel Instrumentation and Applications

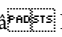
Brandon Lee Barney  
*Brigham Young University - Provo*

Follow this and additional works at: <https://scholarsarchive.byu.edu/etd>

 Part of the [Biochemistry Commons](#), and the [Chemistry Commons](#)

---

## BYU ScholarsArchive Citation

Barney, Brandon Lee, "Image-Charge Detection  Novel Instrumentation and Applications" (2015). *All Theses and Dissertations*. 5616.

<https://scholarsarchive.byu.edu/etd/5616>

This Dissertation is brought to you for free and open access by BYU ScholarsArchive. It has been accepted for inclusion in All Theses and Dissertations by an authorized administrator of BYU ScholarsArchive. For more information, please contact [scholarsarchive@byu.edu](mailto:scholarsarchive@byu.edu), [ellen\\_amatangelo@byu.edu](mailto:ellen_amatangelo@byu.edu).

Image-Charge Detection – Novel Instrumentation and Applications

Brandon Lee Barney

A dissertation submitted to the faculty of  
Brigham Young University  
in partial fulfillment of the requirements for the degree of

Doctor of Philosophy

Daniel E. Austin, Chair  
David V. Dearden  
Adam T. Woolley  
Matthew R. Linford  
James E. Patterson

Department of Chemistry and Biochemistry

Brigham Young University

October 2015

Copyright © 2015 Brandon Lee Barney

All Rights Reserved

## ABSTRACT

### Image-Charge Detection – Novel Instrumentation and Applications

Brandon Lee Barney  
Department of Chemistry and Biochemistry, BYU  
Doctor of Philosophy

Image-charge detection is an analytical technique in which a highly-charged particle is detected by the magnitude of the image current that it generates in a detecting electrode. This current is represented as a voltage between the charged particle and the sensing electrode. It is a single particle detection method, ideal for the analysis of large, variable mass particles such as biological cells.

Some of the physical properties of *Bacillus subtilis* spores were explored using different applications of image-charge detection. *B. subtilis* is a gram-negative spore-forming bacteria that has been shown to exhibit extremophile behavior. The particular extremophile behavior that was investigated in this study is the resistance to extreme mechanical stress.

The effects of high-velocity impacts upon these spores were studied using image-charge detection. The elastic properties of these spores as well as spore survivability to high-velocity impacts were investigated. Spores were shown to survive impacts at velocities up to  $299 \pm 28$  m/s. The average kinetic energy loss experienced by impacting spores, regardless of velocity at impact, was between 71 and 72%. Both conventional and novel image-charge detection techniques were used for these studies.

The novel version of a charge detector that was demonstrated was fabricated using patterned metal electrodes on printed circuit boards. The simplicity and versatility of this method was demonstrated with a multi-stage charge detector, a unique bouncing detector, and charge-detection mass spectrometry detector which is capable of measuring the absolute mass of a single highly-charged particle.

Keywords: bacteria, charge detection, spores, planetary protection, high-velocity impact, mass spectrometry

## ACKNOWLEDGEMENTS

I would like to thank Dr. Daniel Austin for all of his support throughout this project. He has been consistently supportive through all of my ups and downs. He was also a constant source of innovative, out of the box ideas which meant that my research never stayed stalled for long. I would like to thank all of the DEA group members that helped and supported me throughout this project. I would also like to thank my wonderful wife, Kristin, and my children for all of their tireless support through this entire endeavor. Kristin was my rock and I could not have done this without her. I would like to thank John Pantazis of Amptek for helping me to understand the operation of his company's amplifiers that were an integral part of this research. I would like to also thank the Precision Machining Lab for their prompt and accurate machining of the various system components that I required throughout this research. I am very appreciative to the NASA Planetary Protection Program for the funding of a portion of this research. And finally, I would like to thank the BYU department of Chemistry and Biochemistry for this wonderful opportunity and all of the friendship and support that I have been given here.

## TABLE OF CONTENTS

LIST OF FIGURES .....	vi
Chapter 1: Introduction .....	1
Chapter 2: Studying High-Velocity Impacts of Bacteria .....	24
Introduction .....	24
Experimental .....	33
Results .....	42
Conclusion .....	48
Chapter 3: An Image-Charge Detector Made from Printed Circuit Boards .....	49
Introduction .....	49
Experimental .....	60
Results and Discussion .....	64
Conclusion .....	71
Chapter 4: Measuring elasticity via kinetic energy loss in bouncing bacterial spores .....	72
Introduction .....	72
Experimental design .....	84
Results and Discussion .....	90

Conclusion .....	98
Chapter 5: Determination of the exact mass of <i>Bacillus subtilis</i> spores.....	99
Introduction.....	99
Preliminary work and results .....	103
Conclusions.....	109
Chapter 6: Future directions.....	110
References.....	114

## LIST OF FIGURES

Figure 1 - Conventional image-charge detector. A charged particle passes through three metal tubes housed within a grounded cylinder or box. As the particle enters the central (sensing) cylinder a voltage is produced, causing a flow of charge into or out of the sensing cylinder. This image charge is amplified and recorded. A direct measurement of the image charge would produce the top signal, while a differentiating amplifier—essentially measuring image current—would produce the signal shown below .....	3
Figure 2 - Overview of spore impact experiment. Spores are electro sprayed from suspension, then desolvated, and then accelerated within a beam tube. Final acceleration occurs as spores pass through two differentially-pumped skimmers. The spores are detected using an image charge detector prior to impact on a glass surface within a collection vial .....	34
Figure 3 – Photograph of impact experimental setup showing the electro spray source, the acceleration region, the charge detection region, and the impact region.....	35
Figure 4 - The process of electro spray charging. Charged droplets break apart as they evaporate, eventually resulting in bare, charged spores. The spores are drawn into the vacuum system through a small aperture .....	37
Figure 5 – Impact receptacle showing plastic lid with a hole in the center for particle entry and irregular glass bead surface on the interior preventing spores from bouncing back out of the receptacle. ....	40
Figure 6 - Typical signals recorded at the charge detector resulting from charged spores passing through. Top, a spore with measured velocity of 185 m/s; Bottom, spore velocity 348 m/s.....	43
Figure 7 - Velocity distribution of <i>B. subtilis</i> (ATCC 1A308) spores using three different vacuum skimmer arrangements. Average velocities of (from left to right) $155 \pm 9$ , $284 \pm 11$ , and $299 \pm 28$ m/s.....	44
Figure 8 – Rifampicin-containing agar plate showing bacterial colonies that were grown from impacted spores. The spores on this plate survived impact at an average velocity of 184.9 m/s.....	45
Figure 9 - Multi-stage cylindrical detector with alternating cylinders connected to the amplifier and ground. The detector shown has 5 sensing stages. Below, the signal expected from detection of a positively-charged particle using a differentiating amplifier. ....	52
Figure 10 - Top: Design of a PCB for a 5-stage charge detector. Center left: two PCBs used for a single-stage detector. Center right: two PCBs for a 5-stage detector. Large photo: The 5-stage detector assembled and wired. Bottom: flight path of a charged particle through the PCB charge detector .....	61

Figure 11 - Typical signals produced using electrosprayed 1-micron polystyrene particles using (top) single-stage PCB and (bottom) 5-stage PCB charge detectors and differentiating amplifier..... 65

Figure 12 - Representative signals each showing a charged particle passing through both 5-stage PCB (left of each trace) and conventional charge detectors (right of each trace) in series. For each particle, the peak areas generated by both types of charge detectors are equivalent, demonstrating similar sensitivity ..... 67

Figure 13 - Representative signal from a single-plate, 5-stage PCB detector. The peak area steadily decreases as the particle travels from one sensing stage to the next. In contrast to the 2-PCB design, a single-PCB charge detector is unable to measure particle charge. .... 69

Figure 14 – Variation in peak area generated by one particle using a single-plate detector. The peak area varies between approximately 2.9 and 1.8  $\mu$ Vs..... 70

Figure 15 - Vacuum setup for the bouncing experiments. Spores are electrosprayed then pass through a beam tube and a skimmer cone. They then pass through the detector, bounce off of the surface and pass through the detector again. .... 84

Figure 16 – PCB-based bouncing detector. Due to the differently sized detection stages, the direction of the traveling particle is easily determined. Spores travel lengthwise across the detector. They initially travel left to right. After bouncing, they travel right to left..... 88

Figure 17 – Distribution of percent kinetic energy loss for the bacterial spores upon impacting a glass surface at two average velocities. The bin numbers on the horizontal axis indicate a range between the number indicated and the preceding number. For example “100” indicates 95-100. .... 92

Figure 18 - Values for the cellular spring constant  $k$  as a function of the depression distance  $x$  ..... 94

Figure 19 – Signal produced by a charged spore passing through the charge detector, bouncing, and then passing back through again. The peak area for a peak produced by the spore on the return trip is significantly smaller than the peak area corresponding to the initial passage through the detector. Velocities derived from peak spacing were used to verify that signal produced by a bouncing spore was being observed..... 97

Figure 20 – PCB designed for use as planar 6-stage CD-MS detector. DC acceleration region in center of detector designed to change particle velocity for  $m/z$  measurement..... 104

Figure 21 – Trace showing the portion of the signal used for velocity measurement. During this time the particle is traveling over the DC acceleration region. .... 106

Figure 22 – Signal generated by a charged polystyrene particle of 3.36  $\mu$ m diameter passing through all 6 sensing stages of the CD-MS detector. Peak amplitude changes while peak area remains the same for a given particle..... 107



Figure 23 - % relative standard deviation is compared for 20 different CD-MS traces. The % RSD is calculated by comparing the peak areas generated by a single polystyrene sphere traveling through all 6 sensing stages of the detector..... 108

## Chapter 1: Introduction

Portions of this chapter were taken from: Barney, B. L.; Daly, R. T.; Austin, D. E., A multi-stage image charge detector made from printed circuit boards. *The Review of Scientific Instruments* 2013, 84 (11). Copyright [2013], AIP Publishing LLC. Reprinted with permission.

The mass of biological structures, such as bacterial spores, viruses, and various types of cells, is difficult to determine with a high degree of precision or accuracy. This is due primarily to the size and complexity of these objects. Such structures include, but are not limited to: viruses, bacteria, lipoproteins, and blood cells. An assumption could be made that little significant variability is to be expected for the mass of each cell in a group of cells of the exact same type. However, cells tend to exhibit a high degree of mass and size variability. Using sufficiently sensitive analytical methods, a study of the extent and nature of this variability could be made. A method with the ability to measure the mass of cells individually would be ideal for such a study.

The size and mass of individual cells of the same type vary widely from one cell to another. At first glance, mass spectrometry would be the ideal method for the characterization of the mass and size of individual cells in a system. Mass spectrometry (MS) has become the gold standard for the characterization of unknown molecular samples. However, the problem is complex. As has been mentioned, an inherent variability in size and mass among a cell population exists in most biological systems. In order for a mass spectrometer to be able to analyze cells, they will first need to be charged. Variation in cell size comes with variation in the number of charge carriers present on the surface of a cell and hence a large range of charge states

within a group. A wide range of mass coupled with a wide range of charge states makes a distribution of mass-to-charge ratios ( $m/z$ ) all but meaningless. If the  $m/z$  and charge for a specimen could be determined independently, the absolute mass of each cell could be determined, providing a mass distribution for a collection of cells.

Charge detection mass spectrometry (CDMS) is emerging as an important tool for the analysis of particles of large, variable mass. Such particles include biomolecules,<sup>1,2,3</sup> polymers,<sup>4,5,6</sup> aerosols,<sup>7</sup> and even intact cells.<sup>8,9</sup> CDMS is ideal for large particle detection as there is virtually no upper-mass limit for this method. Other types of MS detectors suffer from reduced detection efficiency at masses greater than a few hundred kDa ( $10^3$  Da).<sup>1</sup> Biological cells have masses that are orders of magnitude larger than the effective range for these detectors. Their masses are typically in the MDa to TDa range ( $10^6$ - $10^{12}$  Da). Because of the natural variability in size of these particles, it is desirable to measure the mass of each particle individually—in contrast to conventional techniques in MS where packets of identical ions arrive at a detector at a given time and are detected together.

At the center of the CDMS technique is the image charge detector, a simple device that detects the charge of a particle passing through a section of metal tube. Charge measurement is accomplished through the conversion of the image current into a voltage followed by amplification. Direct amplification of the signal results in a constant voltage offset during the time the particle is within the tube.<sup>1</sup> With a differentiating amplifier, which is more popular in recent work, the signal is converted into a pair of peaks, one positive and one negative, corresponding to the particle's entry and exit from the tube (Figure 1).<sup>1</sup> Particle velocity may be obtained from these two peaks simply by dividing the length of the detector by the elapsed time between the two peaks. The differentiating amplifier produces a larger signal for a given particle

$$\text{Particle velocity} = \frac{\text{length of detector}}{\text{transit time}} \quad (1-1)$$

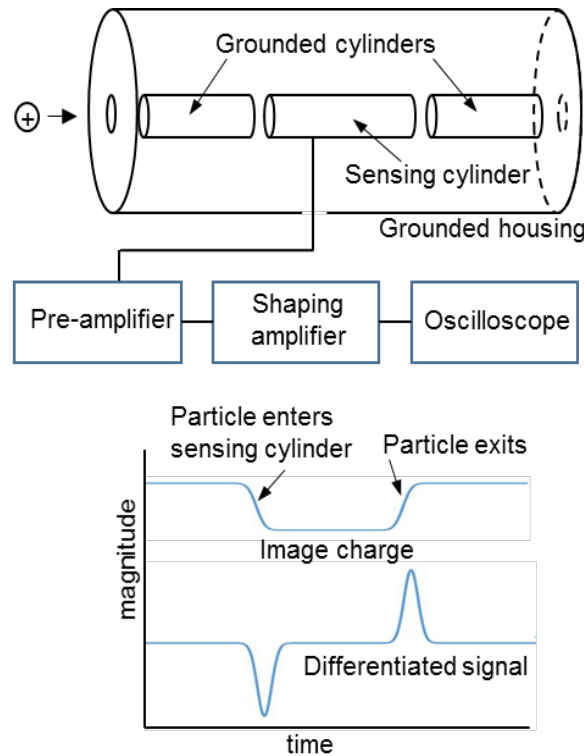


**Figure 1 - Conventional image-charge detector.** A charged particle passes through three metal tubes housed within a grounded cylinder or box. As the particle enters the central (sensing) cylinder a voltage is produced, causing a flow of charge into or out of the sensing cylinder. This image charge is amplified and recorded. A direct measurement of the image charge would produce the top signal, while a differentiating amplifier—essentially measuring image current—would produce the signal shown below. (Reprinted with permission from [Barney, B. L.; Daly, R. T.; Austin, D. E., A multi-stage image charge detector made from printed circuit boards. *The Review of Scientific Instruments* 2013, 84 (11)]. Copyright [2013], AIP Publishing LLC.)

because the rise-time of the signal is short compared with the time the particle traverses the tube. The rise-time is governed by the spacing between the sensing tube and the adjacent, grounded tube segments, and the position of the particle relative to those electrodes. The signal from both

types of amplifiers may be used to calculate the charge of the particle as well as the velocity at which it is traveling.

If the charged particle has been electrostatically accelerated from rest, the accelerating voltage is used to determine the  $m/z$  of the particle. Mass is then determined by multiplying measured charge by  $m/z$ . Thus the charge, velocity,  $m/z$ , and mass of a charged particle are determined using the signal from a single charge detector. For particles that are not electrostatically accelerated from rest (for example, electrosprayed particles entering vacuum through a differentially pumped inlet), it is possible to measure absolute mass using two charge detectors, one with a DC bias, and measuring the change in velocity of the particle as a function of the DC potential drop between the detectors.<sup>10</sup>

Charge detection (CD) was first used in the United States in the 1960s as a method to study micrometeoroid simulants.<sup>11</sup> Using CD, it was possible to measure the velocity of a particle prior to the particle impacting a surface. It was then possible to measure the effect of an impact as a function of the particle velocity. This was done in order to determine what effect the high-velocity impact of a micrometeoroid would have on the hull of a spacecraft while traveling through space. The technique was used to characterize a variety of analytes. These analytes were either seen as useful simulants for the micrometeoroids mentioned or for other related applications.

This method was first reported in 1960 by Shelton *et al.*,<sup>11</sup> who used pairs of conducting metal plates inside a shielded cylinder to detect charged iron spheres in a microparticle accelerator system. Iron microspheres were used as micrometeoroid simulants. It was important that the spheres be highly charged as more highly charged particles receive a greater acceleration

in an electric field. The spheres were brought into this highly charged state by directing them onto a spherical metal electrode that was maintained at a high potential. The charged spheres were then passed between two metal detection plates where a voltage was induced between particle and plate. From this signal, both the particle charge and time-of-flight were generated. They were then able to compute the mass from these data. Considering the sensitivity of their detector, they were able to calculate the mass with 20% accuracy. Using electrostatic acceleration, they were able to accelerate particles up to 1-2 km/s. They used this electrostatic acceleration to simulate micro-meteor impacts with a known particle mass and known particle velocity to observe the effects on a metal surface.

Friichtenicht et al. used a similar setup to Shelton with the aim of improving the particle acceleration pre-impact.<sup>12</sup> They constructed an accelerator out of a 2 MV Van de Graaff generator which they used to achieve velocities up to 14 km/s. This was done so that the range of velocities at which impacts could be simulated could be expanded.

Oil droplets that were charged by passing them through a highly charged needle were studied by Hendricks et al., similar to electrospray ionization.<sup>13,14</sup> It was necessary that the droplets possess a charge of at least  $10^{-15}$  coulombs in order to be detected. This was not thought to be a severe limitation as the charging method produced a large quantity of droplets of this or greater charge. They were detected using a metal electrode plate that had a hole cut into the center of it. As the droplets passed through the hole, they were characterized by the voltage that they induced.

No further experimental studies were published using image-charge detection for more than twenty years. This was due to the fact that the American scientists had become convinced

that these micrometeoroid impacts posed no significant threat to the hull of a traveling spacecraft. Consequently, all governmental funding for such projects was suspended.<sup>15</sup> A small amount of experimentation continued in the 70s and 80s due to interest in the Halley's Comet flyby. This technique revived in the 1990s, with several different researchers using charge detection to simulate micrometeorites and characterize aerosols and other particles. Similar to the micrometeorite studies of the 1960s, each of these studies used conducting metal plates or tubes, attached to an amplifier, to detect charged particles.

Keaton et al. developed a 6 MV Van De Graaff accelerator for the purpose of studying high-velocity impact effects of microparticles on a surface.<sup>15</sup> Charged particles were accelerated and passed through a series of 4 "pick-off" detectors that were each attached to a charge-sensitive pre-amplifier. Velocities were calculated by dividing the distance between two of these detectors by the elapsed time between the signals that were produced by them. The charge was determined by the magnitude of the signal produced by each pick-off detector. Using these two pieces of information, along with the known accelerating voltage, particle masses were calculated. They also used the known densities of the analyte particles to determine size, assuming sphericity. The materials that they were studying, carbonyl iron and conducting polymers, are typically made spherical, so this was a good assumption. Their detection limit was based on the noise level from the pre-amplifiers as well as the noise from the accelerator environment. They reported a lower detection limit of 0.3 fC or about 2000 charges. With accelerating velocities between 1-100 km/s, they were able to study particles with masses of  $10^{15}$  to  $10^{12}$  grams. They used these data to study the relationship between particle velocity, particle energy, and the size of the impact craters produced by these particles.

Vercoulen et al. developed an instrument to detect the charge on individual aerosol particles.<sup>7</sup> For this particular run of experiments, glass beads that were greater than 200  $\mu\text{m}$  in diameter were studied. For detection, they used a series of two charge detection electrodes. Each electrode consisted of two concentric copper rings, the inner for detection and the outer for shielding. This was the first reported instance of any kind of shielding being used for a charge detection device. The image currents in this device were sent directly to an oscilloscope without amplification.

Stradling used a similar setup to the one described above that was reported by Keaton.<sup>16</sup> Their aim was to increase the accuracy of the charge and velocity measurements over what had previously been achieved in order to more accurately characterize the energies and velocities of particles in relation to the impact craters produced by these particles. They studied particles of carbonyl iron dust that were between 1  $\mu\text{m}$  and 10 nm in size. These particles were electrostatically accelerated to 3-30 km/s depending on the particle size. Smaller particles were able to be accelerated to higher velocities. They accelerated the charged spheres along an 8 m flight path that had charge detection devices spaced throughout the path. By so doing they were able to average all signals produced for a single particle leading to greater accuracy in charge, velocity, and mass measurements. They investigated impacts on a variety of different target materials and compared what effects particle energy and velocity had on the cratering of each.

An induction detector for the detection of charged particles was demonstrated by Park et al.<sup>17</sup> The detector itself consisted of 3 metal plates positioned separately in a sandwich-like arrangement, perpendicular to the flight path of the analyte particles. In the center of each plate was a 90% transmission mesh grid. The first and last plate were used for shielding purposes while the central one was connected to amplifiers in order to magnify the induced current for



optimal detection efficiency. There was also a micro-channel plate positioned after the induction detector for the purpose of comparing results between the two detectors. They used a CsI and Ag colloid as a low mass standard. They also analyzed a number of proteins with this setup, including myoglobin, leu-enkephalin, and insulin. It was determined that the induction detector gave slightly better resolution than the MCP detector, in part due to the fact that the detection efficiency did not depend upon the particle velocity, but also due to the fact that it was not possible to saturate the induction detector.

In 1995, Fuerstenau and Benner refined the technique and produced an instrument that most subsequent work has been based on.<sup>1</sup> This was the first instance of a charge detection device being called a mass spectrometer. They detected megadalton DNA ions passing through a metal tube connected to an amplifier with two co-linear grounded tubes, one before and one after the detection tube. Their limit of detection was 425 electrons or the equivalent positive charge. This LOD was significantly lower than any previous reported LOD for an image-charge detection device. A hexapole ion guide was used for the purpose of focusing the ion beam towards the detector. There was also an MCP located at the terminus of the particle stream that they used for diagnostic purposes. They presented mass spectra as well as mass distribution histograms of the DNA ions that were studied. Both the mass spectrum and the histogram show two maxima, one corresponding to single-stranded DNA and one corresponding to the double-stranded version.

The rest of this introductory literature review will focus on charge detection as it relates to advancements in the types of analytes studied. Those papers that concern themselves with using charge detection mass spectrometry as a tool to further understanding of the natural world, will be discussed in this chapter. Studies that instead focus on the development of novel

instrumentation and the improvement of the sensitivity and accuracy of this technique, will be discussed in chapter 3. Naturally, there are studies that will focus both on novel instrumentation and novel analyte analysis. Such studies will be assigned to a particular chapter based on what seems to be the main focus of the paper.

Schultz et al. used CD-MS to characterize both double and single-stranded circular DNA.<sup>2</sup> These molecules contained 2500 – 8000 base pairs that had masses in the range of 1.5 – 5.0 MDa. Their aim was to find a method better suited to the automated sampling of DNA than gel electrophoresis. The instrument used for this study was the same developed by Benner discussed above.<sup>1</sup> Over a period of about 10 minutes, they were able to detect some 3000 ions of the electrosprayed DNA. Combining the  $m/z$  and charge data, they generated a histogram that represented the mass distribution of a single, unfragmented DNA sample. There was some fragmentation naturally present in each sample but no fragmentation method was used as a part of the analysis. They observed much more fragmentation in the single-stranded samples than in the double-stranded ones resulting in more complex spectra for the single-stranded DNA. The single-stranded spectrum showed maxima around the average mass for the monomer as well as the dimer and some fragmentation for each.

The same research team used the same setup to investigate polymerase chain reaction (PCR) products.<sup>3</sup> They analyzed samples consisting of 1525 base pairs (bp), 1982 bp, 2677 bp, as well as a longer double-stranded linear DNA sample. The mass spectra generated showed that about half of the DNA sample passed through the detector in fragmented form. They assigned a band above the mass of the unfragmented DNA to clusters of DNA fragments. They compared the results obtained to those generated using gel electrophoresis and found the accuracy to be equal to and in some cases greater than what was possible with electrophoresis. Also, the mass

of each DNA ion was directly measured, and the analysis time was much shorter than is possible with gel electrophoresis.

Fuerstenau and Benner again collaborated to use CD-MS to measure the mass of an intact virus.<sup>8</sup> They had previously faced difficulties in the analysis of viruses with a quadrupole mass spectrometer. The  $m/z$  ratios produced were simply too high to be accurately detected with that particular mass analyzer. In addition, the large variation in charge states made it difficult to assign mass or charge states to the peaks they observed. Using the same experimental setup that they had used previously, they studied both rice yellow mottle virus (RYMV) and tobacco mosaic virus (TMV). The analysis of thousands of individual virus particles was carried out over about 30 minutes for each viral sample. They recorded an average mass for RYMV between 6-7 MDa and for TMV of 39-42 MDa. Both of these values agreed with previously published values for these virus particles.

CD-MS was next used to study charged water droplets by Maze et al.<sup>18</sup> Using positive-mode electrospray, they observed a significant number of negatively charged droplets. They investigated the droplet fission processes that could produce negatively charged droplets from positively charged droplets. Because of the large positive bias on the electrospray needle, it would have been impossible for negatively charged droplets to not be drawn back towards the needle if they were formed near the needle. They advanced several theories concerning how the negatively charged droplets could be formed. They determined that the most likely scenario involved a bipolar fission process. In this model, a negatively charged droplet fragment forms between two positively charged droplet fragments during the charged droplet fission stage of electrospray ionization. The charge detection setup that they used for these experiments was modeled after that developed by Fuerstenau and Benner and was essentially the same instrument.

Benner et al. studied aerodynamically focused particle beams using CD-MS.<sup>19</sup> The analyte studied here was polystyrene latex spheres. The intended application of this study was finding a way to aerodynamically align a particle beam with a laser. The charge detection setup was used to monitor the size and mass of the polystyrene spheres during the focusing. In this particular experimental setup, two charge detectors were used in series to aid in the particle beam alignment with the laser. They used the detector to not only measure charge and velocity but also to monitor the particle concentration of the aerosol being studied.

Returning to the question of how positive-mode electrospray produces negatively charged water droplets, Zilch et al. compared results of both positive and negative-mode electrospray experiments using dual charge detectors.<sup>20</sup> They also compared water droplets produced by electrospray with those produced by sonic spray and a vibrating orifice aerosol generator (VOAG). They observed that less than 1% of the droplets produced in positive-mode electrospray were negatively charged but surprisingly, greater than 70% of the droplets produced by negative-mode electrospray were positively charged. Both VOAG and sonic spray produced predominantly positively charged droplets. They determined that this preference for positively charged droplets for all ionization techniques studied is primarily due to the way in which the droplets break up when entering the capillary interface at the entrance of their vacuum system. They used a voltage ramp between the two charge detectors in this setup to provide an accelerating voltage between the two charge detection regions. This enabled them to measure the mass of the water droplets.

Zilch again investigated electrosprayed water droplets using dual image-charge detectors with an applied potential drift region between them.<sup>21</sup> In these experiments, he used sonic spray only as an ionization method. He found that droplets often changed their charge state between

detectors and even occasionally switched polarity. He investigated what role droplet freezing had in this process. In order for freezing to be a factor in the apparent change of charge-state, it would need to be possible for droplets to freeze in the space between detectors. The size of the water droplet as well as the times spent passing between the two detectors were thought to be the main determining factors. They determined that at the particle velocities relevant to this study, water droplets with a radius of 1-2  $\mu\text{m}$  were likely to freeze during the transit between the two detectors.

Alexander et al. developed an image-charge detector, which they described as a pick-up ring, for use in the analysis of biological targets resulting from matrix assisted laser desorption ionization (MALDI).<sup>22</sup> For this particular study, they described the calibration of the detector as well as experiments analyzing 2 different proteins. They used clusters of  $\text{Ar}^+$  ions for the calibration. In order to be able to differentiate the signal from the background noise, they found that clusters of at least 3,000 ions were necessary. The two proteins used for this study were bovine serum albumin (BSA) and meso-tetrakis-(pentafluorophenyl) porphyrin (F20TPP). As with the Argon ions, it was necessary to analyze these ions in bunches that were produced using magnetic focusing. They were able to differentiate different charge states of the two proteins in the mass spectra produced as well as dimers and trimers of the BSA.

Poly(ethylene oxide) (PEO) samples were analyzed using CD-MS by Doussineau et al.<sup>5</sup> These PEO particles had masses ranging from 1 to 7 MDa. They investigated the charging capacity of these PEO particles as a function of particle size, concentration, and the type of alkali ions present in solution with the PEO particles. The results were compared with a previous model for the charging of these polymer particles based on the affinity of certain alkali cations for oxygen sites on PEO. Their CD device consisted of a single shielded cylindrical electrode

connected to a charge-sensitive pre-amplifier. They compared velocities measured after electrostatic acceleration to velocities measured field-free due to free gas expansion to estimate particle masses. An average velocity due to free gas expansion is used for each mass measurement, reducing the accuracy of their mass determination.

Doussineau again approached the analysis of polymers using CD-MS in a second study.<sup>6</sup> He presented the first determination of the molar mass of self-assembled amphiphilic block copolymer nanoobjects prepared via living radical emulsion polymerization. Samples were prepared with molar masses in the MDa to GDa range and the CD-MS results were compared to results obtained using transmission electron microscopy and dynamic light scattering. The detector used here was again composed of a single CD device as described above. They did not describe their exact method of mass determination in this particular paper but one can assume that it is the same method that was described in their first study and would suffer from the same accuracy limitations for their mass measurements. They were able to determine the molar mass of several block copolymer samples and found the results to be comparable to the other two methods that they studied. Each method was found to have certain advantages over the other methods, the main advantage of their particular type of CD-MS being speed of analysis.

Antoine et al. investigated the products of laser-induced decay of PEO ions using CD-MS. They used a dual charge detector system for these experiments.<sup>23</sup> The two detectors were arranged in series, the second one being capped on either end by electrostatic potential ramps, turning this second charge detector into an electrostatic ion-beam trap. There was an ion gate positioned at the terminus of the first trap in order to select the energy of the ions entering the second detector. They were able to detect product ions having at least 400 charges. The masses of the products being analyzed were in the low megadalton range. They were able to record

several novel fragmentation pathways that would not have been possible to determine from studies based on statistically averaged reaction rates only.

In order to better understand cosmic dust impacts, Daly et al. used a charge detector to investigate particles composed of minerals, mineral-ice aggregates, and ice that had been charged using electrospray.<sup>24</sup> The particular mineral used for these studies was quartz and the ices under investigation were composed of water and methanol. They used a single-cylinder charge detector that was surrounded by copper shielding and that was connected to a charge sensitive pre-amplifier as well as three differentiating and shaping amplifiers. The detector was calibrated by pulsing a known voltage through the pre-amplifier's 2 pF test capacitor. They determined that a peak area of 1  $\mu$ Vs was equivalent to approximately 168,000 protons or the equivalent negative charge. This was the first reported charge detector calibration where actual numbers were reported for the calibration. They were able to propose protonation mechanisms for quartz during the charging process based on experimental results. From their results they proposed that electrospray charging would couple well with a dust accelerator, used to calibrate current cosmic dust analyzers.

Doussineau et al. used CD-MS to investigate the charging capacity of block copolymer nano-objects that had been charged using electrospray ionization.<sup>25</sup> The charge detection setup used was the single detector setup described previously for this research group. As a control, they took a ratio of the peak areas of the two peaks produced for each particle. Any data set producing a ratio that was less than 0.75 or greater than 1.50 was rejected, the rationale being that the signal producing two such peaks could not be reliably linked to a single particle entering and exiting the detector. They compared the charge states of these polymer micelles to the Rayleigh limit for a water droplet of comparable size. A ratio of 0.6 – 0.65 of the actual charge

versus the Rayleigh limit for the particles studied was reported. Particle masses were then determined by comparing an average field-free velocity to the electrostatically accelerated velocity for an individual particle.

The cosmic dust experiments were next expanded upon by Kerby et al.<sup>26</sup> In these experiments, microparticles of olivine and chondrite were electrosprayed and analyzed using the same charge detection setup described above by Daly. Neither one of these minerals are normally conductive. One of the main aims of this study was to show that non-conductive minerals could be analyzed using electrospray charging, expanding the types of analytes that could be analyzed by a cosmic dust accelerator. They demonstrated that electrospray ionization could be used to charge non-conductive minerals to a requisite level to be used in current cosmic dust accelerators.

Ouadah et al. continued the CD-MS analyses of Doussineau and Antoine discussed above.<sup>27</sup> They used latex polymeric nanoparticles to investigate the relationship between the surface charge present on these particles in solution and their charge states in the gas phase after electrospray ionization. The charge detection setup is the single-stage detection setup described in their previous papers and discussed above. They used mass measurements from the CD-MS detector and the known densities of the polymers to calculate sizes of the particles. These sizes were compared to those obtained using dynamic light scattering (DLS) and were found to be lower. They attributed this difference to an overestimation of size by the DLS method. However the uncertainty in their mass measurement may also have been a factor. By using the ratio of the nanoparticle charge in solution to that measured using CD-MS in the gas phase they suggested a method for measuring the polydispersity of polymer particles in solution using their CD-MS setup.



Pyruvate kinase multimers were investigated by Pierson et al. using a modified cone trap in conjunction with a CD-MS detector.<sup>28</sup> The cone trap was first described by Schmidt.<sup>29</sup> It consisted of three electrodes, one cylindrical positioned between two conically shaped electrodes. Potentials were applied to all three electrodes for trapping purposes and ion detection was done outside of the trap once the ions had been ejected. Pierson's trap simply substituted the cylindrical electrode with a charge detector. Particles that had been charged via electrospray passed through several ion guides before passing either through the charge detector or an orthogonal time-of-flight (TOF) mass analyzer. The charge detector was contained within a modified cone trap. In this fashion they were able to compare mass spectra generated through both methods. They were able to detect up to octomer and dodecamer aggregates of the protein using the TOF mass analyzer. By way of comparison, much greater detail was obtainable with the CD-MS detector and peaks representing aggregates of up to 40-mers of the pyruvate kinase were able to be baseline resolved. By comparing concentration dependent studies to a model, they were able to determine that these higher-order aggregates occur in solution and are not simply an artifact of the electrospray process. Also with the long trapping time possible in their charge detection cone trap, the rms deviation in the charge measurement was reduced to 1.3 electrons.

Keifer et al. used the same CD-MS setup as Pierson above to analyze electrosprayed bacteriophage P22 procapsids.<sup>30</sup> From a mass distribution histogram generated using the measured masses of multiple analytes, they reported that the procapsid peak was centered at 23.60 MDa. This indicated that each capsid was composed of approximately 112 scaffolding proteins. The mass distribution of the entire sample was 31 scaffolding proteins wide. Unexpectedly, they observed a collection of masses centered at 19.84 MDa, indicating that these

masses were attributed to empty capsids. They observed that the empty capsids exhibited much lower charge states than the intact procapsids. This seemed to indicate that they had contracted in the gas phase.

The CD-MS work on viruses that was started by Keifer was continued by Pierson et al.<sup>31</sup> They investigated the assembly intermediates of an icosahedral virus capsid. The CD-MS system described for this study was the same as used by both Keifer and Pierson as described above. Late stage intermediates for the hepatitis B virus capsid were trapped by assembly under high salt conditions. It was confirmed using cryo-electron microscopy that these fragments were in fact from an incomplete virus capsid rather than from an aberrant structure of some kind. Three different dimer intermediates were identified and proposed structures were derived from their kinetic accessibility as well as the stability of the structures.

The conventional charge detection setup whereby charged species pass through charge detecting pickup electrodes has been modified by a group of researchers working primarily on the mass spectrometry of whole cells. This method involves using a quadrupole ion trap for  $m/z$  selection and then colliding the selected analytes onto a plate electrode that is connected to an amplifier. By monitoring the current that is generated as the charged particle approaches the electrode, the absolute charge of the analyte species is determined. Mass is then calculated by multiplying the charge by the  $m/z$  that was determined in the ion trap.

Peng et al. first described this method using laser-induced acoustic desorption (LIAD) ionization to produce ions that then entered the trap.<sup>32</sup> While in the trap, a mild corona discharge was produced in order to increase the charge on the trapped particles. The charged particles were mass selectively ejected from the ion trap before colliding with the detection plate. This

plate was connected to a JFET transistor and an operational amplifier. Signal was obtained after being processed by a low-pass filter. They examined various types of mononuclear cells and were able to distinguish CD3<sup>+</sup> lymphocytes from CD14<sup>+</sup> monocytes. Mass distributions were obtained that allowed differentiation between normal T lymphocytes and CEM cancer cells derived from the T lymphocytes. As will be shown, this technique has been shown to effectively analyze numerous varieties of whole cells.

Several types of gas phase animal cells were analyzed by Nie et al. using the method that was reported by Peng above.<sup>33</sup> Red blood cells (RBC) of humans, goats, cows, pigs, mice, and chickens were detected and differentiated. The average masses ranged between 5.8 and 28 TDa or 9.6 – 46.5 pg. They also looked at different types of human RBCs and measured masses for cells belonging to a healthy male adult, a patient with iron-deficiency anemia, and a patient with thalassemia. The reported masses for the human cells were consistent with those generated using more established methods. In addition, they were able to discern mass differences between RBCs too minute to be attributed to different hemoglobin content alone. This demonstrated the ability to analyze cells with masses of greater magnitude than other CD-MS studies had reported. In addition they were able to resolve different cells of the same type and, to a degree, describe the physiological differences that caused the cell variability. After reporting such remarkable results, it was deemed prudent to provide further detail as to how this method worked.

Peng et al. reported on the details of the design of this instrument.<sup>34</sup> At this point they started calling the technique charge monitoring cell mass spectrometry (CMCMS). A low RF frequency on the quadrupole ion trap (QIT) along with the corona discharge that was used to increase the charge on their analyte particles both served to increase the mass range of the QIT. Particles would exit the trap at approximately 20 m/s and an image charge would be generated as

the particle approached the electrode, which they referred to as a Faraday cup. A homemade charge detector circuit with a long discharge time constant was designed to accurately integrate the CD signal. They demonstrated the operation of the device by measuring the mass of Jurkat cancer cells.

Given what had been shown to be possible with this technique, it was thought that it could be coupled with existing methods to improve the overall performance of these methods. A MALDI source was coupled with a CMCMS setup by Chen et al. with the aim of designing a way to improve the detection efficiency of large biomolecules coming from a MALDI source.<sup>35</sup> Using this setup, several different proteins were analyzed. For example, they analyzed immunoglobulin M (IgM) and reported an average  $m/z$  of 980,000. By applying a step frequency scan to the data obtained, they were able to resolve separate peaks for  $IgA^+$  and  $IgA_2^+$  for immunoglobulin A. It was next decided that this method could be used to monitor small modifications to individual cells.

Lin et al. used what they termed CMS (cell mass spectrometry – same method as CMCMS) to monitor the uptake of different sized gold nanoparticles into NTERA2 cells.<sup>36</sup> This study was undertaken due to the interest in utilizing nanoparticles for drug delivery applications. They were able to determine the number of gold nanoparticles that had been absorbed into an individual cell in contrast with the analysis possible with ICP which provides a mean value for all cells. Using polystyrene, they were also able to demonstrate that CMS could be used to monitor the uptake of non-metal nanoparticles as well.

As CMS had been shown to be able to monitor small modifications to cells, it was next shown to have the ability to determine the cause of variability for other large particles. The

packing material of high-performance liquid chromatography (HPLC) columns was analyzed by Xiong et al.<sup>37</sup> They use the same device that was described above for the CMS experiments. Their method was entitled charge-detection quadrupole ion trap mass spectrometry. The packing material that they analyzed was composed of silica spheres with alkyl chains bonded to the surface. Using the mean mass and the mass distribution of these spheres, they were able to calculate the specific surface area of unbonded silica, the carbon load of the bonded silica, as well as the particle size distribution of the samples.

Given that the ability to characterize a large variety of high-mass particles had been shown, the data analysis method was then examined. Xiong et al. next turned their attention to the shape of the RF waveforms that drive the QIT in the CMS method.<sup>38</sup> These waveforms are typically sinusoidal in nature. They experimented with both triangular and rectangular waveforms and compared the trap performance with the conventional method. They tested the method by attempting to differentiate normal from anemic RBCs and were successful. Their results indicated that trap performance was comparable using all three types of RF waveforms but that the frequency scan for the QIT was easier to do using the triangular and rectangular waveforms than it was using sinusoidal waveforms.

Charge detection mass spectrometry has the ability to characterize the mass of high mass biological systems with a high degree of accuracy. There has already been very important work done with this method. However there are new directions that need to be explored in order for the full potential of the method to be realized. There are two major areas of investigation that can be used to further explore the potential of CD-MS. One area deals with the systems to be analyzed. This includes both the types of analytes to be studied as well as the amount of

information that can be obtained studying these systems. The other avenue to explore is the improvement of the instrumentation itself.

The work that has already been done with viruses, DNA, proteins, and cancer cells is important work. Much has been learned about the exact mass distributions of these populations and some investigation has been done into the structure of individual cells, but there is more that can be learned. There are other systems that could be analyzed using this method: lipoproteins, RNA, bacterial and fungal spores to name a few. It is possible that the mass distribution histograms obtained from a cell population could be used to identify bacterial and viral unknowns. This technique would have implications for biological terrorism threat prevention using CD-MS to identify an unknown pathogen.

To date, the improvements in instrumentation have focused mainly on improving the detection limit, precision, and accuracy of this technique. There are improvements that can be made in other areas. The detector itself could be made simpler if methods other than the precise machining and alignment of identical, collinear metal tubes could be employed to make the detection electrodes. Also, the pressure limits of this technique need to be explored. The pressure requirements for an analytical system dictate how much pumping hardware is needed for the system. This in turn determines the power requirements of said system. These three factors together determine whether or not the method could be made portable. A portable charge detector could be used to detect unknown biological threat agents in the field. It could also be used for on-site lipoprotein or blood analysis for mobile medical teams or rural point-of-care healthcare facilities.

Several studies will be presented that seek to either expand what is known about certain biological systems or that seek to focus on improving the charge detection instrumentation itself. Some of these studies could be said to support both goals. It will be shown that CD-MS is an excellent method for the analysis of large, biological systems and that it is an exciting method with much potential for future advances.

In chapter 2, the survivability of bacterial spores to high-velocity impacts will be investigated. A simple charge detector is used to measure the velocities of these spores prior to impact. There were numerous types of analytes discussed above that have been investigated using CD-MS. To date, no other researchers have attempted to study bacteria using image-charge detection. This study is an example of a novel application for CD-MS. The velocity of each spore is measured individually, giving a realistic picture of the distribution of velocities experienced by the surviving spores.

A novel, multi-stage charge detector will be presented in chapter 3. This is a planar device that seeks to simplify the instrumentation of CD-MS. The detector consists of two printed circuit boards facing each other having charge detection electrodes patterned onto the surface. The performance of the detector is compared to a more conventional CD that is composed of machined metal electrodes. The function and reliability of the device are tested using polystyrene spheres. The versatility of the design and fabrication process are also explored.

Chapter 4 presents a novel application to charge detection, previously unexplored. A specially designed planar CD is used to monitor the velocities of bacterial spores both before and after impact. Using the measurements from this bouncing detector, the kinetic energy loss of these spores is monitored. This study uses the design and fabrication technique described in

chapter 3 to investigate a unique phenomenon. By studying two separate initial velocities of spores, the question of whether or not the kinetic energy loss due to impact is dependent upon this initial velocity is investigated.

A planar PCB-based detector for the measurement of particle mass is presented in chapter 5. By adding a DC acceleration region between two charge detection regions, the  $m/z$  of a particle can be measured. The  $m/z$  combined with the charge measurement yields the absolute mass of a particle. Preliminary tests of the device using polystyrene spheres are presented. The reliability and precision of this detector are investigated without any potential applied to the DC acceleration region. Also, a discussion of the performance and potential of the device is given.

Finally, chapter 6 presents some of the future directions for this research. These possibilities are presented in terms of instrumentation and application. The analysis of a few different biological specimens is previewed. Also, some of the instrumental design possibilities are introduced including a discussion on the feasibility of this technique becoming portable.

With CD-MS, it is important to explore the possibilities of both instrumentation and applications. There are many exciting things that have been done, some of them by me. It is hoped that the potential of this analytical technique will be further explored in the years to come.



## Chapter 2: Studying High-Velocity Impacts of Bacteria

Portions of this chapter have been submitted to *Planetary and Space Science* for publication.

### *Introduction*

The question of how life began on this planet has fascinated scientists for centuries. There exist a wide number of theories concerning this origin. Much is known about how life has evolved from simple to more complex lifeforms over the course of this planet's history. How life began in the first place however, remains a mystery. One theory postulates that microbial life may have been transferred to this planet from elsewhere in the solar system by means of a meteorite impact. Much research has been done with the aim of providing evidence that such a transfer is possible.<sup>39</sup>

The potential transfer of life from one planetary body to another within our solar system depends upon the survival of an organism to the various stresses encountered during transfer, including exposure to vacuum, exposure to extreme radiation, and survival through dynamic events that remove the organism from one body and deposit it on the other.<sup>40</sup> This last factor may involve impact at high velocity of an organism contained within a larger projectile (such as contained within a meteorite), or the organism may be unprotected. Bacteria exhibit significant natural resistance to a wide variety of environmental stresses and are therefore excellent candidates for studies of the possibility of survivability between planetary bodies. In general, bacterial resistance is increased when bacteria are in spore form rather than in vegetative form,<sup>41</sup> when bacteria are grouped together such as when they are part of a biofilm,<sup>42</sup> or are enclosed in some other solid or liquid material that offers protection from environmental stress. Although many studies have examined impact and shock survival of bacterial spores contained within or

associated with other materials, survivability of bacteria during a surface impact in the absence of any other material has not been studied. In other words, investigation of the isolated interaction between a bacterial spore and a hard surface as the result of an impact is currently an area of research that is unexplored.

Potential transfer of life between planetary bodies is of interest both in the context of panspermia and planetary protection. Panspermia focuses on the potential transfer of life from one body in our solar system to another through natural means, such as a meteorite.<sup>43</sup> For instance, a meteorite traveling from Mars to Earth, containing viable microbes, has been proposed as a mechanism by which life first came to Earth.<sup>44</sup> On the other hand, the idea of planetary protection arises from the concern that the search for signs of life elsewhere in our solar system could be compromised by terrestrial microbe contaminants; or that microbes, if present elsewhere in the solar system, could disrupt the ecosystem when introduced to another body, particularly the Earth. These microbes could be transferred from a spacecraft to a planetary body, either by way of a crash or a hard landing. Planetary protection is of particular concern as sample return missions to Phobos are considered, or as the usage of Phobos as a staging area for exploratory missions to Mars is considered.<sup>45</sup> For instance, Ramsley has shown that some fraction of ejecta from Mars will impact and remain on the surface of Phobos, and has suggested that as much as 250 ppm of the Phobos regolith consists of material that originated recently from Mars.<sup>46</sup> Both panspermia and planetary protection therefore require knowledge of the resistance of microbes to the various types of stress that would be encountered during such a transfer.

In order to survive an interplanetary transfer, organisms must be able to survive an impact at some (presumably high) velocity. Several prior experimental studies have explored

this question. Most of these studies have been done within the context of panspermia. They seek to answer the question of whether or not bacteria embedded in a meteorite could survive planetary impact.

Mastrapa et al. investigated the resistance of bacterial cells to extreme accelerations and changes in acceleration or “jerk”.<sup>47</sup> Cells of *Deinococcus radiodurans* and spores of *Bacillus subtilis* were tested by subjecting the spores of *B. subtilis* to ultracentrifugation as well as firing both the spores and the cells into plasticene targets using a rifle. Ten percent of the *B. subtilis* spores survived centrifugation at 100,000 RPM ( $4.27 \times 10^6 \text{ m/s}^2$ ) for 65 hours. For the impact experiments, both spores and cells were loaded into the rear cavity of lead pellets and fired into a chilled plasticene target. Two separate rifles, one firing at approximately 100 m/s and the other firing at approximately 300 m/s were used for these experiments. Impacts at these velocities produced jerks of  $1.5 \times 10^{10}$  and  $1.5 \times 10^{11} \text{ m/s}^3$  respectively. They recorded survival rates of 40-100% for all experiments.

Impact resistance of both *B. subtilis* and *B. pumilus* were tested by Bernardini et al.<sup>48</sup> They harvested these spores from near-subsurface basalt rocks located in the Sonoran desert near Tucson, Arizona. It was thought that wild-type spores that were naturally present in surface and sub-surface rocks were good candidates to investigate survivability to a planetary impact event. The setup used to test impact resistance was the same as described for Mastrapa above. As before, the spores were subjected to impacts at velocities of 100 or 300 m/s. Survival rates of 70-100% were observed for all tests. This would seem to indicate that wild-type bacteria do, in fact, exhibit a higher resistance to severe mechanical stress than do their laboratory-grown counterparts.

Burchell et al. investigated the survivability of bacteria to impacts on icy surfaces.<sup>49</sup> Cells of *Rhodococcus erythropolis* were loaded onto either aluminum spheres or porous ceramic fragments and fired into sterilized ice targets. These projectiles were fired using a light gas gun and velocities of approximately 5 km/s were achieved. They conducted experiments both with bacteria loaded into the projectiles and with bacteria on the surface of the ice that was used for the impact experiments. They found no surviving bacteria for any of the experimental runs. They postulated that there could have been a problem with the collection method and that their results are therefore not conclusive.

Fajardo-Cavazos et al. embedded spores of *B. subtilis* into granite samples then placed these samples into the telemetry module of a sounding rocket.<sup>50</sup> The spores were attached to the irregular surface of the granite samples by submerging the samples in a suspension of the spores and then drying them by repeated application and release of vacuum (at least 20 times). The rocket was launched to an altitude of 120 km before it began its descent. The velocity of the rocket, just prior to impact, was measured to be 1.2 km/s. The survival rate of spores on each of the granite samples ranged from 1.2 % to 4.4 % on all but the forward facing samples. No surviving spores were found on the forward facing samples. This could indicate that bare spores are unable to survive impacts at velocities of this magnitude.

The same research team as described in the last paragraph sought to simultaneously subject spores of *B. subtilis* to extreme compressional shock, heating, and acceleration.<sup>51</sup> These are all stresses that a microorganism would be subjected to during a spallation type event in which ejecta are flung into space following a high velocity impact with a planetary surface. To this end the researchers embedded spores onto the surface of a granite target and fired aluminum projectiles at the target. These projectiles were fired at 5.4 km/s and a spore survival rate of  $10^{-5}$

was measured. They calculated that the shock pressure at the point of impact was 57.1 GPa although collected post-impact fragments were shown to have endured a much lighter 5-7 GPa shock pressure.

Price et al. enclosed yeast spores and agar in nylon cylinders and fired them at a water target using a light gas gun.<sup>52</sup> The water target was composed of HPLC grade water enclosed in a sterilized polystyrene bag. By controlling the amount of gunpowder that was loaded into the light gas gun for each individual shot, they were able to control the velocities of the projectiles. They studied cylinder velocities between 1 and 7.4 km/s and found surviving spores at all velocities tested. The survival rate fell from approximately 50% at 1 km/s to 10<sup>-3</sup>% at 7.4 km/s. The velocities tested correspond to shock pressure values of 2-10 GPa. They observed that above approximately 4 km/s, the survival rates dropped off drastically, perhaps indicating that a critical threshold of cell wall damage had been reached.

All of these studies investigated the question of impact survivability for spores with some type of protection, and under conditions where the specific forces on individual spores were not well-controlled or known. For instance, for a given velocity, spores suspended in agar within a nylon cylinder will experience a significantly different acceleration during the impact process (which may take many microseconds to milliseconds) than bare spores impacting a surface (which takes roughly a nanosecond). The agar may also alter the impact process experienced by the spores in a way that is not well characterized. Further, the organisms used in some of these studies may have formed agglomerates that might act to cushion bacteria at the center of the agglomerates.

The question of whether or not bacteria can survive the force of an impact has been approached in a slightly different way. Several studies have been done to determine the magnitude of shock pressures that bacterial spores can withstand. In some of the studies discussed above, both impact velocity and shock pressure are taken into consideration. The following studies tended to focus more on shock pressure survivability.

Horneck et al. subjected spores of *B. subtilis* to explosive shock pressures that were generated by a flyer plate being propelled into the bacterial sample using a controlled explosion.<sup>53</sup> The spores were coated on the surface of a quartz disk by placing a droplet of spore suspension on the disk and letting it dry overnight. Bacterial survival rates of  $10^{-4} - 10^{-6}$  were recorded. They reported that these results indicated that bacteria should be able to survive a planetary ejection event.

Burchell et al. tested spores of *B. subtilis* as well as *Rhodococcus erythropolis* with high-velocity impacts, causing extreme shock pressures.<sup>54</sup> Spores were loaded onto aluminum projectiles and fired at varying velocities using a light gas gun. Particle velocities between 0.3 to 6.0 km/s resulted in shock pressures between 1-78 GPa. The calculated shock pressure was also dependent upon the surface that the projectiles were impacting. Both agar gel and ice targets were used for these experiments. Survival rates for *R. erythropolis* when striking the icy target were measured at  $10^{-4} - 10^{-7}$ , the lowest survival rate corresponding to a shock pressure of 78 GPa. By way of comparison, the *B. subtilis* spores had a survival rate of  $10^{-5}$  when colliding with the icy target at the higher shock pressure. When impacting the agar targets, the *B. subtilis* spores had only twice the survival rate of *R. erythropolis*.

Shock pressures applied to bacteria in a liquid medium were investigated by Willis et al.<sup>55</sup> They studied cells of *E. coli* in an effort to understand the cell mortality mechanism when subjected to high shock pressures. A suspension of the bacterial cells was loaded into a small cavity in a stainless steel container. This cavity was struck by a flyer plate that had been propelled by a powder gun. Velocities of 0.6 to 1.5 km/s produced shock pressures of 2.2 – 14.9 GPa. Survival rates of  $10^{-2}$  –  $10^{-4}$  were reported. TEM images of shocked cells indicated that cell wall rupture was likely the main mechanism of cell mortality in these experiments.

Stoffler and Horneck investigated shock pressures ranging from 5-50 GPa for *B. subtilis*, *Chroococcidiopsis* sp., and *Xanthoria elegans*.<sup>56</sup> These species were chosen because they are natural inhabitants of rocks. The microorganisms were sandwiched between two thin layers of gabbro, a Martian analogue rock. Using an explosively propelled flyer plate, the cells were subjected to pressures of 5-50 GPa. This is the range of pressures that had been observed in Martian meteorites. *B. subtilis* spores were shown to survive up to 42 GPa, where the survival rate was  $10^{-4}$ . The *Chroococcidiopsis* sp. cells were reported to survive pressures up to 10 GPa where the survival rate was  $10^{-3}$ . *X. elegans* exhibited similar survival rates to *B. subtilis*. All of these survival rate calculations were contingent upon the detection threshold of each species which was defined by the initial cell concentration as well as the cell counting method.

Moeller et al. investigated DNA damage as a possible mechanism for spore mortality when exposed to extreme shock pressures.<sup>57</sup> They also investigated some additional factors, other than shock pressure that could lead to DNA damage and contribute to the mortality rate at certain shock pressures. These factors included host rock composition, water content, and temperature. In order to determine what role DNA damage had in cell mortality rates, they experimented with both wild type spores of *B. subtilis* as well as spores engineered to be

deficient in the DNA repair mechanism. Spore suspensions were coated and dried onto several mineral samples. A high-explosive plane wave setup was used to generate shock pressures of 10-50 GPa in the samples. They found that survival rates were higher for the wild type spores. They also determined that lower pre-shock temperatures raised the survival rate. Being embedded in more porous, irregular minerals seemed to also raise the survival rate.

The survival rate of 3 different species of microbes in a liquid emulsion subjected to high shock pressures was investigated by Hazell et al.<sup>58</sup> Cells of *E. coli*, *Enterococcus faecalis*, and *Zygosaccharomyces bailii* were used in these experiments. The purpose of this study was to investigate what role cavitation had on shock induced survival of bacteria in a liquid medium. They designed a capsule that could shock compress a volume of liquid while suppressing cavitation in the liquid that was being compressed. Impact velocities of 345 and 446 m/s were studied. These flyer plate velocities generated shock pressures in the liquid samples of 0.64 and 0.87 GPa respectively. No significant reduction in microorganism population was reported for any of the species studied at either shock pressure.

Meyer et al. subjected *B. subtilis*, *X. elegans*, and *Chroococcidiopsis* sp. 029 to 5-50 GPa shock pressures while at the same time varying the temperature as well as the composition of the host rock.<sup>59</sup> The bacteria laden mineral samples were placed in an iron container next to a high explosive plane wave generator to create the desired shock pressures. Their aim was to find the combination of shock pressure, pre-shock temperature, and host rock composition that was most favorable to bacterial survival. A variety of tests were performed varying the organism under study, the host rock composition, the pre-shock temperature, and the applied shock pressure. Both *B. subtilis* and *X. elegans* showed high survival rates at shock pressures below 10-20 GPa



and in host rocks with a low porosity. The *Chroococciopsis* sp. cells exhibited extremely low survival rates under all experimental conditions.

As a part of a high pressure homogenization process for cow's milk, bacteria were tested for survival at pressures up to 250 MPa.<sup>60</sup> This pressure was attained using a raw milk homogenizer, 90% of the desired pressure being applied to the primary valve and the rest applied to the secondary valve. *Staphylococcus aureus* populations were monitored for these experiments and no surviving specimens were found at 250 MPa. Psychotrophic bacteria populations underwent a 2.73 log cycle reduction at this pressure while mesophilic bacteria underwent up to a 3.06 log cycle reduction.

A common result of all of these studies was that survivability varies widely between different organisms and different experimental setups. This may reflect a large variance in the amount of stress experienced by each individual organism. For instance, variations in microscopic structure of the projectile and the local environment of the spore may have resulted in wide ranges of conditions even within a single experiment. Although these experiments clearly demonstrated the feasibility of bacterial survival in the context of panspermia, the mechanism and specific limits of shock- or impact-induced death remains unknown. In addition, because of the great time and expense required for light-gas gun and explosive shock experiments, only a very narrow range of bacterial types, shock pressures, impact velocities, and other impact variables were studied.

I report on a set of experiments in which individual bacterial spores impact a solid surface at high velocity and under very controlled impact conditions. The velocity of the impacting spores, the composition of the surface on which they impact, as well as the

environment in which the collision happens are all carefully controlled. This is in contrast to the experiments described above, in which the specific impact conditions experienced by individual cells is not controlled or known. These experiments are intended to further understanding of the underlying process of spore survival (or death) due to impact, in the absence of the complicating factors discussed above. In these experiments, bare spores of *B. subtilis*, aerodynamically accelerated one at a time to velocities up to 299 m/s, impact a glass surface. Measurement of the spore velocities and observation of subsequent spore viability demonstrate survivability under these impact conditions. Three separate velocity ranges were tested. At the fastest velocity range tested, up to 75% of the impacted spores survived, showing that a significant number of spores would be able to survive impact at all of the velocities tested in the case of a planetary impact.

### *Experimental*

An overview of the experimental setup is shown in Figure 2. Spores of *B. subtilis* were electrically charged using electrospray, introduced into a vacuum system, and accelerated aerodynamically. The velocities of the accelerated spores were measured using an image-charge detector. Upon exiting the charge detector (CD) they impacted a glass surface within an impact receptacle (Figure 2). After a suitable number of impacts, this receptacle was removed from the vacuum chamber and the spores were collected from the receptacle to determine whether any of the impacted spores had survived.

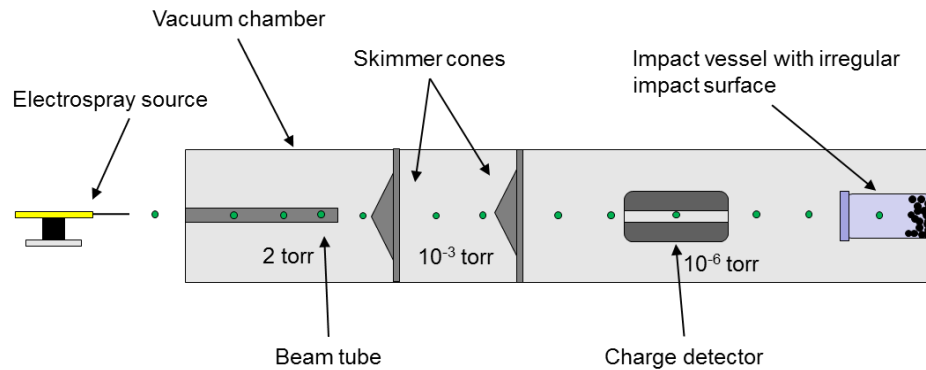


**Figure 2 - Overview of spore impact experiment. Spores are electrospayed from suspension, then desolvated, and then accelerated within a beam tube. Final acceleration occurs as spores pass through two differentially-pumped skimmers. The spores are detected using an image charge detector prior to impact on a glass surface within a collection vial. (Under review for publication in Planetary and Space Science)**

Figure 3 shows the exterior of the vacuum setup. The electro-spray inlet can be seen on the far left of the photograph. Three main vacuum chambers are pumped down by the two turbomolecular pumps seen on top. The third main chamber with the electrical connections contains the image-charge detector. The small chamber at the terminus of the system contains the impact receptacle.

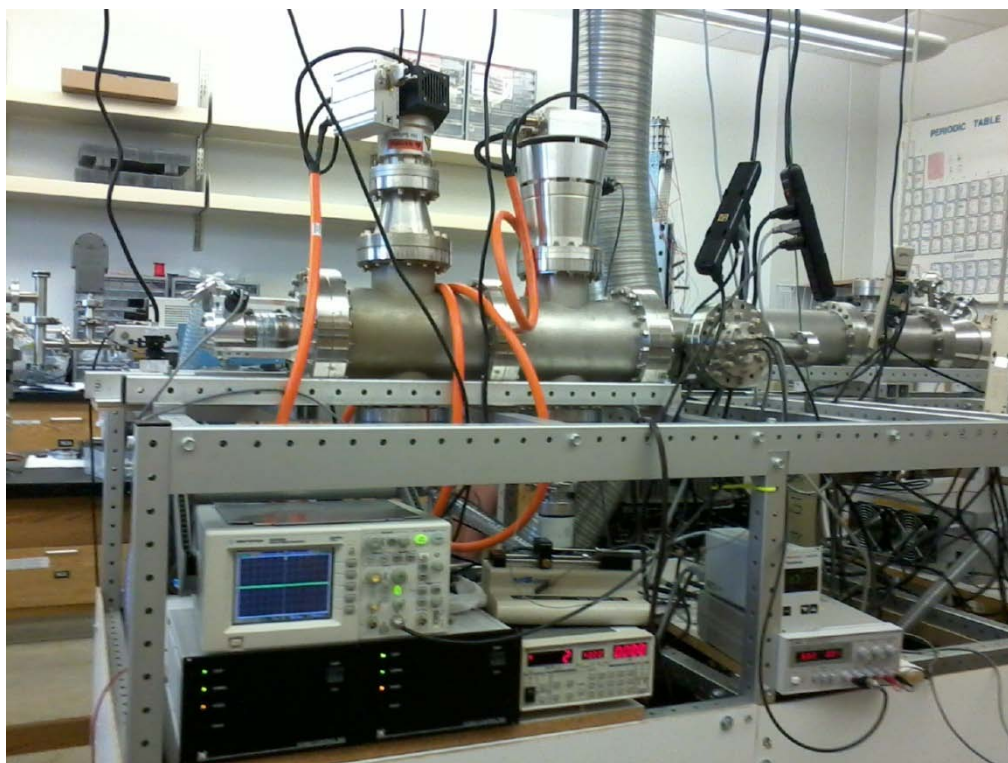


**Figure 3 – Photograph of impact experimental setup showing the electro spray source, the acceleration region, the charge detection region, and the impact region**

All tests were done with a strain of *B. subtilis* (1A308, ATCC, Manassas, VA) that is resistant to the antibiotic rifampicin. Impacted spores were cultured on a rifampicin-containing nutrient agar. The resistance to rifampicin was used as a control to ensure that bacteria were not accidentally introduced to the collection vial between the pre-experiment sterilization and post-experiment sampling. The rifampicin in the agar should kill any present bacteria other than the strain that was used in these studies. Therefore, all detected spores must have passed through the full experimental sequence.

Vegetative *B. subtilis* cells were subjected to a standard sporulation protocol<sup>41</sup> in which the cells were placed on a nutrient agar where they grew and multiplied until the nutrients were

exhausted. The cells then formed endospores. This is a dormant stage that some types of gram positive bacteria have the ability to form. Spores are unable to reproduce but are extremely resistant to stress. This stress could consist of nutrient deprivation, mechanical damage, radiation, or desiccation. These spores, once formed, were collected and suspended in sterilized HPLC-grade water (Thermo Fisher, Waltham, MA) at a concentration of  $10^7$  CFU/mL (colony forming units per mL). This concentration was chosen such that there would rarely be more than one spore per electrospray droplet.<sup>61</sup> It was also important to ensure that no spore agglomerations were present and that individual spores only were detected. The absence of spore agglomerates was demonstrated in previous experiments by comparing the number of colony forming units both with and without passing the suspension through a 0.2  $\mu\text{m}$  filter.<sup>62</sup>

The spores were introduced into the vacuum system via electrospray. Electrospray is a technique commonly used for ionizing molecules in mass spectrometry, and also used to electrically charge microparticles, including microorganisms.<sup>63</sup> Watson et al. have shown that bacterial spore coats contain a large number of charge carriers, consisting mainly of carbonyl and ammine groups, making electrospray an efficient technique to put electrical charges on spores.<sup>64</sup> It has been shown that *B. subtilis* spores survive the electrospray process.<sup>62</sup> In electrospray, a solution containing analyte is sprayed from a capillary in the presence of a strong electric field, yielding charged droplets of the solution. These initial droplets have a large enough ratio of surface area to charge to remain stable. As the droplets evaporate, the magnitude of coulombic repulsion increases until it exceeds the surface tension. Droplets then rupture into several smaller droplets, all electrically charged. This process of evaporation and droplet dissociation continues until essentially all of the solvent has evaporated and only bare, charged analyte particles remain (Figure 4).<sup>65</sup> In the present experiments, the spore suspension was

electrosprayed using a custom-made tip at 100  $\mu\text{L/h}$  using a KD Scientific (Holliston, MA) syringe pump. The electrospray tip was biased at 4000 V using a 25 W high-voltage power supply (PS350, Stanford Research Systems, Sunnyvale, CA). Both gas flow and the electric field drew the charged droplets/spores to a grounded metal plate containing a pinhole that served as the entrance to the vacuum system.

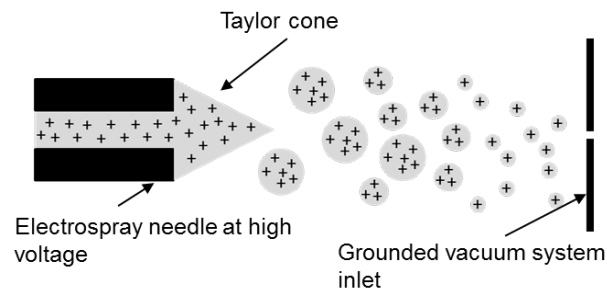


**Figure 4 - The process of electrospray charging. Charged droplets break apart as they evaporate, eventually resulting in bare, charged spores. The spores are drawn into the vacuum system through a small aperture. (Under review for publication in Planetary and Space Science)**

After entering the vacuum system, spores were accelerated by the flow of low-pressure gas through the 6-mm I.D. beam tube. The purpose of the beam tube was to focus and accelerate the spores. Spores and accompanying gas then passed through two skimmers, which further reduced the gas pressure. The velocities of gas and entrained spores increased through each skimmer due to the pressure differential across each skimmer aperture. In addition, skimmers reduced the variation in velocity of gas molecules and spores, as is typical in a supersonic expansion.<sup>66</sup> The resulting spores would be expected to have a narrow distribution of velocities as the sole accelerating force for the spores was the velocity of the gas flow itself. This follows the Bernoulli equation for compressible flow which states that along parallel streamlines fluid

velocity will increase as pressure decreases.<sup>67</sup> In this equation,  $p_1$  and  $p_2$  are the initial and final pressures, respectively,  $\rho$  is the density of the fluid, and  $V_1$  and  $V_2$  are the initial and final fluid velocities.

$$p_1 - p_2 = \frac{1}{2}\rho(V_2^2 - V_1^2) \quad (2-1)$$

Changes to the dimensions of the skimmers and the speed of the turbomolecular pumps allowed different spore velocities to be tested. System pressure decreases as the speed of the turbomolecular pumps increase. As the pressure decreases, the pressure differential across the skimmer in question increases, thus increasing the velocity of the gas flow. Reducing the inner diameter of the skimmer cones has a similar effect, increasing the pressure differential and thereby increasing gas flow velocity. Three different arrangements of skimmer cones and turbo pumps were used in these experiments in order to achieve three separate particle velocities.

After acceleration, the velocity of each spore was measured using an image-charge detector. Image-charge detection, first demonstrated by Shelton and Friichtenicht,<sup>11-12, 68</sup> allows measurement of the velocity of small, highly-charged particles as they pass through a metal sensing tube as well as two grounded tubes. The purpose of the grounded tubes is to shield the sensing electrodes from the incoming charged particle and increase the sharpness of the peaks produced by the interaction between the charged analyte particles and the sensing electrodes.<sup>10</sup> Charged particles induce a current when they enter and exit the sensing tube. The length of the tube and the time between entrance and exit provides the particle velocity. The length of the sensing electrode was 13.9 cm. The tubular electrode was connected to the JFET (junction gate field-effect transistor) input of a charge-sensitive preamplifier (A250, Amptek, Bedford, MA). The output from the preamplifier alone is one small, broad peak that represents the potential

change during the time that the particle is being detected by the sensing electrode. The preamplifier was in turn connected to three shaping amplifiers (Amptek A275) in series, used to differentiate and further amplify the signal. The final processed signal shows a pair of sharp peaks, one produced when the particle enters the sensing electrode and one when it exits. The output from the amplifiers was recorded using a 500 MHz digital oscilloscope (Waverunner 6050A, Lecroy, Chestnut Ridge, NY). Upon exiting the charge detector, bacterial spores entered the impact receptacle.

The impact receptacle was designed to provide a hard surface for impact, while at the same time containing the spores so that they could be collected for later analysis. After the initial impact, the accelerated spores tended to bounce around. An impact vial design was needed to reduce, as much as possible, the loss of impacted spores prior to viability analysis. This receptacle was constructed from a 40 dram glass vial with a plastic lid. A hole was drilled into the lid to allow the spores to enter the vial. To prevent the spores from bouncing straight back out, several spherical glass beads were epoxied to the bottom of the vial, providing a non-normal impact angle (Figure 5).



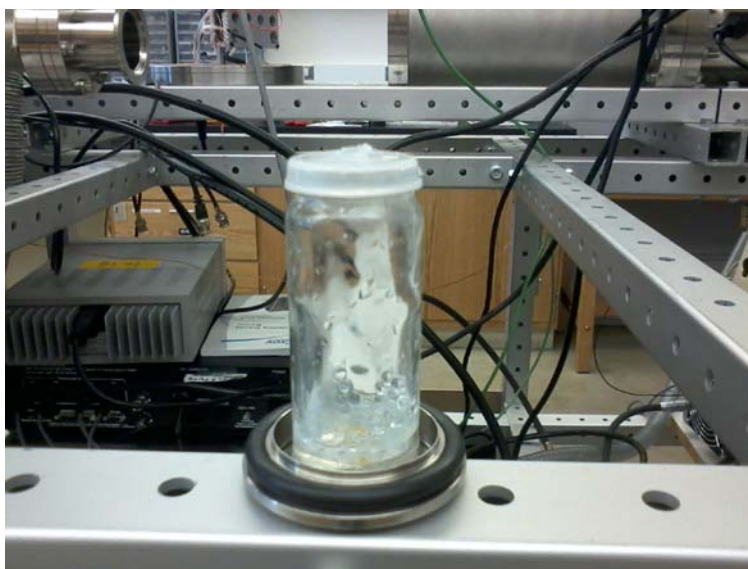


**Figure 5 – Impact receptacle showing plastic lid with a hole in the center for particle entry and irregular glass bead surface on the interior preventing spores from bouncing back out of the receptacle.**

The vial interior was tested for viable bacteria after each impact experiment by placing a sterile cotton swab into sterilized HPLC-grade water and thoroughly swabbing the interior of the vial with the swab. The purpose of this was to cause any spores in the impact vial to adhere to the wet swab. The swab was then swept completely over the surface of a rifampicin-containing nutrient agar so as to cover the entire plate. The agar plate was then placed in a 32° C incubator for 12 hours to encourage surviving spores to form colonies, which were then visually counted and recorded.

Prior to each experiment, aqueous solutions of 40% v/v ethanol and 4.31% v/v sodium hypochlorite were used to sterilize the impact vial and the entire electrospray source (including the aperture to vacuum) to prevent false positive detection. The sterilizing solutions served to kill any contaminant bacteria that may have been present in the system as well as any remaining *B. subtilis* spores that were still present from the previous experiment. In order to check this sterilization procedure for effectiveness, the interior of the impact vial was swabbed after it had

been sterilized. The swab was then swept over the rifampicin-containing agar and left to incubate overnight. The absence of growth after 12 hours indicated that no spores had survived the sterilization process.

For further controls, two separate plates of the rifampicin-containing agar were prepared. Onto the first plate, a sample of HPLC-grade water that had been sterilized by autoclaving was spread using a sterile cotton swab. A sample of the  $10^7$  CFU/mL suspension of the rifampicin-resistant *B. subtilis* was spread onto the second plate. Both plates were placed in the 32° C incubator for 12 hours in order to detect the presence of viable spores. As expected, the plate containing only sterile water exhibited no growth, demonstrating that the procedure was free from contamination. The plate onto which the bacteria had been deliberately spread was covered in a film of bacterial colonies after incubation, as expected. This served to demonstrate that the strain of *B. subtilis* used in these experiments was resistant to the antibiotic rifampicin, as expected.

The control that was done with the rifampicin-containing agar did not prove what it was intended to prove. This control was intended to demonstrate that no other microbes other than the strain of *B. subtilis* that was being investigated could grow on the antibiotic-infused agar. In order to demonstrate this exclusivity, it would have been more prudent to spread a sample of known contaminant onto this agar, even a sneeze onto the agar plate would have produced compelling evidence that the experiments could only produce false positives in the event that some bacteria remained in the vial from a previous experiment. As was mentioned above, that particular source of contamination was prevented using the ethanol and bleach solutions to sterilize the experimental equipment between experiments.

## *Results*

The velocity of each spore was determined from the image charge as the spore entered and exited the charge detector. As mentioned above, one peak is seen as the spore enters the detector while a second peak is shown as the spore exits (Figure 6). For velocity measurements, the length of the detector was divided by the elapsed time between the two peaks. Experiments were conducted with three skimmer and vacuum pump setups, resulting in three different spore velocity ranges:  $155 \pm 9$ ,  $284 \pm 11$  and  $299 \pm 28$  m/s. These values represent the average velocities for each vacuum setup followed by the standard deviations of these groupings. For each velocity range, a fairly narrow distribution of measured spore velocities was observed, as expected. Figure 7 shows the full range of velocities recorded for all three vacuum setups. It can be concluded from the data presented that no spores passed through the system at lower velocities than those shown.

Spores survived impact at all velocity ranges tested. In the fastest velocity range, 43 colonies were recorded out of 57 recorded signals, or an apparent 75% survival rate. Unfortunately, survival numbers were not recorded for the lower two velocities, although surviving spores were observed. Presumably a large fraction survived at the lowest velocity, as they did at higher velocities.

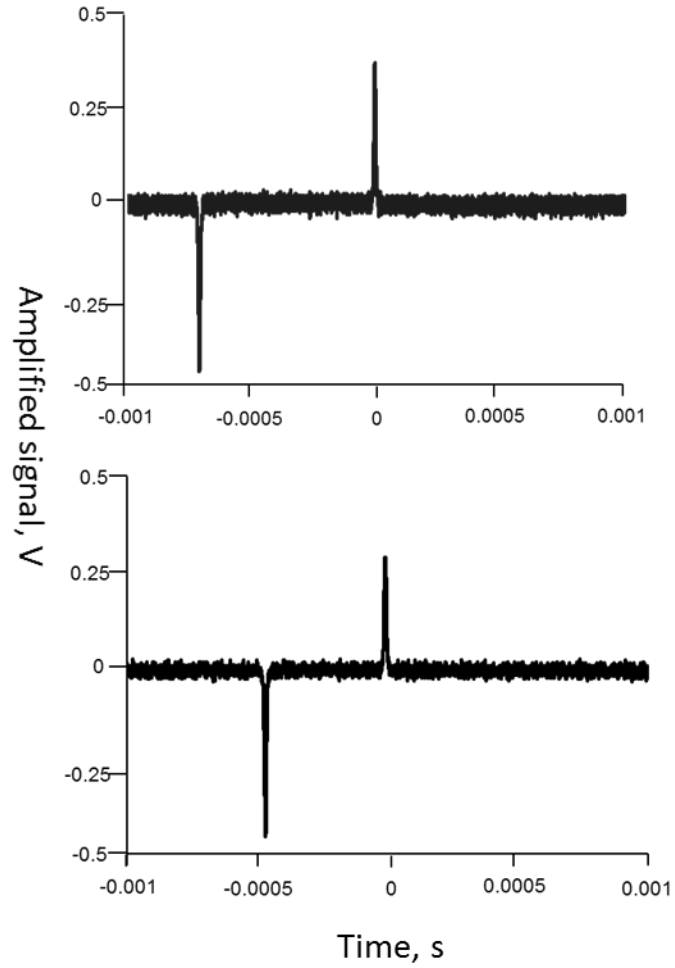


**Figure 6 - Typical signals recorded at the charge detector resulting from charged spores passing through. Top, a spore with measured velocity of 185 m/s; Bottom, spore velocity 348 m/s. The recording electronics triggered off of the second peak, hence the zero on the time base. (Under review for publication in Planetary and Space Science)**

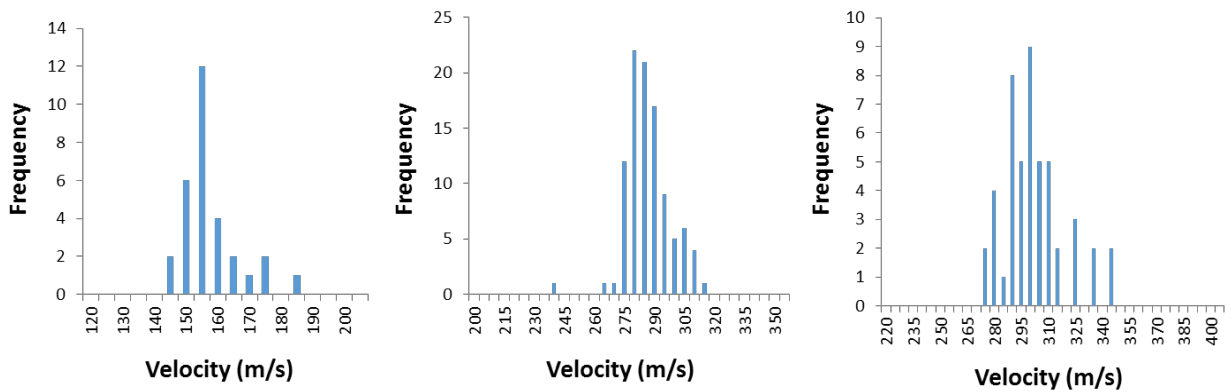


**Figure 7 - Velocity distribution of *B. subtilis* (ATCC 1A308) spores using three different vacuum skimmer arrangements. Average velocities of (from left to right)  $155 \pm 9$ ,  $284 \pm 11$ , and  $299 \pm 28$  m/s. (Under review for publication in *Planetary and Space Science*)**

Part of the reason for this lack of data was the type of oscilloscope that was used to record signal for early experiments. Initially, an older oscilloscope (Agilent 100 MHz DSO3102A) was used to record velocity data. This particular scope had a manual-save-only functionality that required the user to press a button whenever a desired signal appeared on the screen. As one might expect, this led to a lot of missed signal. Because of the missed signal, only a small fraction of the signal for the accelerated bacteria was available for comparison with the number of surviving colonies. The number of these colonies far exceeded the number of recorded signals, making a comparison between the number of counted colonies and the number of recorded signals all but meaningless. The fact remains, however, that for the early, lower velocities tested the velocities reported are accurate for the experiments in question and a large number of surviving spores were observed to produce colonies (Figure 8).

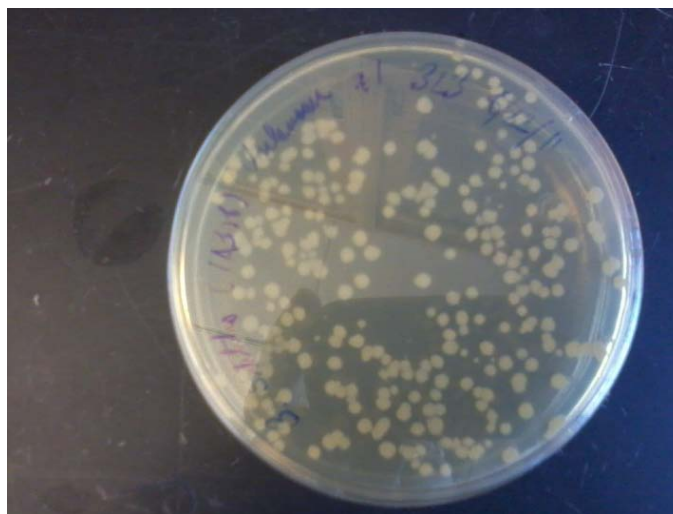


**Figure 8 – Rifampicin-containing agar plate showing bacterial colonies that were grown from impacted spores. The spores on this plate survived impact at an average velocity of 184.9 m/s**

As a comparable amount of spore suspension was electrospayed for each of these experiments, it is a reasonable conclusion that the survival rates for the two lower velocities were approximately the same if not greater than the calculated survival rate for the higher velocity.

The acceleration experienced by the spores during impact may be estimated from the measured velocity and the average dimensions of the spores. The mean length of a *B. subtilis* spore is  $1.07 \pm 0.09 \mu\text{m}$  and the mean diameter is  $0.48 \pm 0.03 \mu\text{m}$  as described in the literature.<sup>69</sup> Assuming the spores that survived experienced a maximum compression of 50% during the impact, then the change in velocity from initial contact to the point of maximum compression yields an average deceleration of  $2\text{-}4 \times 10^{11} \text{ m/s}^2$ , depending on the orientation of the spore. Acceleration is not a factor that has typically been measured by previous researchers. Mastrapa et al. did investigate the effects of extreme acceleration on bacterial cells by placing them in an

ultracentrifuge for 65 hours at 100,000 RPM.<sup>47</sup> This equates to  $4.27 \times 10^6 \text{ m/s}^2$  or about 5 orders of magnitude below the acceleration experienced by the spores in my experiments. Insufficient data is available to predict the amount of compression spores would experience under these conditions, but even with 100% compression (squashed completely flat) the deceleration would be lower by only a factor of 2. Less compression would give a higher deceleration as the spores would be subjected to the same change in velocity but over a shorter distance.

Collection of spores from the vial using a swab likely missed some fraction of the spores, and may explain why the survival rates were not closer to 100%. This is a difficult factor to test, as intentionally introducing a known quantity of spores into the vial (such as through a volume of diluted suspension) would leave spores adhered to the glass in a way that was different from the impact experiment, and may result in different collection efficiency when swabbing.

The narrow velocity distribution, along with the experimental controls mentioned above, demonstrate that the observed bacterial colonies must originate from endospores that survived impacts at velocities within the reported ranges.

In contrast to previous work, the present study isolates the fundamental impact between spore and surface and examines survivability on an individual spore basis. Survivability could not have been enhanced due to agglomeration of bacteria or due to liquid media effects. The magnitude and duration of deceleration was well constrained and always below a well-defined upper limit (defined by the diameter and velocity of the spores). The spore was directly involved with the impact, whereas spores embedded in some material (e.g., granite) may have been located in pores or may have been otherwise removed from the immediate impact surface.

Although previous studies have established spore survivability under some conditions relevant to the interplanetary transfer of bacteria within meteorites, there are also scenarios where bare spore impacts may occur. For instance, aerosolized spores may have been transferred from Mars to Phobos as part of an atmosphere disruption event. Ramsley et al. has shown<sup>46</sup> that many particulates from the Mars atmosphere that are lost due to such an event will impact Phobos at velocities in the range of 1 km/s. If spores can survive such an impact, then there is a possibility that microbes, if present on Mars, may also be present and viable within the Phobos regolith. This possibility may introduce planetary protection considerations for missions involving sample return from Phobos or using Phobos as staging for Mars missions. An additional implication of these results to planetary protection is the possibility that bacterial spores present on the surface of a spacecraft component may be dislodged during a hard landing, with the spore directly impacting regolith and released to the surface.

Spore survivability rates are very high even at the highest velocities achievable with the present experimental setup. Likely the lethal velocity is much higher. Although the present results do not constrain the survivability limits, they do demonstrate survivability under conditions of extreme deceleration that are relevant to microbe transfer in space. These results complement other studies that show survivability under other conditions. Bacterial spores frequently demonstrate extremophile behavior and resistance to many adverse environmental factors (extreme pH, radiation, temperature, salinity, etc.)—the present studies add one more item to that list: the ability to withstand high velocity impact.



## *Conclusion*

I have shown that isolated, individual spores are capable of surviving high velocity impacts up to  $299 \pm 28$  m/s. Bacterial spores may be able to survive planetary impact at similar or higher velocities. Further investigation is needed in order to explore the limits of bacterial survivability to impacts at even higher velocities. These studies will advance understanding of the survival limitations of bacterial spores to impact, including potential transfer events between planetary bodies.

## Chapter 3: An Image-Charge Detector Made from Printed Circuit Boards

Portions of this chapter were taken from: Barney, B. L.; Daly, R. T.; Austin, D. E., A multi-stage image charge detector made from printed circuit boards. *The Review of Scientific Instruments* 2013, 84 (11). Copyright [2013], AIP Publishing LLC. Reprinted with permission.

### *Introduction*

Image-charge detection has been shown to be a versatile method with great potential for future growth. In the first two chapters, the focus has been on the types of analyses that this method is well suited for. In this chapter, an inherent shortcoming of this method will be addressed and studies that have sought to improve the instrumentation of this technique will be reviewed. Following this literature review, the design and testing of a novel multi-stage image-charge detector made from printed circuit boards will be presented.

A weakness of image charge detectors is the detection limit. Individual particles with a single charge or a few charges cannot be detected. Charge detectors can only detect particles with a charge of at least hundreds of electrons (or the corresponding positive charge). As a result, this technique is usually used with a charging method—such as electrospray—that produces highly-charged particles. Methods to lower the detection limit include cooling the detection electronics,<sup>70</sup> passing charged particles through the same charge detector multiple times using electrostatic mirror electrodes<sup>71,72,73</sup> or using multiple detection tubes in series.<sup>10,74,75</sup> Multi-pass reflection-type charge detectors can only analyze particles with low enough kinetic energy and high enough charge-to-mass ratio that they can be electrostatically reflected. In order

to study higher mass systems, it is necessary to use multiple detection stages for improved sensitivity and accuracy.

Multiple detection tubes attached to the same amplifier circuit provide essentially an ensemble averaging effect, as the particle is measured multiple times in sequence. This technique improves the S/N ratio, lowers the detection limit, and increases the accuracy of the charge measurement.<sup>10,74,75</sup> Because the mass of the particle is obtained using the charge measurement, an improvement in the accuracy of the charge will also improve the accuracy of the measured mass.

Gamero-Castano presented a six-stage induction charge detector.<sup>10</sup> He used water droplets produced by electrospray ionization as the sample source. The detector was fashioned from six collinear tubular electrodes with one grounded tubular electrode on each end of the series. For the detection electrodes, every other one is connected to a different amplifier. These amplifiers produced a rectangular wave for each particle, the amplitude of which was proportional to the charge. There was a charge collection calibration detector at the terminus of the electrode array for the purpose of correlating the amplitude of the rectangular wave with the charge on the particle. He reported a limit of detection of 100 charges.

Also using multiple detection regions, Mabbett et al. designed a two stage detector with a pulsed acceleration region between them.<sup>76</sup> They used this setup to study charged water droplets and more specifically the desolvation mechanism of electrosprayed ions. For acceleration, a high-voltage pulse generator was attached to a metal tube that was shielded inside a grounded cylinder to prevent the voltage from the accelerator affecting the charge detection signal. They

measured masses of  $10^{10} - 10^{14}$  Da and charge states of  $10^3 - 10^6$  positive charges. The mass uncertainty was 10% at  $10^{14}$  Da but dropped to 0.1 % at  $< 10^{12}$  Da.

Gamero-Castano again approached the improvement in charge detector instrumentation by coupling a charge detector with a differential retarding potential analyzer.<sup>74</sup> The differential retarding potential analyzer consisted of an electrostatic mirror that was situated in such a way as to deflect the charged particles into the charge detector. The particle exited the mirror when its retarding potential was equivalent to the potential between the plates that made up the analyzer. The time that it took to achieve this potential, along with the charge and velocity measurements from the charge detector were used to calculate mass. Nano droplets from electrospray were analyzed in these particular experiments.

Smith *et al.* used 45 co-linear metal tubes, of which every other one was grounded, giving 22 detection tubes and 23 grounded tubes.<sup>75</sup> The first 11 of the detection electrodes were operated field free, while the second 11 were floated at a potential of 1 V. By comparing the velocities measured in each set of detectors with each other, particle masses were measured. They analyzed particles of poly (ethylene oxide) and reported an average mass of 300 KDa and a charge ratio of approximately 2 kDa/e. By averaging the 22 charge measurements together for each particle, they reported a calculated LOD of 10 charges.

The limits of detection for these methods were extrapolated based on an ensemble average of the signals produced by the various sensing stages. Thus, particles possessing 10 or 100 charges in these cases do not produce a signal large enough to trigger recording electronics, and therefore cannot be individually detected. But because the signal from multiple stages is periodic, it can in theory be deconvoluted from the resulting trace. The advantages of using

multiple detection stages include a lower LOD and improved accuracy for the charge and mass measurements (Figure 9).

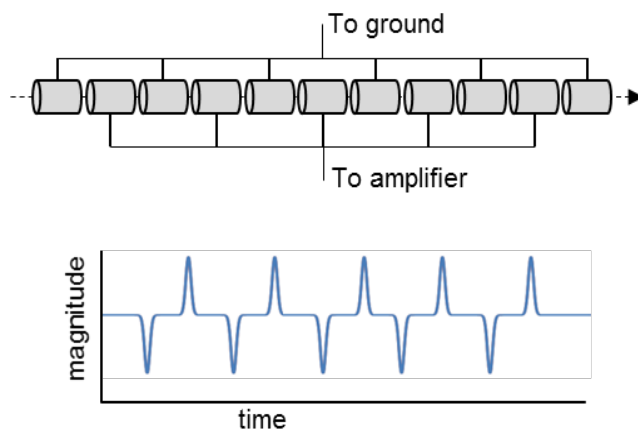


**Figure 9 - Multi-stage cylindrical detector with alternating cylinders connected to the amplifier and ground. The detector shown has 5 sensing stages. Below, the signal expected from detection of a positively-charged particle using a differentiating amplifier. Reprinted with permission from [Barney, B. L.; Daly, R. T.; Austin, D. E., A multi-stage image charge detector made from printed circuit boards. *The Review of Scientific Instruments* 2013, 84 (11)]. Copyright [2013], AIP Publishing LLC.**

By positioning a single charge detector between two electrostatic mirrors, the velocity and charge of a particle may be measured multiple times by the same detector. This type of device is typically called an electrostatic ion beam trap (EIBT). Similar devices, such as the cone trap, operate on the same principle. The  $m/z$  is measured as a function of the number of cycles that a particle remains trapped, which is determined by the charge and energy of the particle. Usually, these traps are designed with one or more CDs in the center of the trap. There are other designs that have been reported for this type of trap, however. For the purposes of this review, only EIBT devices that are coupled with charge detection will be discussed.

Benner designed the first EIBT by placing a tubular charge detector between two separate arrangements of metal sheet electrodes with holes in the centers, arranged in a wafer like fashion.<sup>71</sup> The set of electrodes furthest downstream from the ion source had different potentials applied to them in order to reflect ions back into the detector. Initially, the first set of electrodes had no potential applied to them. When an electrosprayed ion of sufficiently high charge entered the trap, it triggered a circuit that enabled the entrance electrodes, trapping the ion. By measuring the charge and velocity of each ion as it passed over the charge detector, mass was measured. The analyte used for these experiments was 2.88 MDa DNA ions.

The method of extracting a mass spectrum from an EIBT signal through the use of Fourier transform was first demonstrated by Ring et al.<sup>77</sup> They were able to generate mass spectra for  $\text{Ar}^+$  and  $\text{Xe}^+$  as well as the heavier ions of  $\text{PEG}_n\text{Na}^+$  and bradykinin. The noble gas ions were generated by an electron impact source while the heavier ions were produced using a MALDI source.

Pederson et al. investigated the mechanism behind both synchronization of ion motion and rapid debunching in an EIBT.<sup>78</sup> This is an extension of the work described by Ring above, and  $\text{Ar}^+$  and  $\text{Xe}^+$  ions were used for this analysis. They determined that one of the primary mechanisms that determines whether a cluster of ions will remain bunched or begin to diffuse is related to the kinematical and collisional properties of the bunch of ions in question. A correlation between the ion velocities and their positions within the bunch was created by the kinematical properties of the potential well. The repulsive interactions of the ions in the bunch along with this kinematical factor determined whether the bunch moved with synchronized motion or experienced enhanced diffusion.

The ability of the EIBT to resolve clusters of different mass ions was investigated by Zajfman et al.<sup>72,79</sup> They injected bunches of Ar<sup>+</sup> and Xe<sup>+</sup> ions into their trap and observed bunching behavior similar to what would be observed in a Fourier transform ion cyclotron resonance (FTICR) mass analyzer. The instrument performance is compared to an FTICR as well as a time of flight (TOF) mass analyzer. Preliminary results generated by the EIBT showed similar performance to FTICR-MS. It was determined that this method would couple well with TOF-MS as a way to increase the mass resolution of the technique.

In an effort to further improve the performance of the instrument described in the previous paragraph, Zajfman et al. added a set of “cooling” electrodes after the initial ion mirror but before the charge detector.<sup>80</sup> This set was composed of 2 grounded electrodes with a variable potential electrode in between them. Using this setup, they were able to resolve peaks for <sup>132</sup>Xe<sup>+</sup> and <sup>131</sup>Xe<sup>+</sup>. A resolution in terms of  $\Delta m/m$  of  $7 \times 10^{-6}$  was reported.

Attia et al. wanted to understand more about the beam dynamics within an EIBT.<sup>81</sup> Specifically they investigated the transverse velocity distribution (TVD) of the ion beam. They hoped this would help define the trapping efficiency of the EIBT as well as aid in the understanding of beam loss processes within the trap. Singly charged ions of gold, argon and angiotensin II were used in these experiments. The trap that was used was the same as described in the preceding two paragraphs. To measure ion loss and beam distribution, they positioned a microchannel plate (MCP) coupled with a phosphor screen at the terminus of the detector. As ions lost charge due to collisions, they were able to pass through the electrostatic mirrors and hit the MCP. They were able to determine that the TVD was mass dependent and represented about 1% of the longitudinal beam velocity.

A low energy electron target was added to the center of this same trap by Heber et al.<sup>82</sup> This allowed them to study the interaction between electrons and vibrationally cold molecular ions and clusters. Using  $C_2^-$  ions they were able to study the proportionality between the measured collector current and the effective electron density that was seen to interact with the ion beam.

The design of an EIBT operated without magnetic fields for mass selection was reported by Bhushan et al.<sup>83</sup> They used electrostatic fields only to guide the ion stream into the trap. Magnetic fields typically select for a certain energy, resulting in some of the ions generated at the source not making it into the trap. Magnetic fields also tend to alter the relative natural abundances of ions in the sample. These effects were avoided through the use of electrostatic fields. They studied  $Ar^+$  and  $Xe^+$  ions and reported average storage lifetimes of approximately 100 ms. A resolving power of over 20,000 was reported.

Aviv et al. further modified the design first demonstrated by Zajfman in the creation of a bent EIBT.<sup>84</sup> An electrostatic deflector was positioned at the center of the trap that deflected ions towards a third electrostatic mirror positioned equidistant from the center of the trap as compared to the regular exit mirror. By placing MCPs at the terminus of both exit mirrors, they were able to monitor the decay of stored  $Al_n^-$  clusters into neutral and charged fragments.

The EIBT that the Zajfman group designed and which had been modified several times in the previous paragraphs was further modified by Toker et al. who added a mass selector to the center of the trap just before the charge detector.<sup>85,86</sup> The mass selector consisted of a deflection electrode surrounded by two grounded electrodes. As the storage time for an ion bunch increased, the bunch tended to split into smaller bunches of the same mass. Once this separation



had occurred it was possible to set the voltage of the mass selector to “kick out” particles of a certain mass while retaining the rest for further analysis.

Doussineau et al. built a two-stage charge detection device with the second stage being an EIBT.<sup>4</sup> They also had an ion gate at the entrance of the first CD to mass select the ions of a certain  $m/z$  for further analysis. Using this device they analyzed PEO ions of approximately 7 MDa. During the trapping time, ions of interest were irradiated with a CO<sub>2</sub> laser and the fragmentation patterns of the ions were monitored.

An alternative method of extracting mass spectra from the signal produced by an EIBT was presented by Greenwood et al.<sup>87</sup> They operated with an EIBT of a similar design as that which has been discussed for others above. The novel aspect of the trap itself was that it contained three collinear charge detectors between the two ion mirrors. They termed their data analysis method CHIMERA (comb-sampling for high-resolution impulse-train frequency extraction). This algorithm used a comb function to produce frequency coefficients as opposed to the sinusoids produced by a Fourier transform. By applying this analysis to EIBT data that was obtained for xenon ions, they showed that the spectra generated by CHIMERA showed much better agreement with the natural abundance of xenon isotopes than the FFT analysis did.

Another new form of data analysis for the signal produced by an EIBT was presented by Sun et al.<sup>88</sup> Orthogonal projection method (OPM) was introduced as an alternative to fast Fourier transform (FFT) for the analysis of the data produced by an EIBT. OPM used induced signals of the EIBT as basis vectors whereas FFT used harmonics within the signal itself for basis vectors. This method was shown to produce more readable spectra with a faster sampling time than FFT. They reported a resolving power of 75,000 and determined that quantitative MS

could be accurately performed in a sampling time range that was proportional to  $M^{3/2}/\delta M$  as specified by a linear regression analysis.

Doussineau et al. reported a further application for their instrument that was described above.<sup>89</sup> Again dual charge detectors were used, the second of which was positioned in the center of an EIBT. They used the trap along with the infrared multiphoton dissociation fragmentation method to investigate the relative activation energies for the unimolecular dissociation of megadalton DNA ions. They were able to extract the activation energy from a log plot of the first order rate constants versus the laser intensity.

Contino et al. presented a modified cone trap that operated much the same as an EIBT.<sup>90</sup> A charge detector was positioned between two conical electrodes that can function as ion mirrors. They had a dual hemispherical deflection analyzer (HDA) positioned at the entrance of the trap that was used for mass selection. The HDA was a novel mass selector composed of two curved path electrodes connected to each other in an s shaped formation. By applying a selected potential to these electrodes, they were able to mass select ions before entering the trap. Using this trap, they analyzed molecules of bovine serum albumin (BSA). They were able to trap the BSA for an average of 1139 cycles, producing a calculated 3.2 elementary charge (e) limit of detection.

The same instrument described in the above paragraph was further modified by Contino et al. by cryogenically cooling the JFET that received the charge detection signal.<sup>70</sup> This lowered the thermal noise and improved their S/N. They analyzed charged molecules of alcohol dehydrogenase as well as cytochrome c with this particular arrangement. They were able to detect single ions with as few as 9 e. The detection efficiency was calculated to be more than

95% for ions with more than 13 e. They were able to trap ions for approximately 1500 cycles and postulated that the number of cycles was mainly limited by collisions with background gas.

The study of DNA ion activation energies was again presented by Doussineau et al.<sup>91</sup> They used an EIBT with a continuous wave CO<sub>2</sub> laser for a fragmentation source. The analytes that they trapped were single strand circular M13mp18, double strand circular M13mp18, and double strand linear lambda phage DNA fragments – all in the 2.23 – 31.5 MDa range. They determined that the activation energies increased slightly as a function of molecular weight. It was shown that it was possible to differentiate hybridized from non-hybridized structures based solely on their activation energies.

Pierson et al. were able to further refine the instrument demonstrated by Contino to achieve longer trap times and thereby lower the LOD as well as the accuracy of the charge measurement.<sup>92</sup> The analytes studied here were ubiquitin, cytochrome c, and pyruvate kinase. They were able to extend trapping times in 3 ways. The ion optics alignment was improved, providing greater focus for the ion beam. The HDA was operated in a high resolution mode, so that ions entering the trap had a narrower energy distribution. Lastly, the intensity of the ion beam was minimized, increasing the chances for single-ion trapping events. With these improvements, the uncertainty in the charge measurement was reduced to 0.65 e while the LOD was lowered to 7 elementary charges.

In spite of the advantages in sensitivity and accuracy, a charge detector with multiple stages requires that multiple sections of metal tubing be carefully machined, aligned and connected. This process is time-consuming and subject to alignment difficulties. Multi-pass devices such as the EIBT are not able to trap cells such as bacterial spores. The momentum of

these larger analyte species upon entering the trap becomes too great to be repelled by the electrostatic ion mirrors.

I demonstrate a charge detector in which the detection elements and associated wiring are patterned onto two printed circuit boards (PCBs) placed in a sandwich arrangement with a space in between. The facing surfaces of each PCB contain a linear array of copper rectangles, with electrodes connected alternately to either the charge sensitive pre-amplifier or to ground. Charged particles are detected as they pass through the space between the two identical PCBs. Such a device can contain one or many sensing stages depending on the pattern used in creating the PCBs. Each of these stages approximates the sensitivity of a single cylinder. A multiple-stage PCB charge detector requires no additional production overhead and no additional alignment compared with a single-stage device, in contrast with conventional multi-stage charge detectors comprised of a series of metal tubes. These PCBs are easy to make, easy to modify the pattern, easy to connect up, and simple to operate. It is possible using this approach to improve CDMS measurements while greatly reducing complexity. Although demonstrated for a single device, the broader novelty of this report is the ability to use patterned circuit boards to create ion optics devices. This approach will revolutionize both the construction and the possible variations of devices for detection and manipulation of charged particles. One example of such a variation will be described in chapter 4.

## *Experimental*

The charge detection devices were designed using PCBs patterned with metal electrodes. These electrodes consist of alternating regions that are either grounded or connected to a charge sensitive pre-amplifier. The plates were designed using Eagle Layout Editor 6.4.0 and were fabricated by Quick Turn Circuits (Salt Lake City, UT). Two identical plates face one another, parallel to the flight path of the incoming charged particles. Copper electrodes ( $45 \pm 10 \mu\text{m}$  thickness) were patterned and deposited on the circuit boards. A tin-lead finish was hot-air soldered over the top of the electrodes. The purpose of the tin-lead finish was to allow for easier soldering. The PCBs for both the one-stage and five-stage detectors were 63.5 mm wide and 101.6 mm long. For the single stage PCB detector, the sensing stage was 38.1 mm wide and was separated from the 28.7-mm-wide grounded stages on either side by a 1.0-mm gap. For the five-stage PCB detector, alternating grounded and sensing stages were 7.9 mm wide and spaced 1.0 mm apart. The sensing stages on each PCB are connected by a patterned metal strip located away from the particle path along the side of the PCB. Grounded stages are similarly connected on the other side of the PCB. The array of sensing stages on facing plates are connected to each other as well as the charge-sensitive pre-amplifier by wires that are connected to vias on each plate. A plate spacing of 4 mm between the two plates was maintained using ceramic spacers (Figure 10). This spacing is equal to the inner diameter of the cylindrical electrodes in my conventional tubular CD. There are additional spacers positioned on the bottom of the device that maintain the correct distance between the detector and the electronics box that assures alignment with the particle beam.

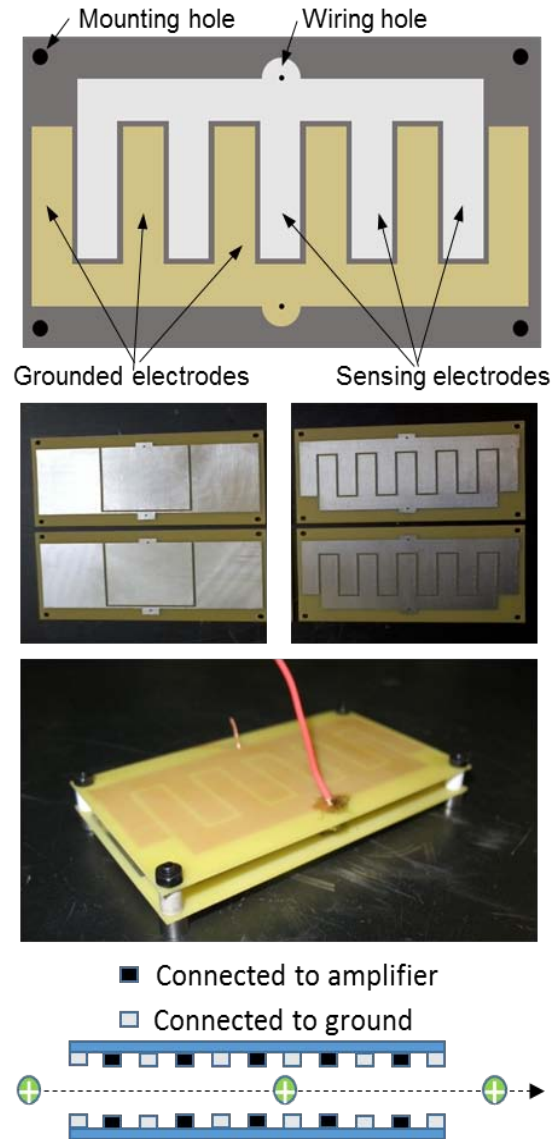


Figure 10 - Top: Design of a PCB for a 5-stage charge detector. Center left: two PCBs used for a single-stage detector. Center right: two PCBs for a 5-stage detector. Large photo: The 5-stage detector assembled and wired. Bottom: flight path of a charged particle through the PCB charge detector. Reprinted with permission from [Barney, B. L.; Daly, R. T.; Austin, D. E., A multi-stage image charge detector made from printed circuit boards. *The Review of Scientific Instruments* 2013, 84 (11)]. Copyright [2013], AIP Publishing LLC.

Several different PCB charge detector designs were developed and compared: a single-stage, two-PCB detector; a 5-stage, two-PCB detector; and also a 5-stage detector using only one

PCB. Each of the different designs was tested according to the same procedure. The detector itself, as well as the box containing the amplifiers, was mounted on a vacuum flange that was situated at the terminus of the vacuum system. No efforts were made to shield the PCB detectors at this time as noise levels were not a major concern for these experiments. All sensing elements of the PCBs were connected together to the JFET input of a charge-sensitive preamplifier (A250, Amptek, Bedford, MA). The preamplifier was in turn connected to three shaping amplifiers (Amptek A275) in series. The output from the amplifiers was connected to a 500 MHz digital oscilloscope (Waverunner 6050A, Lecroy, Chestnut Ridge, NY).

The performance of each PCB charge detector was demonstrated using polystyrene particles charged by electrospray and introduced into vacuum. The analyte used in all tests was 0.91- $\mu\text{m}$  amino-terminated polystyrene beads (Spherotech, Lake Forest, IL) at a concentration of 0.05% w/v in a solution that was 4:1 methanol to water. The solution was acidified to a pH of 3.9 with formic acid. The polystyrene solution was pumped through a custom-made electrospray needle by a syringe pump operating at 100  $\mu\text{L}/\text{h}$ . The needle was biased at 3000 V relative to the grounded vacuum system using a 5000 V, 25 W high-voltage power supply (PS350, Stanford Research Systems, Sunnyvale, CA). The electrosprayed solution entered the vacuum system through a 150- $\mu\text{m}$  pinhole before passing through a beam tube (4.5 mm I.D.) inside a differentially pumped (using a turbo-molecular pump) stage that was separated from the detector by a 0.7-mm I.D. skimmer cone. The charged particles then passed through the detector where an image current was generated and the signal was amplified.

The purpose of the amplifier setup was to convert the very small current generated by the interaction between the charged particle and the detector electrodes into a measurable signal. This initial conversion was done with a charge-sensitive pre-amplifier (Amptek A250). The

voltage output from the pre-amplifier was passed on to three differentiating and shaping amplifiers (Amptek A275) connected in series. At this point, the voltage reading was converted into two sharp peaks, one positive and one negative. The area of either of these peaks was directly proportional to the total charge on the particle. The first of the pair of peaks occurred when the particle entered the detector while the second signified when the particle exits. By dividing the physical length of the detector by the length in time between these two peaks, the velocity was obtained.

In order to correlate peak area to charge, any charge detector using a differentiating amplifier must be calibrated. The published procedures use a pulse generator which is connected to the test-line of the charge-sensitive pre-amplifier.<sup>1</sup> A known voltage is passed through a 2 pF test capacitor producing a known charge at the input of the preamplifier. Once this approach has been applied, a simple correlation coefficient between the voltage and the charge is obtained.

In order to determine whether the sensitivity of the PCB charge detector was comparable to that of a conventional charge detector, the two detectors were placed in series such that each charged particle passed through both detectors, one after the other. A given particle passing through presented exactly the same charge to both detectors, so the resulting image charges were directly comparable. The sensing elements of both the PCB charge detector and the tubular charge detector were electrically connected to the JFET input of the same pre-amplifier so that both signals could be analyzed under identical conditions. Under these conditions, the ratio of the peak areas between the two detectors will be equal to the ratio of the sensitivities of the detectors, even if the sensitivities are different. However, if the sensitivities of the two detectors are similar, the peak areas will be equivalent. The results of this test are independent of the



accuracy of the calibration and unaffected by low-frequency fluctuations in the detector or electronics.

A similar test was made to compare the performance between a PCB detector consisting of just a single plate and the conventional tubular charge detector. This test would determine whether the second PCB is necessary for accurate charge determination using this type of charge detector.

### *Results and Discussion*

All three designs have been tested and shown to function as expected. The signal from the single-stage PCB charge detector shows the same features and appears equivalent to the signal produced by a single cylindrical detector. The five-stage detector shows a series of five negative and five positive peaks (Figure 11).

In some of the spectra acquired from the 5-stage PCB detector the peak amplitudes steadily increase or decrease as the particle passes through the different stages of the detector. However, in each of these cases the peak areas remain constant. Because charge measurement is based on peak areas and not peak amplitudes, accurate charge measurement can still be obtained. A possible explanation of the inconsistent peak amplitudes is that the particle traverses the

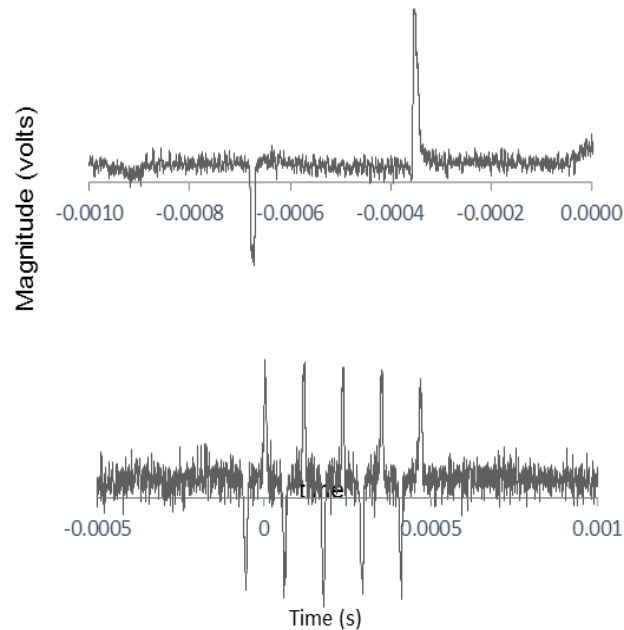


**Figure 11 - Typical signals produced using electro sprayed 1-micron polystyrene particles using (top) single-stage PCB and (bottom) 5-stage PCB charge detectors and differentiating amplifier. Reprinted with permission from [Barney, B. L.; Daly, R. T.; Austin, D. E., A multi-stage image charge detector made from printed circuit boards. *The Review of Scientific Instruments* 2013, 84 (11)]. Copyright [2013], AIP Publishing LLC.**

detector at a slight angle. Assuming that the image charge is proportional to the solid angle projected by the analyte particle onto the sensing elements, a particle that is off-center will exhibit a varied rise-time as it approaches the set of sensing electrodes for a given sensing element. This results in a varied amplitude of the differentiated signal. The peak areas remain constant because as the particle moves away from one electrode, it moves closer to the electrode on the opposite plate. The reduced solid angle on one electrode is partially cancelled out by the increased solid angle of the opposing electrode, giving the same net image charge. Referring

back to the undifferentiated signal shown in Figure 1, the net offset remains the same regardless of the position of the particle in the device. The net offset is due only to the particle charge and the corresponding voltage produced on the detector plates due to the capacitance of the system. However, the amplitude of the differentiated signal reflects the rise-time, which is influenced by the geometric relationship of the charged particle to one or the other electrodes. The rise-time is not a result of the magnitude of the charge, hence the amplitude of the differentiated signal does not reflect particle charge. Note that the particle velocity does not change in any of the measurements made.

The results of the experiments utilizing both a tubular detector and a 5-stage, 2-PCB detector in series demonstrate that the two detectors produce a similar response for a given particle (Figure 12). For each detected particle, signal was generated from both detectors and the peak areas were compared. A paired t-test was used to determine if the conventional and PCB detectors were equivalent methods for the measurement of charge. The analysis was carried out using data from 47 different charged particles that were detected by both the multi-stage PCB detector and a tubular CD. The average difference in peak areas between these two methods was  $0.032 \mu\text{Vs}$  with a standard deviation of  $0.40 \mu\text{Vs}$ . Within the 95% confidence interval, the two methods are not statistically different. It is a reasonable supposition that this correlation applies equally to any of the planar detector designs that were tested. Similar to multi-stage charge detectors made with tubular electrodes, in the two-PCB device the ensemble averaging provided by multiple measurements of the particle charge improve the S/N of the charge measurement.<sup>10,32,33</sup>

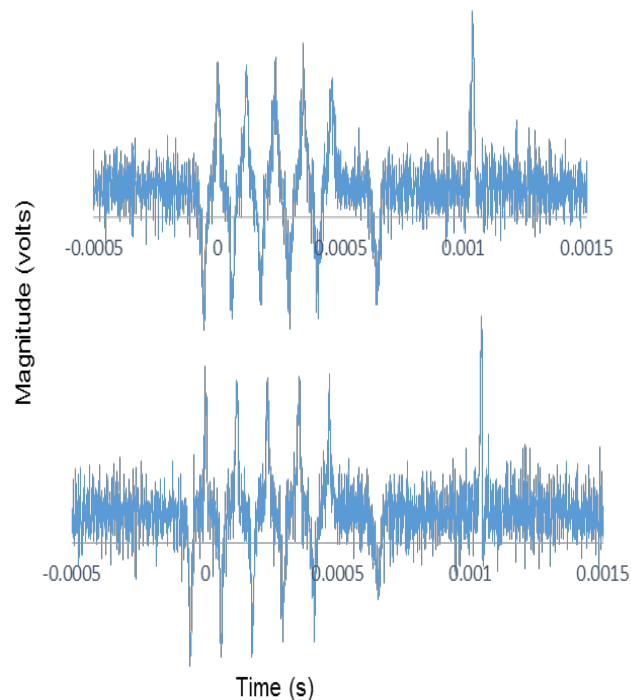


**Figure 12 - Representative signals each showing a charged particle passing through both 5-stage PCB (left of each trace) and conventional charge detectors (right of each trace) in series. For each particle, the peak areas generated by both types of charge detectors are equivalent, demonstrating similar sensitivity. Reprinted with permission from [Barney, B. L.; Daly, R. T.; Austin, D. E., A multi-stage image charge detector made from printed circuit boards. *The Review of Scientific Instruments* 2013, 84 (11)]. Copyright [2013], AIP Publishing LLC.**

To determine whether reliable charge measurements could be made with a single PCB, particles were detected with only one plate of the 5-stage PCB detector. This “open-faced” detector only had one set of sensing elements, testing the necessity of the two-plate approach. It was anticipated with this experiment that the peak area would vary with the distance between the particle and the PCB, a factor that was neither controlled nor measured. A comparison was made

between the areas of the peaks for each particle to see if the areas were still reproducible. Unfortunately, not only the peak amplitudes, but also the peak areas from one stage to the next varied significantly for most of the particles detected (Figure 13). For one of the traces that was evaluated, the ratio in areas between the first and last peaks was  $2.9 \mu\text{Vs}/1.4 \mu\text{Vs}$  (Figure 14). This was essentially a 2 to 1 ratio. Because of the direct area to charge correlation the charge of the particle appeared to decrease by half as it passed through the detector. Without a consistent ratio of particle charge to peak area, the single-PCB device could not be used for accurate charge measurement. Whereas the two-PCB charge detector provides consistent peak areas and charge measurement, the single-PCB device is unable to accurately measure charge.

An initial concern in these experiments was that the skin depth of the sensing electrodes would be a factor in the sensitivity of the device. For signals in the 10 kHz range (typical of the signals measured in these experiments) the skin depth of copper is roughly 0.2 mm,<sup>93</sup> which is thicker than the copper layer deposited onto the PCBs. The cylindrical CD was made of stainless steel, which at these same frequencies has a skin depth of approximately 1 mm, comparable to the thickness of the electrode used. The comparable charge detected in the test discussed above (with two detectors in series) shows that skin depth is not an important factor in the magnitude of the image current generated.

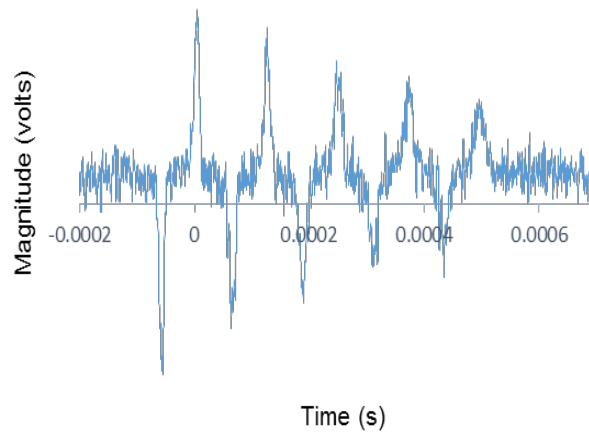


**Figure 13 - Representative signal from a single-plate, 5-stage PCB detector. The peak area steadily decreases as the particle travels from one sensing stage to the next. In contrast to the 2-PCB design, a single-PCB charge detector is unable to measure particle charge. Reprinted with permission from [Barney, B. L.; Daly, R. T.; Austin, D. E., A multi-stage image charge detector made from printed circuit boards. *The Review of Scientific Instruments* 2013, 84 (11)]. Copyright [2013], AIP Publishing LLC.**

The device that has been demonstrated is the first instance of an image-charge detector being made using lithographically patterned circuit boards. This work shows that devices for detection, analysis, and/or manipulation of charged particles, including ions, can be made in this fashion rather than using separately-fabricated metal electrodes. Although the present design does not improve the sensitivity or detection limit over a conventional device with a similar number of stages and similar dimensions, this approach has many other advantages. First, the

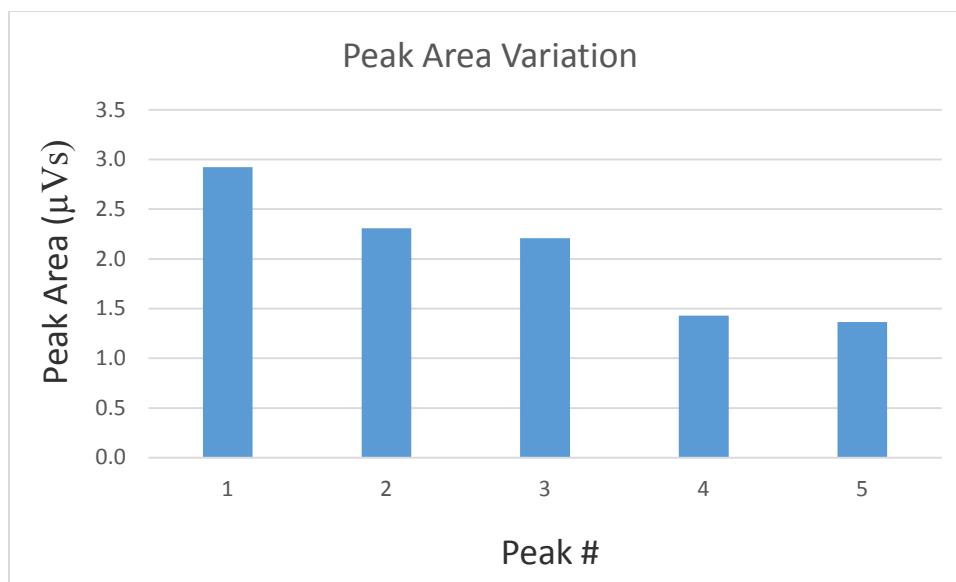


**Figure 14 – Variation in peak area generated by one particle using a single-plate detector. The peak area varies between approximately 2.9 and 1.8  $\mu\text{Vs}$**

simplicity of construction and design afford the opportunity to test a variety of detector layouts with minimal expertise and expense. In this study, single-stage and five-stage detectors were demonstrated. Switching between these two designs did not involve any additional mounting hardware other than a redesign of the PCBs. This approach enables even larger numbers of stages to further improve the S/N and the accuracy of charge and mass measurement in CD-MS. Secondly, the two-plate design greatly alleviates alignment difficulties for multiple sensing stages when compared with multiple collinear tubes. It is no more difficult to align two PCBs with twenty sensing stages than it is to align two PCBs with one sensing stage. The technique also benefits from the high dimensional precision with which PCBs can be patterned. Furthermore, the PCB design facilitates integration of other electronic elements, such as ion optics or amplifier circuitry, onto one of the same PCBs with the sensing stages. Electrostatic

acceleration would permit mass to be determined along with the charge and velocity measurements that are already demonstrated with this device.

### *Conclusion*

Variations on a PCB-based image-charge detector have been demonstrated. Charged particles have been detected using these detectors which have metal electrodes patterned onto printed circuit boards. The signal generated from the single-stage device closely resembles signal that was generated from a conventional single-stage tubular-electrode detector. The two 5-stage devices that have been tested show five clear up and down peaks, representing each of the five stages of the device. Peak areas for a given particle from cylindrical and planar devices are not statistically different. The fabrication method is simple, precise, and inexpensive, especially as compared to the conventional method of machining tubular electrodes for detection purposes. With the addition of a DC acceleration region, this detector will be able to measure the mass of a charged particle as well as the charge. The ability to measure mass will allow a planar PCB-based image charge detector to be used to determine the mass distribution of large variable mass systems. These results also demonstrate that printed circuit boards can be used to construct ion optics devices with several significant advantages over techniques using conventional electrodes.



## Chapter 4: Measuring elasticity via kinetic energy loss in bouncing bacterial spores

### *Introduction*

An understanding of the physical properties and characteristics of biological cells has many possible applications. For instance, the mechanical properties of bacterial spores, when understood, have potential design applications for nanomaterials. Nanoparticles based on biological models are already in use. Both particles based on proteins and DNA have been tested for nano-medicine.<sup>94</sup> Bacterial spores are another model that could potentially be of use in this field. These materials are of interest for drug delivery and other medicinal applications.

Much has been done investigating the tolerance of stationary bacterial and fungal spores and vegetative cells to the steadily increasing force of an AFM stylus. Heinz and Hoh first envisioned using AFM to explore the intermolecular interactions in biological structures including bacteria.<sup>95</sup> They wanted to better understand how the intermolecular forces that tie biological systems together are specifically distributed in the space between the atoms that make up the surface of a biological target. In AFM, a mechanical spring attached to a stylus is used to measure force as a function of distance. It was developed primarily as an imaging tool to provide finer detailed surface mapping than other methods that were available at the time. The AFM has a sharp tipped stylus (around 10-100 nm) that is well suited for molecular work as the radius of curvature of the AFM tip is on the scale of the molecular interactions that it would be used to probe. Specifically, the AFM probe could be used to map surface adhesion, elasticity, hardness, and electrostatic interactions. All of these different types of forces could be mapped together to generate an interaction surface for a particular object.

A number of researchers have used AFM measurements to generate force-distance curves for the surfaces of bacterial and fungal cells and have extrapolated physical properties of the cells from these data. Surface hardness, elasticity, thickness of the cell wall, as well as how these properties vary across the surface of the cell can all be derived from these curves. The two primary properties of the cell membrane or cell wall that researchers have been interested in are the elasticity or Young's modulus and the stiffness or cell spring constant. Elasticity is measured in  $\text{N/m}^2$  or Pa and stiffness is measured in N/m. Both properties are different ways of describing how the force generated by an AFM stylus pressing against the cell affects that cell mechanically.

It is possible to generate a range of possible values for the cellular spring constant as well as the Young's modulus for the spores in this study based on the change in kinetic energy data that was collected. However, with the current experimental setup it is not possible to determine exact values for these two constants. The reason for this is that both values require a knowledge of the degree of spore depression that occurs at impact. Without values for the depression distance or area as a result of impact, the most that can be reported is an estimate of a range of values based on possible spore depression conditions. A more detailed discussion of this problem will be given in the results section of this chapter. This is the first study that has been reported that analyzes the elasticity of a spore or a cell based on kinetic energy change due to impact in a dynamic experiments. The studies listed below report values for the elastic properties of cells evaluated in a mostly static environment.

Yao et al. used AFM to measure the elasticity of the murein sacculus, or peptidoglycan layer, of the cell walls of *Escherichia coli* and *Pseudomonas aeruginosa*.<sup>96</sup> At the time, it was assumed that the peptidoglycan layer was the main stress bearing structure in bacterial cells.

These experiments strove for further understanding of the mechanical properties of this structure. The cells were suspended in deionized water and small drops of the suspension were placed on the etched surface of a Si or Si<sub>3</sub>N<sub>4</sub> wafer. The elasticity of the sacculus was measured by determining how much force from the AFM stylus was needed to depress the saccule into the etched grooves on the surface of the wafer. They found the elasticity to be  $2.5 \times 10^7$  N/m<sup>2</sup> for the hydrated cells and between  $3 \times 10^8$  and  $4 \times 10^8$  N/m<sup>2</sup> for the dry cells.

The turgor pressure and the spring constant of *Magnetospirillum gryphiswaldense* were measured by Arnoldi et al. using AFM in conjunction with scanning electron microscopy (SEM).<sup>97</sup> Turgor pressure plays a key role in how bacteria maintain their shape as well as several other cell functions. It was thought that if the turgor pressure could be more precisely defined for a certain cell then a greater understanding of these functions could be reached. Buffer suspensions of the bacterial cells were placed between two glass surfaces and the surfaces were scanned using both techniques. Only data points in which the surface returned to the original position after depression were included as this indicated completely elastic depression. The turgor pressure value was determined to be 85 – 150 kPa. Measured values between 0.04 and 0.07 N/m were generated for the spring constant.

Touhami et al. investigated the variation in elasticity for different regions of the cell membrane for hydrated yeast cells.<sup>98</sup> Specifically they were interested in the region where cell division has occurred, or the bud scar. Cells of *Saccharomyces cerevisiae* were trapped in polycarbonate membranes prior to AFM analysis. Young's modulus values of  $6.1 \pm 2.4$  and  $0.6 \pm 0.4$  MPa were measured for the bud scar region and the surrounding cell membrane respectively.

The mechanism by which the bacterial spring constant of *Shewanella putrefaciens* changed at different pH values was investigated by Gaboriaud et al.<sup>99</sup> Cell membrane stiffness plays a key role in many functions, including bacterial adhesion and surface recognition, among others. The researchers sought to understand how the cell's chemical environment affects this stiffness. Cells were suspended in either pH 4 or pH 10 solutions and then were dried in a polystyrene dish, adhering them to the surface of the dish for AFM measurements. The force curves at both pH values had both linear and non-linear regions. The linear region indicated simply depression of the cell wall by the AFM tip while the non-linear portion was thought to be the result of a polymeric fringe on the surface of the dried cells. They measured bacterial spring constants of 0.05 and 0.02 N/m for pH 4 and pH 10 respectively.

Zhao et al. measured the stiffness and elasticity of *Aspergillus nidulans* spores.<sup>100</sup> They wanted to investigate what influence the protein coverage on the surface of the spore had on these mechanical properties. Thus, they compared wild type spores to isogenic *rodA*<sup>+</sup> and *rodA*<sup>-</sup> strains. The spores were affixed to glass cover slips prior to nanoindentation measurements made using AFM. The stiffness values for wild-type, *rodA*<sup>+</sup>, and *rodA*<sup>-</sup> spores were  $110 \pm 10$ ,  $120 \pm 10$ , and  $300 \pm 10$  N/m respectively. The elasticity measurements for these three spore types were  $6.6 \pm 0.4$ ,  $7.0 \pm 0.7$ , and  $22 \pm 0.2$  GPa respectively.

Cell surface elasticity of two different strains of *E. coli* was studied by Beckman et al using AFM.<sup>101</sup> One strain was a wild-type pathogenic enteroaggregative *E. coli* while the other type was a mutant non-pathogenic strain of *E. coli* that did not exhibit the surface protein dispersin. They wanted to investigate what role the protein dispersin had in the surface elasticity of the bacteria. Individual cells were embedded into a gel that covered a mica surface in water prior to AFM mapping. They presented their results as slopes which may be understood to

indicate standard units of N/m for the elastic moduli of the two different strains of bacteria. They reported values of 0.133 and 0.081 N/m for the wild-type and mutant strains respectively when the cells were grown in broth. Additional values were reported for cells grown on agar and showed that the elasticity was roughly the same for both strains if they were grown on an agar gel as opposed to in a nutrient broth.

Mendez-Vilas et al. used AFM to map the surface elasticity of *Staphylococcus epidermidis* in two studies.<sup>102,103</sup> They wanted to gain further insights into the surface adhesion properties of this particular species. In particular, they wanted to see if there were any sub-cellular features that influenced this adhesion. In the first study, they investigated the difference in elasticity between the outer cell membrane and the inner cell wall, while in the second study they investigated the effect that different fixation methods had on the elasticity of the cells. They found the elasticity of the cell membrane to be  $0.072 \pm 0.009$  N/m while the value for the inner cell was  $0.24 \pm 0.01$  N/m. They also showed that the mechanical trapping of these bacterial cells in a filter membrane altered the mechanical characteristics of the cells.

The cell rigidity of *S. cerevisiae* was investigated by Lanero et al.<sup>104</sup> They postulated that perhaps some of the cell fixation methods used while studying the mechanical properties of these cells could be altering those properties. They compared the elasticity of bare cells to the elasticity of cells that had been embedded in a poly-electrolyte matrix used to affix cells for imaging. Both treated and untreated cells were trapped in a microporous membrane for analysis purposes. By comparing cantilever deflection to piezo-displacement, force curves were generated for the cells. They used these curves to calculate a Young's modulus of  $1.79 \pm 0.08$  MPa for the encapsulated cells,  $1.12 \pm 0.02$  MPa for uncoated cells without a bud scar, and  $2.0 \pm 0.2$  MPa for untreated cells with a bud scar from cell division.

Sullivan et al. compared the surface elasticity of *E. coli* spheroplasts to that of intact cells.<sup>105</sup> A spheroplast is a bacterial cell from which the cell wall has been almost completely removed. They wanted to determine what role the cell wall had in the elasticity of the cell as a whole. They developed new methods for affixing spheroplasts to a surface for study using either aminopropyltriethoxysilane or glutaraldehyde. The bacterial spring constants of the intact bacteria and cell wall deficient spheroplasts were determined to be 0.191 and 0.574 N/m respectively.

The elasticity of two types of yeast cells was mapped by Alsteens et al., *Saccharomyces carlsbergensis*, and *S. cerevisiae*.<sup>106</sup> They wanted to determine how cell wall elasticity and polysaccharide properties differed across the surface of a cell as well as from strain to strain. The cells were trapped in porous polycarbonate membranes for study. Young's modulus values for *S. cerevisiae* were determined to be relatively uniform across the bud scar region as well as the surrounding area at  $0.8 \pm 0.2$  MPa. In contrast, *S. carlsbergensis* exhibited a large amount of variability with Young's modulus values of  $0.7 \pm 0.2$  and  $2.3 \pm 0.8$  MPa for the mother cell and the bud scar respectively. By analyzing the mechanical data obtained from the AFM measurements, they were able to determine that the surface of *S. cerevisiae* is relatively rich in manoproteins (highly glycosylated polypeptides that make up much of the surface of the cell), while the surface of *S. carlsbergensis* is not.

Bui et al. measured the elasticity of *S. cerevisiae*.<sup>107</sup> They compared the elasticity of the cells when suspended in deionized water versus those suspended in a phosphate-buffered saline solution. This was another study that aimed to determine what role the cell's environment played in its elasticity. In order to fix the cells in place for analysis, they were first trapped in a polycarbonate membrane. Force-distance curves for cells in both types of solvent were

generated and used to derive Young's modulus values of  $0.15 \pm 0.02$  MPa for the yeast suspended in DI water and  $0.24 \pm 0.03$  MPa for the yeast suspended in the PBS buffer solution.

Further investigations were carried out on the effect of environment on cell elasticity. Wet cells of *Pseudomonas aeruginosa* were studied by Vadillo-Rodriguez et al.<sup>108</sup> They investigated how both the cell spring constant and the effective time constant for these cells changed when glutaraldehyde was added to the cell suspension. Glutaraldehyde served to increase the covalent bonding on the surface of the cell and should have had an effect on the stiffness of the cell membrane. In order to determine the mechanical properties of the cells, the AFM cantilever was lowered at a constant rate until a pre-determined loading force was reached. At this point, the force was held constant and the force distance curves were generated. They obtained cell spring constants of  $0.044 \pm 0.002$  and  $0.11 \pm 0.03$  N/m for the untreated and glutaraldehyde treated cells respectively. They observed that the cells exhibited a time-dependent deformation in response to a constant loading force. The glutaraldehyde-treated cells were observed to be 2.8 times stiffer than the untreated cells.

Cerf et al. measured the Young's modulus of *E. coli* cell walls, both for living cells and those that had been killed by heating.<sup>109</sup> At the time there was considerable difficulty in differentiating between a living bacterial cell, a dead cell, and one that has lost the ability to reproduce. For this reason, the researchers wanted to see what effect cell death had on the mechanical properties of the cell. For cell fixation, they used a novel patterned adsorption method to fix single cells into ordered arrays. Once fixed, the elasticity of each individual cell was evaluated. The same cells were then heated to 45 °C over 20 minutes, after which the elasticity of the cells was measured again. They found that the damaged cells had a Young's modulus of  $6.1 \pm 1.5$  MPa while a value of  $3.0 \pm 0.6$  MPa was observed for the living cells.

The cellular spring constant of *S. cerevisiae* cells was measured by Arfsten et al.<sup>110</sup> In industrial biology, bacteria are used for the synthesis of many products, like synthetic enzymes. In order to recover these products, the cell must be ruptured. This study had for an aim the improvement of a target-oriented disruption process. They investigated the degree of uncertainty in the elasticity measurements of these cells by performing the measurements 40 times for each cell. They found a normal distribution around the median value. From this they determined that the median value for the cellular spring constant could be used as the actual value. This median value that they measured was 0.32 N/m. They also investigated how the osmotic pressure of the cell influenced the spring constant measurement. They found that the spring constant decreased, on average, as the osmotic pressure increased. A range of 0.075 – 0.324 MPa was observed.

Pinzon-Arango et al. measured the Young's modulus of *Bacillus anthracis* cells, in vegetative form, spore form, and as germinated spores.<sup>111</sup> In order to determine what effect different germinants at different concentrations had on the elasticity of the germinated spores, tests were done with both L-alanine and inosine treated spores at two separate concentrations for each germinant. The highest value for the Young's modulus was obtained for the dormant spores, with an average value of  $197.02 \pm 80.48$  MPa. The lowest value obtained was  $12.4 \pm 6.3$  MPa for the vegetative cells. The values obtained for the Young's modulus after different concentrations of the germinants were added for a different length of time varied between these two extremes. The lowest elasticities obtained using one type of germinant alone were  $47.5 \pm 41.7$  MPa for the L-alanine and  $35.4 \pm 15.8$  for the inosine. Combining the two germinants together decreased the elasticity even further. A minimum value of  $23.5 \pm 14.8$  MPa was reported for the two mixed together.



The elasticity, hardness, surface roughness, and adhesion force of *Aspergillus niger* spores was experimentally determined by Fang et al.<sup>112</sup> For analysis, they anchored the spores on a glass slide with a small amount of glue. The loading force for the AFM cantilever was varied in order to generate more data points from which to calculate the mechanical properties under investigation. The average surface roughness of these spores was approximately 33 nm. They found that the adhesion force between the spores and mica was greater in air (30-110 nN) than in water (2-25 nN). They measured Young's modulus values from 0.1 to 21.4 GPa. Between 0.01 and 0.17 GPa was the range of values measured for the spore hardness. Both the Young's modulus and the hardness of the spore increased at a depth of 470 nm from the spore surface where plastic deformation began.

There are methods other than AFM that have been utilized to measure the mechanical properties of bacterial and fungal cells. While the experimental method differs from the studies discussed in the preceding paragraphs, the goal of the next set of studies is the same as those previously discussed – a better understanding of the mechanical properties of bacterial and fungal spores.

Minc et al. constructed polydimethylsiloxane micro-chambers that each held one yeast cell.<sup>113</sup> These chambers were arranged in an array of approximately 10,000 chambers with a volume of about 1 fL each. By buckling the chambers and thereby rupturing the cell walls, they were able to determine the surface elasticity of *Schizosaccharomyces pombe* (a type of yeast) cells. As a control they monitored what forces it took to buckle a yeast cell under the strain of its own growth while confined in the chamber. To test whether or not the stress-response pathways were triggered in the buckled cells, they monitored the stress reporters sty1-green fluorescent protein (GFP) and pap1-GFP. These reporters move from the cytoplasm to the nucleus of the

cell during times of osmotic or oxidative stress. They noticed no change in the distribution of these markers either when the cell was buckling from its own growth or from induced external pressure, indicating that the buckling of the cells was not causing a large amount of stress to the cell. They recorded values of  $20.2 \pm 6.1$  N/m and  $101 \pm 30$  MPa for the cellular spring constant and the Young's modulus respectively.

Individual cells of *S. cerevisiae* were investigated by Stenson et al. They placed the cells between two plates and measured the force required to rupture the cells.<sup>114</sup> There was a fear that many of the previous values obtained for the mechanical properties of cells were good for only the unique conditions that they were tested in. They determined that in order to avoid obtaining non-unique values for the elasticity of the cell, the determination of a few additional properties was required. These included: the initial cell stretch ratio, the initial cell wall thickness ratio, and the cell wall permeability or hydraulic conductivity. For both the cell wall thickness ratio and the initial cell stretch ratio, population mean values were used, leaving the cell wall permeability as the adjustable property. They found that up to 60% compression, the deformation of the cells was completely elastic. They also found that if they compressed the cells rapidly enough then the elastic modulus didn't alter from increased compression speed. This demonstrated that above a certain speed threshold water loss from the cell during compression was negligible. Taking all of these factors into consideration, a mean elastic modulus of  $185 \pm 15$  MPa was measured for the cells.

Nakanishi et al. investigated the spore or cell hardness of *E. coli*, *Staphylococcus aureus*, *P. aeruginosa*, and five *Bacillus* species using the cantilever of a scanning probe microscope, similar to the AFM method.<sup>115</sup> They compared the hardness values that they determined for each species to heat and UV resistance for the species in question. They found no significant

difference in the Young's modulus of the 7 species tested in vegetative cell form, although the values for the 2 gram-negative species did tend to be lower than the values for the 5 gram positive species. They reported Young's modulus value of approximately 0.2 N/m for each of the vegetative cells. It must be noted that these are units for a bacterial spring constant rather than a Young's modulus and can be treated as such. The values for the spores were much higher and ranged between  $0.240 \pm 0.059$  and  $0.811 \pm 0.048$  N/m. They also found that the relationship between the cellular spring constant and both heat and UV resistance was a linear one, demonstrating that for the species studied, high resistance to mechanical stress was also an indicator of high resistance to heat and UV stress.

A nano-needle was used to study the elasticity of wild type yeast cells that had been placed inside an environmental scanning electron microscope chamber by Shen et al.<sup>116</sup> This was another study that looked to determine what effect cell environment has on the stiffness of the cell. In this case the relative humidity of the air was monitored in relation to cell stiffness. The microscope was used to monitor the cell deformation in real time throughout the experiment. As the relative humidity was increased, the stiffness of the cell decreased. Stiffness values of approximately 15.5, 8.0 and 3.5 MPa were recorded for 40%, 70%, and 100% relative humidity.

The previous studies primarily investigate the mechanical properties of cells as a function of their resistance to a steadily increasing force. It is instructive to compare cell response to this type of stress to the mechanical reaction that a cell has to a sudden high velocity impact. Both energy regimes are necessary to more completely understand how these biological structures respond to stress.

The inspiration for the experiments that will be discussed in this chapter arose from an unintended result during the bacterial impact survival experiments discussed in chapter 2. Many initial impact experiments were performed before any surviving bacteria could be found. At the time, I was using an Erlenmeyer flask as the impact vessel. It was thought that perhaps the problem lay in the system alignment. This led to checking the system piece by piece to see if an element of the system was out of alignment. During this process a brownish-orange substance was noticed at the terminal end of the charge detector, at a point before the spores would have entered the impact vessel. The substance was collected and spread onto a rifampicin-containing agar plate. After overnight incubation, bacterial colonies formed on the surface of the agar. The presence of the antibiotic rifampicin in the agar was a strong indication that the colonies originated from the strain of *B. subtilis* that I was studying. This evidence along with the lack of spores in the impact vessel seemed to indicate that the spores were bouncing out of the vessel and back into the vacuum system.

For this study, the elasticity of *Bacillus subtilis* spores as expressed by the kinetic energy loss of individual spores upon impacting a hard glass surface has been measured. This energy loss was calculated using the change in velocity of the spores before and after impacting the surface. Two different initial spore velocities were analyzed. These velocities were measured using a specially designed image-charge detector that was built for this study. Experiments were performed in a vacuum system.

## Experimental design

In these experiments, spores of *Bacillus subtilis* were highly charged using electrospray ionization before being swept into a vacuum system using pressure differentials. After passing through a beam tube and a skimmer cone they passed through the detector. The detector was a 2-stage image-charge detector that was specially designed to detect particle bouncing. After passing through the detector once, the spores impacted a glass surface and bounced back into the detector, where they were detected a second time (Figure 15). The velocity was measured for both passes through the detector and the change in kinetic energy was calculated using these velocities. Two different vacuum setups produced two different ranges of initial velocities. The kinetic energy change upon impact was tested for both ranges of initial velocities and the results were compared with one another.

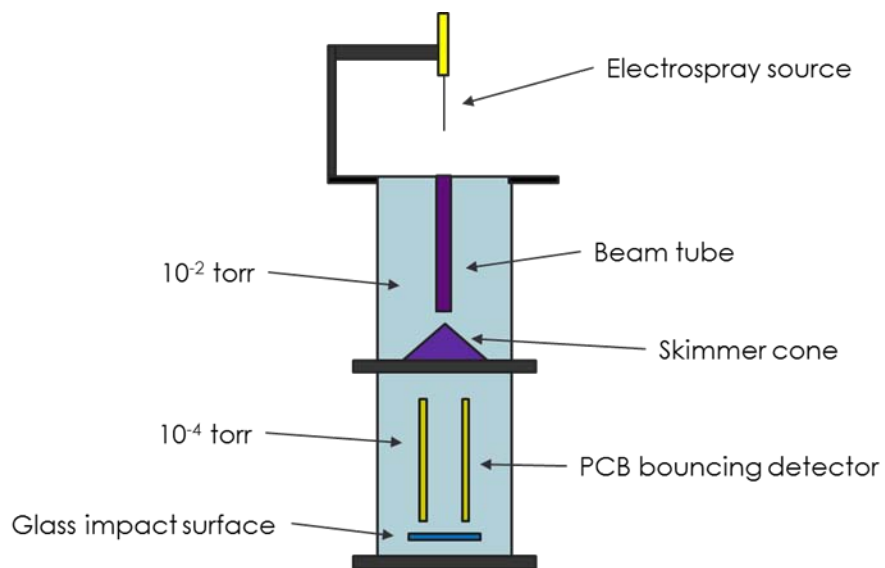


**Figure 15 - Vacuum setup for the bouncing experiments. Spores are electrosprayed then pass through a beam tube and a skimmer cone. They then pass through the detector, bounce off of the surface and pass through the detector again.**

All tests were done with the same strain of *Bacillus subtilis* (1A308, ATCC, Manassas, VA) that was used for the experiments in Chapter 2. In order to carry out the bouncing tests, it was necessary for the live cells to undergo sporulation. Vegetative cells were subjected to a sporulation protocol in which the cells were placed on a nutrient agar where they grew and multiplied rapidly until the nutrients were exhausted. Once the nutrients were exhausted, the cells began to enter a dormant stage, known as the endospore stage. At the completion of this process, the spores were collected and suspended in sterilized HPLC water (Thermo Fisher, Waltham, MA) at a concentration of  $10^6$  CFU/mL (colony forming units per mL). These spores were introduced into the vacuum system via electrospray ionization. The sporulation was done in order to increase the resistance of the cells to mechanical stress. Cells undergo a number of physiological changes as they become spores. Primarily, they are almost completely dehydrated and they develop a thick outer protein coat. Both of these factors help the spores to survive extremely harsh environmental conditions and stresses. By way of comparison, it is not likely that live cells would be able to undergo both the electrospray process and the impact event without being destroyed.<sup>62</sup> Cell rupture could alter the shape of the cells post impact and thereby alter the speed of these cells over what would be expected from a more elastic bounce. This would introduce a degree of uncertainty into the second velocity measurement, taken after the cells had bounced.

ESI was performed using the *B. subtilis* spore suspension mentioned above. The solution was pumped through a custom-made electrospray tip at 100  $\mu$ L/h using a KD Scientific (Holliston, MA) syringe pump. Negative mode electrospray was used for these experiments. Negative mode electrospray was selected because a larger percentage of electrosprayed spores were detectable in negative mode than in positive mode experimentally. The electrospray tip

was biased at -3500 V using a 5000 V, 25 W high-voltage power supply (PS350, Stanford Research Systems, Sunnyvale, CA). After being electrosprayed, the spores entered the vacuum system in a highly charged state, enabling them to be detected by the charge detector.

Once electrosprayed, the spores entered the vacuum chamber through a pinhole. They were then swept through a beam tube and a skimmer cone by the flow of gas through the vacuum system. Through the use of the skimmer cone as well as two turbo-molecular pumps, the pressure was reduced from ambient conditions to approximately  $1 \times 10^{-4}$  torr. In order to produce the second velocity studied, both turbo pumps were turned off, reducing the system pressure to  $7 \times 10^{-2}$  torr. A third initial velocity was attempted by turning off just one of the two turbo pumps. This increased the system pressure by about half an order of magnitude, bringing it up to  $6 \times 10^{-4}$  torr. As the system pressure increased, it was assumed that the particle stream velocity would decrease. This was due both to an increase in the number of collisions with the background gas as well as the reduced difference in pressure from one side to the other of both the pinhole and skimmer cone interfaces. Surprisingly, this higher system pressure had no appreciable effect on the initial particle velocity. One of the two turbo pumps was positioned before the skimmer cone and one was positioned after. Either pump, operating independently, produced approximately the same system pressure and the same initial particle velocity. Only by turning off both pumps was a different initial spore velocity achieved. Without the turbo pumps, the system was pumped down only by two rotary vane roughing pumps, one at the system inlet and one farther downstream, pulling on the location that the two turbo pumps occupy. For velocity measurement, the particles then passed through the charge detector, specially designed to detect bouncing.

The charge detection devices were designed using printed circuit boards (PCBs) patterned with metal electrodes. The board designs and layout were similar to that described in chapter 2. As with the previous design, two identical plates faced one another, parallel to the flight path of the incoming charged particles. Each plate consisted of two sensing regions interspersed by three grounded regions. The two sensing regions were of different length, one of them being 0.64 cm long while the other was 1.91 cm long (Figure 16). The reason for the differing length of the sensing regions was to give the detector the ability to indicate the direction that the spore was traveling. Traveling from the system entrance towards the system terminus, spores passed the shorter sensing region first, followed by the longer sensing region. The signal produced by a spore thus traveling appeared as two closely spaced peaks followed by two that were spaced further apart. Once the spore impacted the hard glass surface and bounced back into the detector, it passed through the two sensing regions in reverse order. Two more widely spaced peaks were followed by two more closely spaced peaks. This design allowed for the signal from a bounced spore to be easily distinguished from the signal for two spores traveling closely together. In contrast, a single or multi-stage charge detector does not have the ability to determine the direction that a particle is traveling. Thus the signal produced by two spores traveling closely together would be indistinguishable from the signal produced by a spore that had bounced.

The plates were designed using Eagle Layout Editor 6.4.0 and were fabricated by Quick Turn Circuits (Salt Lake City, UT). Similar to the multi-stage design in the previous chapter, the two sensing stages on facing plates were connected to each other as well as the charge-sensitive pre-amplifier by wires that were connected to vias on each plate. The grounded regions on both



plates were also wired to each other as well as to outside ground. A plate spacing of 4 mm between the two plates was maintained using ceramic spacers.

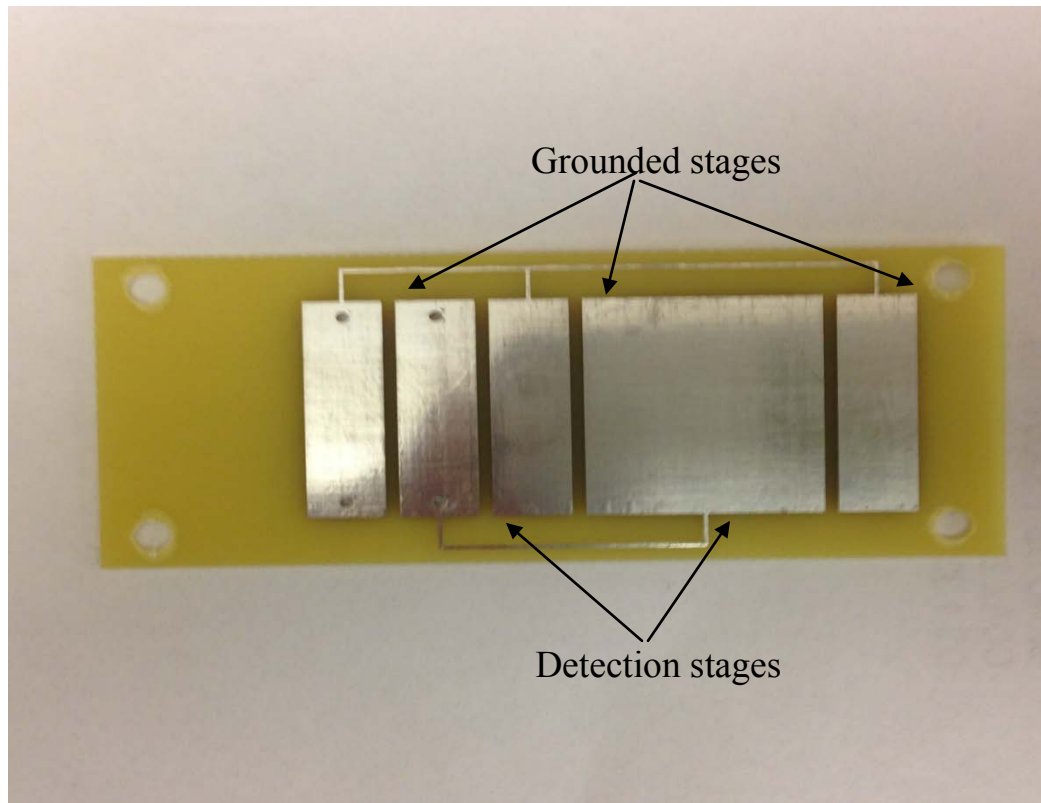


**Figure 16 – PCB-based bouncing detector.** Due to the differently sized detection stages, the direction of the traveling particle is easily determined. Spores travel lengthwise across the detector. They initially travel left to right. After bouncing, they travel right to left.

This novel plate design was engineered to correct problems that were observed in early bouncing experiments done using an 11-stage charge detector. There were two problems with this design for this particular experiment. First, being much longer in length, it was much less likely that bouncing spores would pass all the way through the detector after bouncing. With a shorter detector, the bouncing angle does not need to be perfect in order for the particle to be detected. A spore that has bounced at a small angle from the normal is still detectable by a short 2-stage detector. Secondly, there was no directionality to the signal produced by the 11-stage

charge detector. This caused problems in bouncing measurements as the signal produced by a spore passing back through the detector after having bounced was difficult to distinguish from the signal produced by two spores traveling closely together.

For an impact surface, a square of pane glass that was 15 mm x 15 mm was used. It was positioned at the terminus of the charge detector, normal to the flight path of the spores. This provided a smooth, flat surface that the particles had a better chance of rebounding off of back into the detector. Other surfaces that were attempted included glass covered by adhesive tape, polytetrafluoroethylene (Teflon), and a polished silicon wafer. It was surprisingly difficult to find a surface that generated good signal after the particle had bounced. This was likely due to charge loss of the particle at the point of impact, which would seem to indicate a transfer of charge between the spore and the surface upon which it impacted. Therefore a surface that had a low affinity for electrons should have been the best surface for impact. Based on the triboelectric series, both silicon and adhesive tape should have had a much lower electron affinity than glass. However, the peak areas generated from experiments with both silicon and adhesive tape were significantly smaller than the signal generated from the glass impacts and more difficult to measure accurately. It was decided that the signal generated from the glass impacts was sufficient to measure velocities accurately. Accurate velocity measurement was important for these experiments as it allowed for a more accurate determination of kinetic energy loss.

In order to measure the change in kinetic energy due to impact, it was necessary to measure the velocity of the particles both before and after bouncing. The signal generated by the charge detector provided the time that it took each particle to pass through the detector. By dividing the known length of the detector by this transit time, particle velocities were obtained.

By comparing the velocities of each spore both before and after impact, the change in kinetic energy was calculated for each spore.

### *Results and Discussion*

In order to determine what effect a semi-elastic impact has on the kinetic energy of a bacterial spore, it was necessary to compare the spore's energy before impact to the spore's energy after impact. In order to calculate this change, it was only necessary to know the spore's velocity before and after bouncing. For all experiments performed for this study, the change in kinetic energy was calculated in the following manner:

$$\% \text{ change in kinetic energy} = \frac{\frac{1}{2}mv_1^2 - \frac{1}{2}mv_2^2}{\frac{1}{2}mv_1^2} \times 100\% \quad (4-1)$$

After the  $\frac{1}{2}m$  (m for particle mass) term is cancelled out, the change in kinetic energy becomes simply a question of the change in the square of the two velocities.

$$\frac{v_1^2 - v_2^2}{v_1^2} \times 100\% = \% \text{ change in kinetic energy} \quad (4-2)$$

The average spore velocity for the experiment performed at  $8.6 \times 10^{-4}$  torr was  $197 \pm 16$  m/s. This pressure was achieved by turning off the turbo pump that was positioned before the skimmer cone while leaving the other one on. It must be noted that tests performed with the other turbo pump on as well as tests performed with both turbo pumps on produced the same experimental results, within the margin of error. The average kinetic energy loss after impact for this experiment was  $71 \pm 16$  %.

For the experiments performed with both turbo pumps turned off, the system pressure was  $6.8 \times 10^{-2}$  torr. The average spore velocity at this pressure was  $147 \pm 12$  m/s. The percent kinetic energy loss after bouncing at this velocity was  $72 \pm 10$  %. Impacts at both initial velocities produced very similar energy loss results. In fact, within the margin of error, both energy loss values were essentially the same. This seems to indicate that the energy lost at impact is not dependent upon the initial velocity of the spore impacting the surface.

The distribution of energy losses around the average value for both initial velocities produced a more or less normal distribution as would be expected (Figure 17). The velocities of these spores were governed primarily by the airflow that carried them through the vacuum system. Spores of different sizes traveled at slightly different velocities due to a greater or lesser resistance to airflow. Such natural variations in velocity were encompassed in the normal energy loss distributions of these samples.

One of the early concerns with these experiments was the fact that the bouncing signal that was observed was somewhat infrequent. A large proportion of the signal that was collected showed only a single set of peaks, likely produced by a spore traveling through the detector but not bouncing back into the detector. However, when the spore shape is considered it is not surprising that the signal was so infrequent. As mentioned in chapter 2, these spores have average dimensions of approximately  $1 \mu\text{m} \times 0.5 \mu\text{m}$ . There are only a select few orientations at which a traveling spore could impact a surface in such a way as to rebound directly back into the

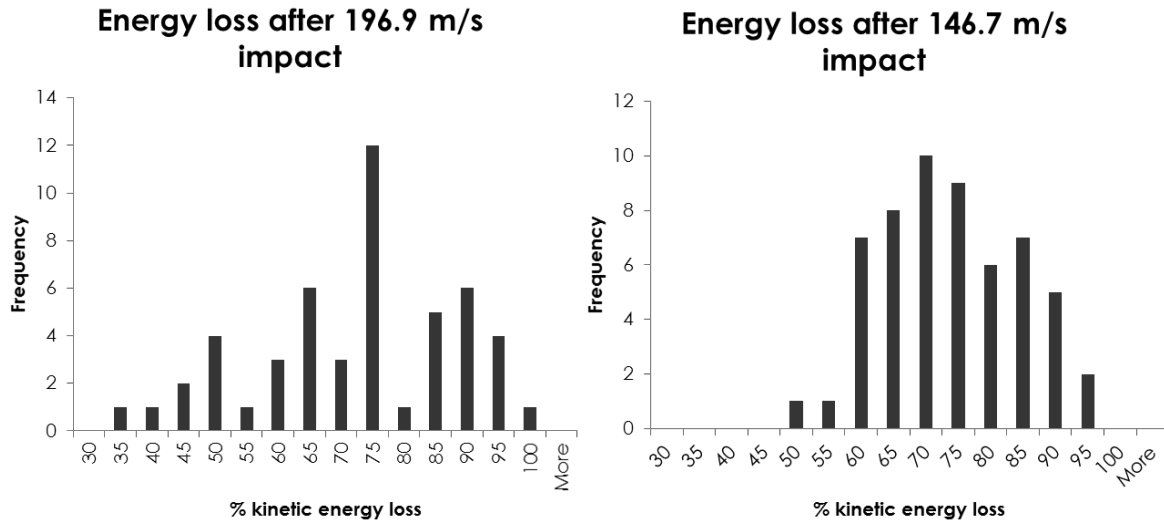


**Figure 17 – Distribution of percent kinetic energy loss for the bacterial spores upon impacting a glass surface at two average velocities. The bin numbers on the horizontal axis indicate a range between the number indicated and the preceding number. For example “100” indicates 95-100.**

detector. Approximately one or two out of every ten recorded signals for a given experiment demonstrated that a bounce had occurred.

It is possible that the energy loss numbers reported here were biased by the oblong shape of the spores themselves along with the experimental conditions. The relatively narrow dimensions of the detector made it so that only impacts resulting from a relatively narrow range of bouncing angles bounced the spores back into the detector. A wider detector would allow a greater percentage of the bouncing spores to be detected. This would result in a more complete picture of the energy loss experienced by a spore upon impact regardless of the orientation of the spores upon impact.

In order to generate a range of possible cellular spring constants for the spores in these experiments, it was necessary to utilize the principle of conservation of energy. As seen in the above results, the kinetic energy of the spores was significantly reduced as a result of the impact with the glass surface. The difference between these two kinetic energies can be expressed by the spring potential energy of the spore.

$$\frac{1}{2}mv_1^2 = \frac{1}{2}mv_2^2 + \frac{1}{2}kx^2 \quad (4-4)$$

In the above equation  $m$  represents the mass of the spore  $v_1$  is the spore velocity before impact,  $v_2$  is the spore velocity after impact,  $k$  is the cellular spring constant, and  $x$  represents the distance that the spore is compressed upon impact. Rearranging the above equation and solving for  $k$  yields the following expression:

$$k = \frac{m(v_1^2 - v_2^2)}{x^2} \quad (4-5)$$

Values for the two velocities were measured using the image-charge detector as reported. The mass used was an average *B. subtilis* spore mass based on published values for the average volume and density for these spores.<sup>69</sup> Based on these numbers, an average mass of  $2.4 \times 10^{-16}$  kg was calculated.

As stated in the introduction, the value of  $x$  was not known. As the average dimensions of the spores were  $1.07 \mu\text{m} \times 0.48 \mu\text{m}$  4 possible  $x$  values were used to calculate a value for  $k$ . The estimated  $x$  values used were: 0.25, 0.5, 0.75, and  $1.07 \mu\text{m}$ . These  $x$  values yielded average  $k$  values for the spores of  $61 \pm 16$ ,  $15 \pm 4$ ,  $7 \pm 2$ , and  $3 \pm 1$  N/m respectively (Figure 18). As can be expected, the  $k$  value decreased as the depression distance increased.

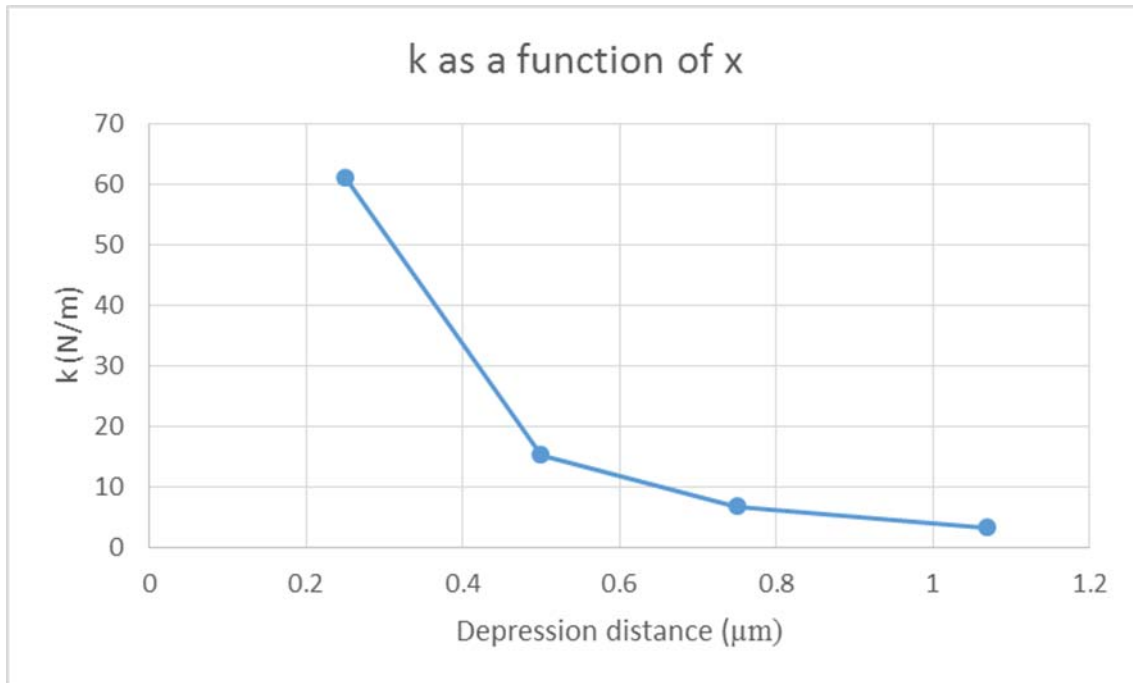


**Figure 18 - Values for the cellular spring constant  $k$  as a function of the depression distance  $x$**

In order to calculate a value for the Young's modulus of these spores I could have used the value for  $k$  to calculate the amount of force necessary to depress the spore a given distance. If this force were then divided by the cross-sectional area of the spore at that particular distance from the surface, a value for the Young's modulus could be obtained. However, as this depression distance is not actually known, it would have to be estimated. Also as the value for Young's modulus depends upon a distance squared rather than just a distance, the range in possible values would be much larger than the range reported for  $k$ . This would limit the usefulness of such a calculation being done for discussion purposes.

The image-charge detector used for these experiments consisted of two sensing regions, one much longer than the other. The different electrode dimensions were designed to detect the direction that a particle was traveling. Each time a charged spore passed over a sensing region, a pair of peaks was produced, the first when the particle first began to pass over the detecting

region and the second when the particle left the detection region. Thus a particle passing through a 2-stage charge detector should produce 4 peaks. A particle passing through the detector and bouncing back out again would produce a total of 8 peaks. Each signal consisting of at least 6 peaks exhibiting the characteristic pattern for a bouncing spore was evaluated. This pattern consisted of a pair of 2 closely spaced peaks followed by 2 pairs of widely spaced peaks. If a particle bounced back into the detector at an angle, it is possible that it would be detected by the longer detecting region but not the shorter. This type of particle could either pass out of the detector to the side or possibly collide with the grounded region between the two detecting regions without being detected by the shorter region. For this reason signals of 6 peaks were considered along with signals showing eight peaks. By only evaluating signal exhibiting the pattern of two sets of peaks spaced far apart, bouncing signals were easily differentiated from signal produced by two spores traveling closely together. By dividing the known length of the sensing region by the transit time between each pair of peaks, each particle's velocity was calculated.

As an additional test to confirm a particular signal represented a bouncing spore, the two velocities that were taken from each bouncing spore signal were compared to a third velocity that was derived from the elapsed time between the signals produced by the forward and reverse trip of a spore through the detector. This third velocity and distance were represented by the time during which the spore traveled from the end of the detector to the impact surface and then rebounded back into the detector. For half of this distance, the spore was traveling at its initial velocity while for the other half of the distance the spore was traveling at the post-impact velocity. With the recorded time that it took to travel this distance, and the two measured velocities, it was possible to calculate what this intermediate bouncing time should have been



theoretically. By comparing this theoretical value with the observed value it was possible to further confirm that true bouncing signal was being observed.

$$\left(\frac{0.0141 \text{ m}}{v_1} + \frac{0.0141 \text{ m}}{v_2}\right) = t_t \quad (4-3)$$

In this equation 0.0141 m is the distance between the end of the final sensing element and the impact surface,  $v_1$  is the pre-impact spore velocity, and  $v_2$  is the post impact spore velocity. The variable  $t_t$  is the theoretical time that it should take the spore to travel from the end of the sensing element, to the impact surface, and back into the final sensing element based on the two recorded velocities. All apparent bouncing signals that had a greater than 10% deviation between the measured and theoretical times were rejected. This resulted in less than 1 in 10 signals being rejected. Interestingly, the rejection of these signals had no appreciable effect on the average energy loss and only a slight effect on the standard deviation. This confirmation was in addition to the confirmation provided by the apparent peak spacing due to the detector design.

As is demonstrated in Figure 17, the area of the peaks produced by the charged spore post-impact was significantly smaller than the area of the peaks corresponding to the initial pass through the detector. These peak areas are directly proportional to the charge of the particle that produced the peaks (Figure 19). Therefore the object that produced the second set of peaks must have a significantly smaller charge than the object that produced the first set of peaks. It has already been confirmed that the signals observed were indeed produced by a bouncing object. It is likely that the loss in peak area after each bounce was due to a charge transfer between the

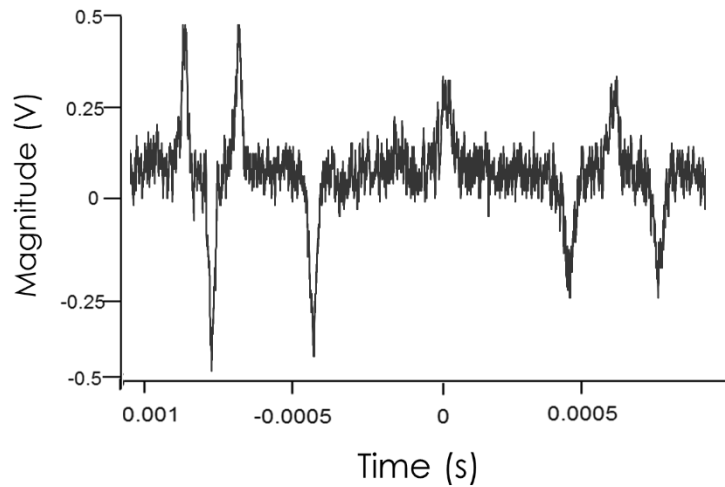


Figure 19 – Signal produced by a charged spore passing through the charge detector, bouncing, and then passing back through again. The peak area for a peak produced by the spore on the return trip is significantly smaller than the peak area corresponding to the initial passage through the detector. Velocities derived from peak spacing were used to verify that signal produced by a bouncing spore was being observed.

charged spore and the glass surface. As mentioned in the previous section, other impact surfaces were tried other than glass. These surfaces included Teflon, a polished silicon wafer, and the back side of adhesive tape. This reduction in peak area was observed under every impact condition tested. For the surfaces other than glass that were tested, this reduction in peak area was significantly greater, making it more difficult to extract any useful information from these data sets. This would seem to indicate that when considering a highly-charged, fast-moving object, impacts on glass tend to result in a relatively low transfer of charge.

## *Conclusion*

The elastic properties of *B. subtilis* spores have been investigated in a novel manner. A unique detector has been introduced that was specifically designed to monitor bouncing particles. By using this detector to measure the velocities of impacting spores, both before and after impact, it was possible to determine how the kinetic energy of a traveling spore is affected by impact with a glass surface. The shape of the spores likely plays a role in the dynamics of these impacts. It can also be inferred from the data presented that a significant amount of charge is transferred from the surface of a charged spore to the glass at the time of impact. The work presented here will serve to supplement other studies that have investigated the mechanical properties of bacterial spores. This enhanced understanding could point the way towards using bacterial spores as models in the construction of nano-particles for use in a variety of applications.

## Chapter 5: Determination of the exact mass of *Bacillus subtilis* spores

### *Introduction*

The determination of the exact mass of a bacterial cell is a challenging problem. As mentioned in chapter 1, the natural variability in mass and size of individual spores of the same type makes this analysis impossible using conventional mass spectrometry methods. Charge detection mass spectrometry (CD-MS) is an analytical method where both the absolute charge and the  $m/z$  ratio are determined for a particle. The two measurements can be combined to generate the mass for each individual particle measured. For this reason, the accuracy of the measured mass of a particle determined by CD-MS is not diminished by the variable mass and size of individual cells within a cell population. It is in fact an ideal method for the investigation of the mass variability of a particular type of cell.

In chapters 2 and 4 it was shown that by combining electrospray ionization with image-charge detection, it was possible to detect individual bacterial spores. Both spore velocity and energy loss due to impact have been measured using this technique. If a known potential is applied between two charge detection regions it is possible to measure the  $m/z$  of a charged particle by comparing the particle velocity inside the field to the velocity in the field-free region. As described in chapter 1, it is also possible to correlate the peak area of the image-charge detection signal to the absolute charge of the particle that produced said signal. With both the charge and the  $m/z$  for an individual cell, the mass of the cell can be obtained.

The small number of studies that have been done measuring the mass of a bacterial or fungal cell have been done with different light scattering techniques. In all of these cases, the

total mass of a bacterial sample is obtained by monitoring the way that light scatters or refracts through a cell suspension. After determining the number of cells in the sample separately, an average cell mass is calculated. The determination of cell mass was usually not the main goal of the study. This mass determination was used to investigate some other property of the cells under study. These methods were used to determine cell size before researchers expanded the calculations to include mass.<sup>117</sup> To the best of my knowledge, no studies have been reported that attempted to measure the mass of an individual bacterial cell.

Coles et al. first reported the measurement of bacterial mass using a light scattering photometer.<sup>118</sup> They looked at cells of *Serratia marcescens*, *E. coli* and *Thiobacillus ferrooxidans*. They used a light source in the IR region with a wavelength similar to the size of the cells being studied. By measuring how the light scattered through the spore suspension compared to pure water alone, a Zimm plot was generated for each species. This type of plot tracks how scattered light intensity changes with the root mean square radius as well as the concentration of the scattering particles. A standard benzene solution was used for calibration purposes. However, the uncertainty in the benzene measurement was large (20-25%). This resulted in the calculated mass values for the cells  $1.2 - 2.6 \times 10^{-13}$  g carrying up to a 60% uncertainty.

The change in mass between wet and dry spores of *Fusarium roseum* was measured by Mumford et al.<sup>119</sup> They diluted a spore suspension until one drop of the suspension contained approximately 40 spores. One drop was placed on a microscope coverslip which was weighed immediately and then 24 hours later, after the water had evaporated - leaving only spores. Using a scattering microscope, the difference in optical path length between the wet and dry spore samples was recorded. This information was used to determine that the percentage of total spore

mass that was composed of lipid bodies decreased from 23% to 10% as the cells dried. They also found that even as the percent lipid body was changing, the mass of approximately 57 pg stayed relatively constant.

The mass of both the fungal spore and germinated cells of *Diplodia maydis* was presented by Pappelis et al.<sup>120</sup> As above, they used quantitative interference microscopy to measure the total cell mass both before and after germination. The mean mass value was then determined using sample spore counts. The masses increased from approximately 297 pg to 550 pg during germination. They concluded, based on the mass increase and available material that the germinating spores incorporated material from spores that did not germinate in order to have the type of mass increase that was observed during germination.

Algie et al. were able to determine both the mass and water content of the core, cortex and coat of *B. stearothersophilis* spores.<sup>121</sup> At the time it had been assumed that the heat resistance exhibited by bacterial spores was a function of partial dehydration during the sporulation process. However, there existed no experimental evidence to support this. Using electron micrographs, they determined the volumes of the different spore components. They then calculated densities using a solvent linear density gradient column. Using measured water isotherms along with the density and size, they were able to determine the relative mass of each spore component. The total spore mass was measured at  $79.36 \times 10^{-14}$  g with the masses of the coat, cortex, core, and protoplasm being 22.77, 41.84, 14.76, and  $4.44 \times 10^{-14}$  g respectively. Using both wet and dry measurements, they determined that both the core and coat of the spore are partially dehydrated.

A method to measure cell volume and mass using flow cytometry was presented by Koch et al.<sup>122</sup> They expanded upon the theory of light scattering measurements that existed at the time by presenting a method whereby particles as small and irregularly shaped as bacteria could be analyzed. By generating algorithms that make use of the integral of the scattered light signal from various sized cells at various orientations, they were able to calculate cell volume as well as wet and dry biomass.

The studies discussed above all report an average mass of the bacterial cells under study. Generally, this information is given in passing as it was not the main goal of most of these experiments. The researchers were more interested in some other property of the cell and calculated an average mass for the cells in the course of their research. In order to more accurately determine spore mass, it is necessary that an instrument be able to analyze spores individually.

The design and preliminary testing of a planar PCB CD-MS (printed circuit board charge-detection mass spectrometry) detector will be presented. This is another example of a specialized PCB charge detection device being designed for a specific task, in this case the mass measurement of individual charged particles. This detector was designed with the analysis of bacterial spores in mind. However it could be used for the analysis of practically any highly charged particle, provided that the charge state was of sufficient magnitude to trigger the recording electronics.

### *Preliminary work and results*

The design of the PCB for the CD-MS detector is very similar to both the multi-stage CD and the bouncing detection CD that have already been presented. The primary differences for this new design are the dimensions and function of the different electrodes. Each plate consists of a 3-stage detection region, followed by a DC acceleration region, followed by another 3-stage detection region. The 3-stage detection regions consist of 7 electrodes that are 0.70 cm long and are 0.10 cm apart. The 1<sup>st</sup>, 3<sup>rd</sup>, 5<sup>th</sup>, and 7<sup>th</sup> electrodes are wired to ground while the other 3 electrodes are wired to the charge-sensitive pre-amplifier and three differentiating and shaping amplifiers that have previously been described. The DC acceleration region is 5.8 cm long and is separated from both detection regions by 0.10 cm. This acceleration region is intended to be wired to a low variable voltage DC power supply. As before, two of these plates are arranged to face each other in a sandwich-like fashion, 4 mm apart. As a charged particle passes over each sensing region, a pair of peaks is generated (Figure 20).

This detector could be used to calculate the mass of a charged particle by combining the charge measurement with the change in velocity due to a known applied electric field.

$$\frac{1}{2}mv_1^2 = \frac{1}{2}mv_2^2 - qV \quad (5-1)$$

$$\frac{1}{2}m\left(\frac{l}{t_l}\right)^2 = \frac{1}{2}m\left(\frac{d}{t_d}\right)^2 - qV \quad (5-2)$$

$$m = \frac{-2qV}{\left(\frac{l}{t_l}\right)^2 - \left(\frac{d}{t_d}\right)^2} \quad (5-3)$$



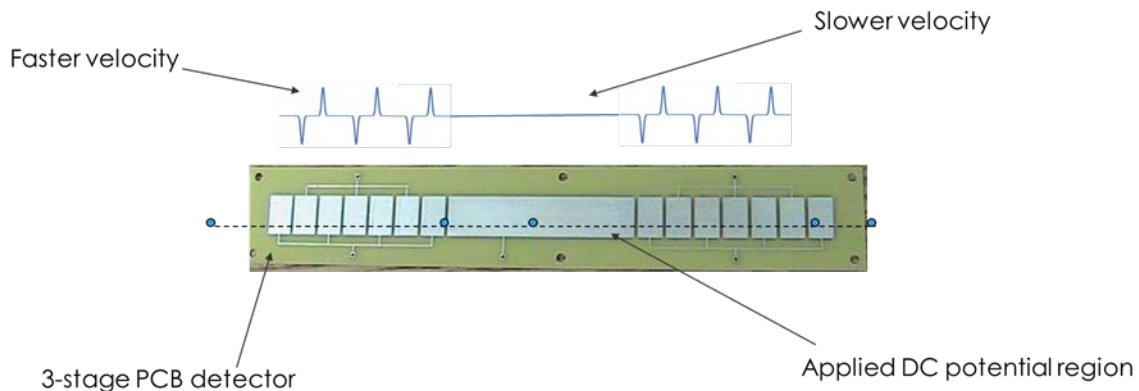


**Figure 20 – PCB designed for use as planar 6-stage CD-MS detector. DC acceleration region in center of detector designed to change particle velocity for  $m/z$  measurement.**

In equation 5-1,  $m$  represents the mass of the particle,  $v_1$  is the velocity of the particle outside of the electric field,  $v_2$  is the velocity of the particle within the field,  $q$  is the charge and  $V$  is the applied voltage that generates the electric field. In equation 5-2,  $l$  is the distance over which the velocity is measured outside of the electric field,  $t_1$  is the time that it takes to travel that distance,  $d$  is the distance over which the velocity is measured within the electric field, and  $t_d$  is the time that it takes to travel that distance.

The testing of this detector was performed using the same vacuum system and electrospray source that has been described for both the bacteria bouncing and multi-stage CD experiments. A system pressure of approximately  $4 \times 10^{-4}$  torr was maintained for the experiments that will be described below. Positive mode electrospray was utilized for all tests with an applied potential of 3500 V between the electrospray needle and the grounded inlet. The charged analyte particles were then swept through the vacuum system and into the detector using

pressure differentials. The signal generated by each charged particle was displayed and recorded by the oscilloscope.

Solutions of various sized amino-polystyrene spheres were electrosprayed and analyzed by the detector with zero potential applied to the DC acceleration region. The goal of these tests was both to establish that all six detection regions were functioning properly and to establish that the detector could be used to detect particles of various sizes. Polystyrene spheres at a concentration of 0.05% w/v with diameters of 0.61, 0.91, 3.36, 6.72, and 8.66  $\mu\text{m}$  were all tested. Signal from all six detection regions was seen for every size of polystyrene sphere tested.

Some more detailed analyses were performed on the signal produced by 20 separate 3.36  $\mu\text{m}$  polystyrene spheres. The purpose of these analyses was primarily to test the consistency of the device in order to determine its suitability for large particle mass measurement. The same data set was analyzed in three separate ways in order to determine this suitability.

First, the velocity of the 20 particles was measured and these velocities were compared with each other. The average velocity for these 20 particles was  $96.0 \pm 8.2$  m/s. The velocity of the particles was determined by dividing the distance between the end of the 3<sup>rd</sup> and 4<sup>th</sup> detection electrodes by the time that it took each particle to traverse this distance. As the long DC acceleration region lay between these two regions, this portion of the detector provided a relatively long distance over which to measure the particle velocities. It was thought that signal from a longer distance would yield the most precise velocity measurements (Figure 21). This is due to the fact that there is a certain amount of subjectivity inherent in each velocity measurement. The researcher needs to visually determine where on each signal trace to begin and end the time measurement for each velocity determination. The edges of the peaks used for

time measurements are not always well defined. The decision of where to place the boundaries for the time measurement could vary from one researcher to another. As this variability in peak shape does not increase with an increase in distance between peaks, it becomes less significant over longer distances.

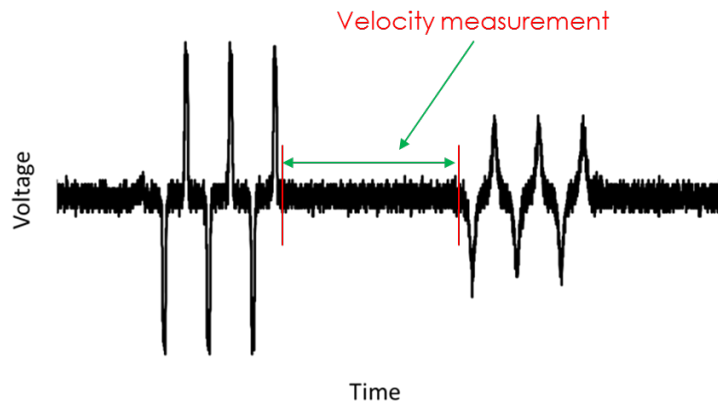


**Figure 21 – Trace showing the portion of the signal used for velocity measurement. During this time the particle is traveling over the DC acceleration region.**

Next, the consistency of the velocity measurement for a given particle was analyzed. The signal generated by different regions of the detector was analyzed for the same 20 particles as before. There are a number of ways that the velocity measurement consistency could be tested. It was decided to measure transit times for 3 separate regions of the detector. These regions were defined as follows: region 1 - the first 3-stage detection region, region 2 - the DC acceleration region, and region 3 - the second 3-stage detection region. The times that it took a particle to traverse these regions were defined as  $t_1$ ,  $t_2$ , and  $t_3$  respectively. It should take a particle approximately the same amount of time to traverse both the 1<sup>st</sup> and 3<sup>rd</sup> regions. If these times are approximately equal then the ratio of  $t_1/t_2$  should be approximately equal to the ratio of  $t_3/t_2$ . For the 20 particles in question, these two ratios were  $0.55 \pm 0.02$  and  $0.58 \pm 0.03$  respectively. As

the two uncertainty values overlap each other, it is reasonable to conclude that the different sensing regions of the detector are performing consistently in regards to velocity measurement.

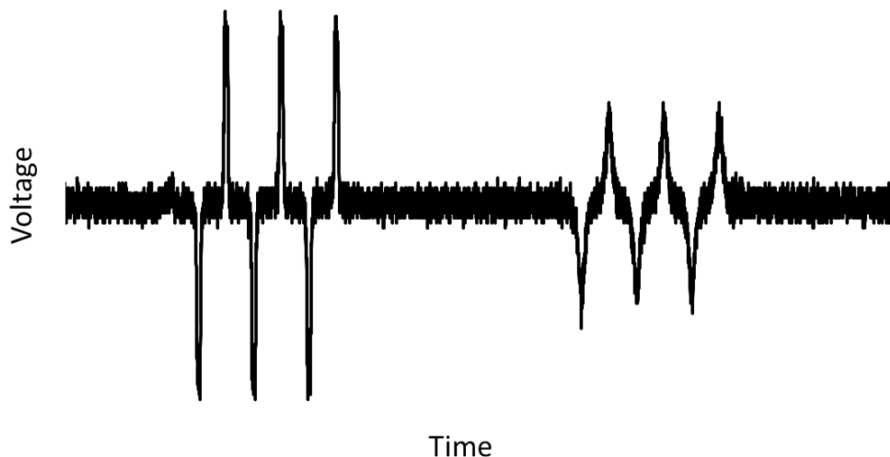


**Figure 22 – Signal generated by a charged polystyrene particle of 3.36  $\mu\text{m}$  diameter passing through all 6 sensing stages of the CD-MS detector. Peak amplitude changes while peak area remains the same for a given particle.**

Finally, the consistency in the charge measurement was explored. In order to investigate this, it was necessary to look at the areas of the peaks generated by a single particle passing through the detector (Figure 22). They were then compared with each other. The areas of the 6 upward facing peaks generated by a single particle were compared for each of the 20 signals under study. These areas were determined using the measurement software of the oscilloscope used to record the signal. While the peak amplitude and shape did vary from one peak to the next, the areas remained consistent. The average % relative standard deviation for the 6 peak areas within a given trace was 6.02313 % (Figure 23). The small variability exhibited by the

difference in peak areas did not demonstrate a pattern of any kind, meaning that there was not any particular detection electrode that generated consistently higher or lower areas than the others. It can be concluded that charge measurements calculated using an average of the six peak areas for a given particle would be more consistently accurate than a determination made using only one of these 6 areas.

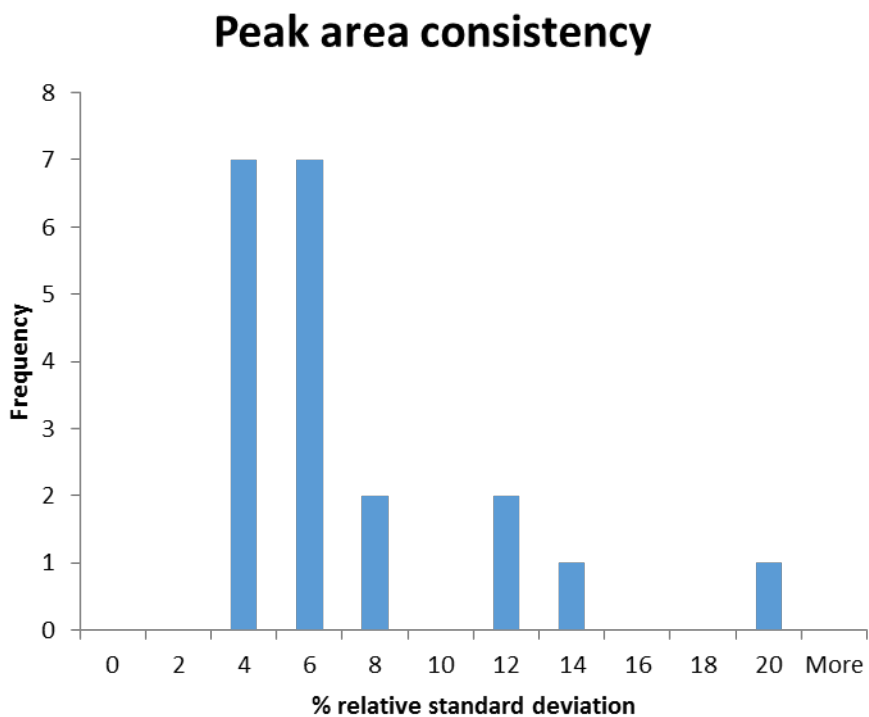


Figure 23 - % relative standard deviation is compared for 20 different CD-MS traces. The % RSD is calculated by comparing the peak areas generated by a single polystyrene sphere traveling through all 6 sensing stages of the detector.

## *Conclusions*

Preliminary experiments performed using the planar CD-MS detector indicate that it could be reliably used to determine particle charge and velocity. Once the DC acceleration region is implemented, the  $m/z$  of a particle can be measured. This along with the charge determination will yield absolute mass values for the particles being analyzed. The wide range of particle sizes that were tested indicate that a large variety of analytes, that are in the size range of bacterial spores or larger, could be studied with this method. These possibilities could include bacteria, fungal spores, and most plant and animal cells.

## Chapter 6: Future directions

Charge detection mass spectrometry is a method that still has much room for future growth. As mentioned in the introduction, there are two primary ways in which this technique has the potential to grow and improve. These two areas are simply an expansion of the types of applications for this method as well as improvements to the instrumentation itself. Both novel instrumentation and novel applications have already been demonstrated, by myself and others. However, there are many directions that research using this technique can go in the future.

The detailed analysis of most biological systems is hampered by the complexity of the systems themselves. Both lipoproteins and red blood cells are excellent examples of this. Both may be found in human blood. However the number of components that are naturally found in human serum makes it challenging to separate the desired analyte from everything else in the medium. This problem becomes less complex with CD-MS. Most of the metabolites, sugars, metal ions, and even small proteins are simply too small to be detected by a charge detector. Therefore to study a system that is detectable by CD-MS it is only necessary to separate the desired analyte system from anything in the matrix that is of requisite size and mass to be seen by the detector. This simplifies the problem considerably. One method that might couple well with CD-MS as a sample preparation method would be size exclusion chromatography. If samples could be separated into fine enough size fractions to separate all of the types of larger analytes from each other, then the fraction of interest could be run through the CD-MS for more detailed analysis. Specific analytes that have been considered for this technique include bacterial spores, viruses, and lipoproteins.

Determining the mass of bacterial spores would be significant simply because it has never been done before. The mass distribution of a spore sample could reveal more detailed information about spore structure than is currently known. The differences in mass from one cell to another could enable us to determine what structures or functional groups are responsible for these differences. Increased knowledge of these cell structures as revealed by mass distribution could lead to their being used as a template for nanoparticle designs. It would also be interesting to see if the mass distribution of a bacterial unknown could reveal the genus of the organism in question or possibly even the species.

The study of viruses would be similar in many ways to the study of bacteria. However, viruses are fundamentally different organisms. They are much simpler in structure than bacteria. While the structure of a bacterial cell is similar in many ways to that of a plant or animal cell, viruses are very different. They are composed simply of a protein capsid surrounding a relatively small amount of genetic material. It would be interesting to see if this greater simplicity made it easier or more difficult to identify a viral unknown based on the mass distribution of a viral sample. That such a distribution is observed for virus samples analyzed by CD-MS was demonstrated by Fuerstenau et al.<sup>8</sup>

Lipoproteins are typically divided into two main categories by size. The relative levels of high density versus low density lipoproteins (HDL vs. LDL) in the blood is viewed as an important indicator of an individual's risk of heart disease. It is possible to separate them into more than two categories as other researchers have done.<sup>123</sup> The mass resolution that is made possible by CD-MS could provide a detailed mass distribution of the separate lipoproteins in the sample. This knowledge could lead to a better understanding of the classifications and numbers of lipoproteins that indicate a greater patient risk.



There are various ways in which the CD-MS instrumentation could be improved. First it will be important to explore the pressure limitations of the method. If CD-MS can be proven to work at higher pressures, then high-vacuum pumps may not be necessary. It is much easier to find small roughing pumps with low power demands than it is to find similar qualities in a high-vacuum pump. The results for a single bouncing experiment performed at  $10^{-2}$  torr were discussed in chapter 4. However, further testing is certainly needed. Once the pressure requirements for effective analysis are determined, it will then be necessary to evaluate the vacuum chamber setup to find the simplest way to achieve the desired operating pressure. The size of the chamber, the number and size of skimmer cones and beam tubes, as well as the number and type of vacuum pumps can be altered. A low vacuum method would be much easier to develop into a portable method.

The second way to simplify the device is to investigate the possibility of integrating the sensing electrodes and the amplifier electronics onto a single circuit board. In order to investigate this question it will be necessary to evaluate the current electronics to see how much of what is currently attached to the amplifiers is strictly necessary for this particular application. The amplifier boards that we currently use as part of the charge detection electronics are pre-made circuit boards that are designed to function in a wide variety of applications. There are likely extraneous circuit elements that are simply not necessary for this particular application. At that point it would be easier to decide how much the method would be simplified by the integration of all necessary circuit elements onto a single board.

The planar PCB-based detectors have a large amount of potential for modification. It has been shown that they can be designed with a differing number of sensing electrodes in order to increase the accuracy and precision of the technique. They can be designed with a unique task in

mind, such as the detection of energy loss in bouncing bacterial spores. It has also been shown that a DC acceleration region can be added for CD-MS measurements. There are likely other designs that could be created for varying applications. Creating a PCB-based electrostatic ion-beam trap is one area that certainly should be explored. The possibilities of impact studies could be greatly expanded by placing a radio frequency linear accelerator and a charge detector onto a single PCB. The ease of production of these PCBs makes it more feasible to experiment with unique ideas that could be too large of a gamble using machined metal electrodes.

Charge detection mass-spectrometry has the potential to become an important method for the analysis of larger mass systems. The simultaneous measurement of both the absolute charge and the mass to charge ratio makes the determination of absolute mass possible, something that is not possible with other MS systems analyzing large-mass particles. It is likely that there are many interesting applications for this technique that have yet to be thought of, in addition to mass determination. The bouncing experiments are a good example of this, as they are the direct result of an unlooked-for outcome in the bacteria impact studies. The biological systems discussed above as potential candidates for CD-MS analysis are only a small sample of the many types of particles that could be analyzed with this method. Aerosol particles, micrometeorites, pollen, and fungal samples are also systems that could be analyzed using charge detection mass spectrometry. These are just a few examples of the many ways in which this technique has the potential to augment our understanding of the natural world.

## References

1. Fuerstenau, S. D.; Benner, W. H., Molecular weight determination of megadalton DNA electrospray ions using charge detection time-of-flight mass spectrometry. *Rapid Commun. Mass Sp.* **1995**, *9* (15), 1528-1538.
2. Schultz, J. C.; Hack, C. A.; Benner, W. H., Mass determination of megadalton-DNA electrospray ions using charge detection mass spectrometry. *J. Am. Soc. Mass Spectr.* **1998**, *9* (4), 305-313.
3. Schultz, J. C.; Hack, C. A.; Benner, W. H., Polymerase chain reaction products analyzed by charge detection mass spectrometry. *Rapid Commun. Mass Sp.* **1999**, *13* (1), 15-20.
4. Doussineau, T.; Bao, C. Y.; Clavier, C.; Dagany, X.; Kerleroux, M.; Antoine, R.; Dugourd, P., Infrared multiphoton dissociation tandem charge detection-mass spectrometry of single megadalton electrosprayed ions. *Rev. Sci. Instrum.* **2011**, *82* (8).
5. Doussineau, T.; Kerleroux, M.; Dagany, X.; Clavier, C.; Barbaire, M.; Maurelli, J.; Antoine, R.; Dugourd, P., Charging megadalton poly(ethylene oxide)s by electrospray ionization. A charge detection mass spectrometry study. *Rapid Commun. Mass Sp.* **2011**, *25* (5), 617-623.
6. Doussineau, T.; Bao, C. Y.; Antoine, R.; Dugourd, P.; Zhang, W. J.; D'Agosto, F.; Charleux, B., Direct Molar Mass Determination of Self-Assembled Amphiphilic Block Copolymer Nanoobjects Using Electrospray-Charge Detection Mass Spectrometry. *ACS Macro Lett.* **2012**, *1* (3), 414-417.
7. Vercoulen, P. H. W.; Roos, R. A.; Marijnissen, J. C. M.; Scarlett, B., AN INSTRUMENT FOR MEASURING ELECTRIC CHARGE ON INDIVIDUAL AEROSOL-PARTICLES. *J. Aerosol. Sci.* **1991**, *22*, S335-S338.
8. Fuerstenau, S. D.; Benner, W. H.; Thomas, J. J.; Brugidou, C.; Bothner, B.; Siuzdak, G., Mass spectrometry of an intact virus. *Angew. Chem.-Int. Edit.* **2001**, *40* (3), 542-544.
9. Fuerstenau, S. D., Whole Virus Mass Analysis by Electrospray Ionization. *J. Mass Spectrom. Soc. Jpn.* **2003**, *51* (1), 50-53.
10. Gamero-Castano, M., Induction charge detector with multiple sensing stages. *Rev. Sci. Instrum.* **2007**, *78* (4).
11. Shelton, H.; C. D. Hendricks, J.; Wuerker, R. F., Electrostatic Acceleration of Microparticles to Hypervelocities. *J. Appl. Phys.* **1960**, *31* (7), 1243-1246.
12. Friichtenicht, J. F., Micrometeoroid simulation using nuclear accelerator techniques. *Nucl. Instrum. Methods* **1964**, *28* (1), 70-78.

13. Hendricks Jr, C. D., Charged droplet experiments. *J. Coll. Sci. Imp. U. Tok.* **1962**, *17* (3), 249-259.
14. Pfeifer, R. J.; Hendricks, C. D., Charge-to-Mass Relationships for Electrohydrodynamically Sprayed Liquid Droplets. *Phys. Fluids* **1967**, *10* (10), 2149-2154.
15. Keaton, P. W.; Idzorek, G. C.; Rowton, L. J.; Seagrave, J. D.; Stradling, G. L.; Bergeson, S. D.; Collopy, M. T.; Curling, H. L.; McColl, D. B.; Smith, J. D., A hypervelocity - microparticle - impacts laboratory with 100-km s projectiles. *Int. J. Impact Eng.* **1990**, *10* (1-4), 295-308.
16. Stradling, G. L.; Idzorek, G. C.; Shafer, B. P.; Curling, H. L.; Collopy, M. T.; Blossom, A. A. H.; Fuerstenau, S., Ultra-high velocity impacts - cratering studies of microscopic impacts from 3-km/s to 30-km/s. *Int. J. Impact Eng.* **1993**, *14* (1-4), 719-727.
17. Park, M. A.; Callahan, J. H., An inductive detector for time-of-flight mass-spectrometry. *Rapid Commun. Mass Spectrom.* **1994**, *8* (4), 317-322.
18. Maze, J. T.; Jones, T. C.; Jarrold, M. F., Negative droplets from positive electrospray. *J. Phys. Chem. A* **2006**, *110* (46), 12607-12612.
19. Benner, W. H.; Bogan, M. J.; Rohner, U.; Boutet, S.; Woods, B.; Frank, M., Non-destructive characterization and alignment of aerodynamically focused particle beams using single particle charge detection. *J. Aerosol. Sci.* **2008**, *39* (11), 917-928.
20. Zilch, L. W.; Maze, J. T.; Smith, J. W.; Ewing, G. E.; Jarrold, M. F., Charge Separation in the Aerodynamic Breakup of Micrometer-Sized Water Droplets. *J. Phys. Chem. A* **2008**, *112* (51), 13352-13363.
21. Zilch, L. W.; Maze, J. T.; Smith, J. W.; Jarrold, M. F., Freezing, fragmentation, and charge separation in sonic sprayed water droplets. *Int. J. Mass. Spectrom.* **2009**, *283* (1-3), 191-199.
22. Alexander, J. D.; Graham, L.; Calvert, C. R.; Kelly, O.; King, R. B.; Williams, I. D.; Greenwood, J. B., Determination of absolute ion yields from a MALDI source through calibration of an image-charge detector. *Meas. Sci. Technol.* **2010**, *21* (4).
23. Antoine, R.; Doussineau, T.; Dugourd, P.; Calvo, F., Multiphoton dissociation of macromolecular ions at the single-molecule level. *Phys. Rev. A* **2013**, *87* (1).
24. Daly, R. T.; Kerby, J. D.; Austin, D. E., Electrospray charging of minerals and ices for hypervelocity impact research. *Planet. Space Sci.* **2013**, *75* (0), 182-187.
25. Doussineau, T.; Santacreu, M.; Antoine, R.; Dugourd, P.; Zhang, W. J.; Chaduc, I.; Lansalot, M.; D'Agosto, F.; Charleux, B., The Charging of Micellar Nanoparticles in Electrospray Ionization. *Chem. Phys. Chem* **2013**, *14* (3), 603-609.

26. Kerby, J. D.; Daly, R. T.; Austin, D. E., A novel particle source based on electrospray charging for dust accelerators and its significance for cosmic dust studies. *Earth Planets Space* **2013**, *65* (3), 157-165.
27. Ouadah, N.; Doussineau, T.; Hamada, T.; Dugourd, P.; Bordes, C.; Antoine, R., Correlation between the Charge of Polymer Particles in Solution and in the Gas Phase Investigated by Zeta-Potential Measurements and Electrospray Ionization Mass Spectrometry. *Langmuir* **2013**, *29* (46), 14074-14081.
28. Pierson, E. E.; Keifer, D. Z.; Contino, N. C.; Jarrold, M. F., Probing higher order multimers of pyruvate kinase with charge detection mass spectrometry. *Int. J. Mass Spectrom.* **2013**, *337*, 50-56.
29. Schmidt, H. T.; Cederquist, H.; Jensen, J.; Fardi, A., Conetrap: A compact electrostatic ion trap. *Nucl. Instrum. Meth. B* **2001**, *173* (4), 523-527.
30. Keifer, D. Z.; Pierson, E. E.; Hogan, J. A.; Bedwell, G. J.; Prevelige, P. E.; Jarrold, M. F., Charge detection mass spectrometry of bacteriophage P22 procapsid distributions above 20 MDa. *Rapid Commun. Mass Spectrom.* **2014**, *28* (5), 483-488.
31. Pierson, E. E.; Keifer, D. Z.; Selzer, L.; Lee, L. S.; Contino, N. C.; Wang, J. C. Y.; Zlotnick, A.; Jarrold, M. F., Detection of Late Intermediates in Virus Capsid Assembly by Charge Detection Mass Spectrometry. *J. Am. Chem. Soc.* **2014**, *136* (9), 3536-3541.
32. Peng, W. P.; Lin, H. C.; Lin, H. H.; Chu, M.; Yu, A. L.; Chang, H. C.; Chen, C. H., Charge-monitoring laser-induced acoustic desorption mass spectrometry for cell and microparticle mass distribution measurement. *Angew. Chem.-Int. Edit.* **2007**, *46* (21), 3865-3869.
33. Nie, Z.; Cui, F.; Tzeng, Y. K.; Chang, H. C.; Chu, M.; Lin, H. C.; Chen, C. H.; Lin, H. H.; Yu, A. L., High-speed mass analysis of whole erythrocytes by charge-detection quadrupole ion trap mass Spectrometry. *Anal. Chem.* **2007**, *79* (19), 7401-7407.
34. Peng, W. P.; Lin, H. C.; Chu, M. L.; Chang, H. C.; Lin, N. H.; Yu, A. L.; Chen, C. H., Charge monitoring cell mass spectrometry. *Anal. Chem.* **2008**, *80* (7), 2524-2530.
35. Chen, C. H.; Lin, J. L.; Chu, M. L.; Chen, C. H., MALDI Ion Trap Mass Spectrometer with Charge Detector for Large Biomolecule Detection. *Anal. Chem.* **2010**, *82* (24), 10125-10128.
36. Lin, H.-C.; Lin, H.-H.; Kao, C.-Y.; Yu, A. L.; Peng, W.-P.; Chen, C.-H., Quantitative Measurement of Nano-/Microparticle Endocytosis by Cell Mass Spectrometry. *Angew. Chem. Int. Edit.* **2010**, *49* (20), 3460-3464.

37. Xiong, C. Q.; Zhou, X. Y.; Chen, R.; Zhang, Y. M.; Peng, W. P.; Nie, Z. X.; Chang, H. C.; Liu, H. W.; Chen, Y., Characterization of Column Packing Materials in High-Performance Liquid Chromatography by Charge-Detection Quadrupole Ion Trap Mass Spectrometry. *Anal. Chem.* **2011**, *83* (13), 5400-5406.
38. Xiong, C. Q.; Xu, G. P.; Zhou, X. Y.; Wang, J. N.; Tang, Y.; Chen, R.; Peng, W. P.; Chang, H. C.; Nie, Z. X., The development of charge detection-quadrupole ion trap mass spectrometry driven by rectangular and triangular waves. *Analyst* **2012**, *137* (5), 1199-1204.
39. Nicholson, W. L., Ancient micronauts: interplanetary transport of microbes by cosmic impacts. *Trends Microbiol.* **2009**, *17* (6), 243-250.
40. Fajardo-Cavazos, P.; Schuerger, A. C.; Nicholson, W. L., Testing interplanetary transfer of bacteria between Earth and Mars as a result of natural impact phenomena and human spaceflight activities. *Acta. Astronaut.* **2007**, *60* (4-7), 534-540.
41. Nicholson, W. L.; Munakata, N.; Horneck, G.; Melosh, H. J.; Setlow, P., Resistance of *Bacillus* endospores to extreme terrestrial and extraterrestrial environments. *Microbiol. Mol. Biol. R.* **2000**, *64* (3), 548-+.
42. Kubota, H.; Senda, S.; Nomura, N.; Tokuda, H.; Uchiyama, H., Biofilm Formation by Lactic Acid Bacteria and Resistance to Environmental Stress. *J. Biosci. Bioeng.* **2008**, *106* (4), 381-386.
43. Valtonen, M.; Nurmi, P.; Zheng, J.-Q.; Cucinotta, F. A.; Wilson, J. W.; Horneck, G.; Lindegren, L.; Melosh, J.; Rickman, H.; Mileikowsky, C., Natural transfer of viable microbes in space from planets in extra-solar systems to a planet in our solar system and vice versa. *Astrophys. J.* **2009**, *690* (1), 210-215.
44. (a) Gualtieri, D. M., Trace-elements and panspermia hypotheses. *Icarus* **1977**, *30* (1), 234-238; (b) Mileikowsky, C.; Cucinotta, F. A.; Wilson, J. W.; Gladman, B.; Horneck, G.; Lindegren, L.; Melosh, J.; Rickman, H.; Valtonen, M.; Zheng, J. Q., Natural transfer of viable microbes in space - 1. From Mars to Earth and Earth to Mars. *Icarus* **2000**, *145* (2), 391-427.
45. Murchie, S. L.; Britt, D. T.; Pieters, C. M., The value of Phobos sample return. *Planet. Space Sci.* **2014**, *102*, 176-182.
46. Ramsley, K. R.; Head, J. W., III, Mars impact ejecta in the regolith of Phobos: Bulk concentration and distribution. *Planet. Space Sci.* **2013**, *87*, 115-129.
47. Mastrapa, R. M. E.; Glanzberg, H.; Head, J. N.; Melosh, H. J.; Nicholson, W. L., Survival of bacteria exposed to extreme acceleration: implications for panspermia. *Earth Planet. Sc. Lett.* **2001**, *189* (1-2), 1-8.
48. Benardini, J. N.; Sawyer, J.; Venkateswaran, K.; Nicholson, W. L., Spore UV and acceleration resistance of endolithic *Bacillus pumilus* and *Bacillus subtilis* isolates obtained from Sonoran desert basalt: Implications for lithopanspermia. *Astrobiology* **2003**, *3* (4), 709-717.

49. Burchell, M. J.; Galloway, J. A.; Bunch, A. W.; Brandao, P. F. B., Survivability of bacteria ejected from icy surfaces after hypervelocity impact. *Origins Life Evol. B.* **2003**, *33* (1), 53-74.
50. Fajardo-Cavazos, P.; Link, L.; Melosh, H. J.; Nicholson, W. L., Bacillus subtilis spores on artificial meteorites survive hypervelocity atmospheric entry: Implications for lithopanspermia. *Astrobiology* **2005**, *5* (6), 726-736.
51. Fajardo-Cavazos, P.; Langenhorst, F.; Melosh, H. J.; Nicholson, W. L., Bacterial Spores in Granite Survive Hypervelocity Launch by Spallation: Implications for Lithopanspermia. *Astrobiology* **2009**, *9* (7), 647-657.
52. Price, M. C.; Solscheid, C.; Burchell, M. J.; Josse, L.; Adamek, N.; Cole, M. J., Survival of yeast spores in hypervelocity impact events up to velocities of 7.4 km s(-1). *Icarus* **2013**, *222* (1), 263-272.
53. Horneck, G.; Stoffler, D.; Eschweiler, U.; Hornemann, U., Bacterial spores survive simulated meteorite impact. *Icarus* **2001**, *149* (1), 285-290.
54. Burchell, M. J.; Mann, J. R.; Bunch, A. W., Survival of bacteria and spores under extreme shock pressures. *Mon. Not. R. Astron. Soc.* **2004**, *352* (4), 1273-1278.
55. Willis, M. J.; Ahrens, T. J.; Bertani, L. E.; Nash, C. Z., Bugbuster - survivability of living bacteria upon shock compression. *Earth Planet. Sc. Lett.* **2006**, *247* (3-4), 185-196.
56. (a) Stoffler, D.; Horneck, G.; Ott, S.; Hornemann, U.; Cockell, C. S.; Moeller, R.; Meyer, C.; de Vera, J. P.; Fritz, J.; Artemieva, N. A., Experimental evidence for the potential impact ejection of viable microorganisms from Mars and Mars-like planets. *Icarus* **2007**, *186* (2), 585-588; (b) Horneck, G.; Stoffler, D.; Ott, S.; Hornemann, U.; Cockell, C. S.; Moeller, R.; Meyer, C.; De Vera, J. P.; Fritz, J.; Schade, S.; Artemieva, N. A., Microbial rock inhabitants survive hypervelocity impacts on Mars-like host planets: First phase of lithopanspermia experimentally tested. *Astrobiology* **2008**, *8* (1), 17-44.
57. Moeller, R.; Horneck, G.; Rabbow, E.; Reitz, G.; Meyer, C.; Hornemann, U.; Stoffler, D., Role of DNA Protection and Repair in Resistance of Bacillus subtilis Spores to Ultrahigh Shock Pressures Simulating Hypervelocity Impacts. *Appl. Environ. Microb.* **2008**, *74* (21), 6682-6689.
58. Hazell, P. J.; Beveridge, C.; Groves, K.; Appleby-Thomas, G., The shock compression of microorganism-loaded broths and emulsions: Experiments and simulations. *Int. J. Impact Eng.* **2010**, *37* (4), 433-440.
59. Meyer, C.; Fritz, J.; Misgaiski, M.; Stoffler, D.; Artemieva, N. A.; Hornemann, U.; Moeller, R.; de Vera, J. P.; Cockell, C.; Horneck, G.; Ott, S.; Rabbow, E., Shock experiments in support of the Lithopanspermia theory: The influence of host rock composition, temperature, and shock pressure on the survival rate of endolithic and epilithic microorganisms. *Meteorit. Planet. Sci.* **2011**, *46* (5), 701-718.

60. Hayes, M. G.; Fox, P. F.; Kelly, A. L., Potential applications of high pressure homogenisation in processing of liquid milk. *J. Dairy Res.* **2005**, *72* (1), 25-33.
61. Cai, Y.; Peng, W. P.; Kuo, S. J.; Lee, Y. T.; Chang, H. C., Single-particle mass spectrometry of polystyrene microspheres and diamond nanocrystals. *Anal. Chem.* **2002**, *74* (1), 232-238.
62. Pratt, S. N.; Austin, D. E., Bacterial Spores Survive Electrospray Charging and Desolvation. *J. Am. Soc. Mass Spectr.* **2014**, *25* (5), 712-721.
63. Fenn, J. B.; Mann, M.; Meng, C. K.; Wong, S. F.; Whitehouse, C. M., Electrospray ionization for mass-spectrometry of large biomolecules. *Science* **1989**, *246* (4926), 64-71.
64. Watson, J. S.; Sephton, M. A.; Sephton, S. V.; Self, S.; Fraser, W. T.; Lomax, B. H.; Gilmour, I.; Wellman, C. H.; Beerling, D. J., Rapid determination of spore chemistry using thermochemolysis gas chromatography-mass spectrometry and micro-Fourier transform infrared spectroscopy. *Photochem. Photobiol. Sci.* **2007**, *6* (6), 689-694.
65. Wang, G. D.; Cole, R. B., Mechanistic interpretation of the dependence of charge-state distributions on analyte concentrations in electrospray-ionization mass-spectrometry. *Anal. Chem.* **1995**, *67* (17), 2892-2900.
66. Goates, S. R.; Sin, C. H., Supersonic jet spectroscopy coupled to chromatography for very high-resolution chemical-analysis. *Appl. Spectrosc. Rev.* **1989**, *25* (2), 81-126.
67. Franklin, W. S.; Deimel, R. F., Pressure energy in an incompressible fluid and bernoulli's principle. *Science (New York, N.Y.)* **1925**, *62* (1609), 397.
68. Friichtenicht, J. F., Two-Million-Volt Electrostatic Accelerator for Hypervelocity Research. *Rev. Sci. Instrum.* **1962**, *33* (2), 209-212.
69. Carrera, M.; Zandomeni, R. O.; Fitzgibbon, J.; Sagripanti, J. L., Difference between the spore sizes of *Bacillus anthracis* and other *Bacillus* species. *J. Appl. Microbiol.* **2007**, *102* (2), 303-312.
70. Contino, N. C.; Pierson, E. E.; Keifer, D. Z.; Jarrold, M. F., Charge detection mass spectrometry with resolved charge States. *J. Am. Soc. Mass Spectr.* **2013**, *24* (1), 101-8.
71. Benner, W. H., A Gated Electrostatic Ion Trap To Repetitiously Measure the Charge and m/z of Large Electrospray Ions. *Anal. Chem.* **1997**, *69* (20), 4162-4168.
72. Strasser, D.; Heber, O.; Goldberg, S.; Zajfman, D., Self-bunching induced by negative effective mass instability in an electrostatic ion beam trap. *J. Phys. B-At. Mol. Opt. Phys.* **2003**, *36* (5), 953-959.



73. Sun, Q.; Ding, L.; Gu, C. X., Modeling and optimization of dual-cylinder image current detector in electrostatic ion beam trap for mass spectrometry. *Int. J. Mass Spectrom.* **2009**, *282* (1-2), 38-44.
74. Gamero-Castano, M., Retarding potential and induction charge detectors in tandem for measuring the charge and mass of nanodroplets. *Rev. Sci. Instrum.* **2009**, *80* (5).
75. Smith, J. W.; Siegel, E. E.; Maze, J. T.; Jarrold, M. F., Image Charge Detection Mass Spectrometry: Pushing the Envelope with Sensitivity and Accuracy. *Anal. Chem.* **2011**, *83* (3), 950-956.
76. Mabbett, S. R.; Zilch, L. W.; Maze, J. T.; Smith, J. W.; Jarrold, M. F., Pulsed Acceleration Charge Detection Mass Spectrometry: Application to Weighing Electrosprayed Droplets. *Anal. Chem.* **2007**, *79* (22), 8431-8439.
77. Ring, S.; Pedersen, H. B.; Heber, O.; Rappaport, M. L.; Witte, P. D.; Bhushan, K. G.; Altstein, N.; Rudich, Y.; Sagi, I.; Zajfman, D., Fourier transform time-of flight mass spectrometry in an electrostatic ion beam trap. *Anal. Chem.* **2000**, *72* (17), 4041-4046.
78. Pedersen, H. B.; Strasser, D.; Amarant, B.; Heber, O.; Rappaport, M. L.; Zajfman, D., Diffusion and synchronization in an ion-trap resonator. *Phys. Rev. A* **2002**, *65* (4).
79. Zajfman, D.; Rudich, Y.; Sagi, I.; Strasser, D.; Savin, D. W.; Goldberg, S.; Rappaport, M.; Heber, O., High resolution mass spectrometry using a linear electrostatic ion beam trap. *Int. J. Mass Spectrom.* **2003**, *229* (1-2), 55-60.
80. Zajfman, D.; Strasser, D.; Heber, O.; Goldberg, S.; Diner, A.; Rappaport, M. L., Dynamics of stored ions in an electrostatic ion beam trap. *Nucl. Instrum. Methods Phys. Res. Sect. A-Accel. Spectrom. Dect. Assoc. Equip.* **2004**, *532* (1-2), 196-202.
81. Attia, D.; Strasser, D.; Heber, O.; Rappaport, M. L.; Zajfman, D., Transverse kinematics of ions stored in an electrostatic ion beam trap. *Nucl. Instrum. Methods Phys. Res. Sect. A-Accel. Spectrom. Dect. Assoc. Equip.* **2005**, *547* (2-3), 279-286.
82. Heber, O.; Witte, P. D.; Diner, A.; Bhushan, K. G.; Strasser, D.; Toker, Y.; Rappaport, M. L.; Ben-Itzhak, I.; Altstein, N.; Schwalm, D.; Wolf, A.; Zajfman, D., Electrostatic ion beam trap for electron collision studies. *Rev. Sci. Instrum.* **2005**, *76* (1).
83. Bhushan, K. G.; Gadkari, S. C.; Yakhmi, J. V.; Sahni, V. C., Electrostatic ion trap and Fourier transform measurements for high-resolution mass spectrometry. *Rev. Sci. Instrum.* **2007**, *78* (8).
84. Aviv, O.; Toker, Y.; Errit, M.; Bhushan, K. G.; Pedersen, H. B.; Rappaport, M. L.; Heber, O.; Schwalm, D.; Zajfman, D., A bent electrostatic ion beam trap for simultaneous measurements of fragmentation and ionization of cluster ions. *Rev. Sci. Instrum.* **2008**, *79* (8).

85. Toker, Y.; Altstein, N.; Aviv, O.; Rappaport, M. L.; Heber, O.; Schwalm, D.; Strasser, D.; Zajfman, D., The kick-out mass selection technique for ions stored in an Electrostatic Ion Beam Trap. *J. Instrum.* **2009**, *4*.
86. Rahinov, I.; Toker, Y.; Heber, O.; Strasser, D.; Rappaport, M.; Schwalm, D.; Zajfman, D., Lifetime measurements in an electrostatic ion beam trap using image charge monitoring. *Rev. Sci. Instrum.* **2012**, *83* (3).
87. Greenwood, J. B.; Kelly, O.; Calvert, C. R.; Duffy, M. J.; King, R. B.; Belshaw, L.; Graham, L.; Alexander, J. D.; Williams, I. D.; Bryan, W. A.; Turcu, I. C. E.; Cacho, C. M.; Springate, E., A comb-sampling method for enhanced mass analysis in linear electrostatic ion traps. *Rev. Sci. Instrum.* **2011**, *82* (4).
88. Sun, Q.; Gu, C. X.; Ding, L., Multi-ion quantitative mass spectrometry by orthogonal projection method with periodic signal of electrostatic ion beam trap. *J. Mass. Spectrom.* **2011**, *46* (4), 417-424.
89. Doussineau, T.; Antoine, R.; Santacreu, M.; Dugourd, P., Pushing the Limit of Infrared Multiphoton Dissociation to Megadalton-Size DNA Ions. *J. Phys. Chem. Lett.* **2012**, *3* (16), 2141-2145.
90. Contino, N. C.; Jarrold, M. F., Charge detection mass spectrometry for single ions with a limit of detection of 30 charges. *Int. J. Mass Spectrom.* **2013**, *345*, 153-159.
91. Doussineau, T.; Paletto, P.; Dugourd, P.; Antoine, R., Multiphoton Dissociation of Electrosprayed MegaDalton-Sized DNA Ions in a Charge-Detection Mass Spectrometer. *J. Am. Soc. Mass Spectr.* **2015**, *26* (1), 7-13.
92. Pierson, E. E.; Contino, N. C.; Keifer, D. Z.; Jarrold, M. F., Charge Detection Mass Spectrometry for Single Ions with an Uncertainty in the Charge Measurement of 0.65 e. *J. Am. Soc. Mass. Spectr.* **2015**, *26* (7), 1213-1220.
93. Tong, X. C., *Advanced Materials and Design for Electromagnetic Interference Shielding*. CRC Press: Boca Raton, FL, 2009.
94. Talekar, M.; Tran, T.-H.; Amiji, M., Translational Nano-Medicines: Targeted Therapeutic Delivery for Cancer and Inflammatory Diseases. *AAPS J.* **2015**, *17* (4), 813-27.
95. Heinz, W. F.; Hoh, J. H., Spatially resolved force spectroscopy of biological surfaces using the atomic force microscope. *Trends Biotechnol.* **1999**, *17* (4), 143-150.
96. Yao, X.; Jericho, M.; Pink, D.; Beveridge, T., Thickness and elasticity of gram-negative murein sacculi measured by atomic force microscopy. *J. Bacteriol.* **1999**, *181* (22), 6865-6875.

97. Arnoldi, M.; Fritz, M.; Bauerlein, E.; Radmacher, M.; Sackmann, E.; Boulbitch, A., Bacterial turgor pressure can be measured by atomic force microscopy. *Phys. Rev. E* **2000**, *62* (1), 1034-1044.
98. Touhami, A.; Nysten, B.; Dufrene, Y. F., Nanoscale mapping of the elasticity of microbial cells by atomic force microscopy. *Langmuir* **2003**, *19* (11), 4539-4543.
99. Gaboriaud, F.; Bailet, S.; Dague, E.; Jorand, F., Surface structure and nanomechanical properties of *Shewanella putrefaciens* bacteria at two pH values (4 and 10) determined by atomic force microscopy. *J. Bacteriol.* **2005**, *187* (11), 3864-3868.
100. Zhao, L. M.; Schaefer, D.; Marten, M. R., Assessment of elasticity and topography of *Aspergillus nidulans* spores via atomic force microscopy. *Appl. Environ. Microb.* **2005**, *71* (2), 955-960.
101. Beckmann, M. A.; Venkataraman, S.; Doktycz, M. J.; Nataro, J. P.; Sullivan, C. J.; Morrell-Falvey, J. L.; Allison, D. P., Measuring cell surface elasticity on enteroaggregative *Escherichia coli* wild type and dispersin mutant by AFM. *Ultramicroscopy* **2006**, *106* (8-9), 695-702.
102. Mendez-Vilas, A.; Gallardo-Moreno, A. M.; Gonzalez-Martin, M. L., Nano-mechanical exploration of the surface and sub-surface of hydrated cells of *Staphylococcus epidermidis*. *Antonie Van Leeuwenhoek* **2006**, *89* (3-4), 373-386.
103. Mendez-Vilas, A.; Gallardo-Moreno, A. M.; Gonzalez-Martin, M. L., Atomic force microscopy of mechanically trapped bacterial cells. *Microsc. Microanal.* **2007**, *13* (1), 55-64.
104. Svaldo Lanero, T.; Cavalleri, O.; Krol, S.; Rolandi, R.; Gliozzi, A., Mechanical properties of single living cells encapsulated in polyelectrolyte matrixes. *J. Biotechnol.* **2006**, *124* (4), 723-731.
105. Sullivan, C. J.; Venkataraman, S.; Retterer, S. T.; Allison, D. P.; Doktycz, M. J., Comparison of the indentation and elasticity of *E-coli* and its spheroplasts by AFM. *Ultramicroscopy* **2007**, *107* (10-11), 934-942.
106. Alsteens, D.; Dupres, V.; Mc Evoy, K.; Wildling, L.; Gruber, H. J.; Dufrene, Y. F., Structure, cell wall elasticity and polysaccharide properties of living yeast cells, as probed by AFM. *Nanotechnology* **2008**, *19* (38).
107. Bui, V. C.; Kim, Y. U.; Choi, S. S., Physical characteristics of *Saccharomyces cerevisiae*. *Surf. Interface Anal.* **2008**, *40* (10), 1323-1327.
108. Vadillo-Rodriguez, V.; Beveridge, T. J.; Dutcher, J. R., Surface viscoelasticity of individual gram-negative bacterial cells measured using atomic force microscopy. *J. Bacteriol.* **2008**, *190* (12), 4225-4232.

109. Cerf, A.; Cau, J. C.; View, C.; Dague, E., Nanomechanical Properties of Dead or Alive Single-Patterned Bacteria. *Langmuir* **2009**, *25* (10), 5731-5736.
110. Arfsten, J.; Leupold, S.; Bradtmoller, C.; Kampen, I.; Kwade, A., Atomic force microscopy studies on the nanomechanical properties of *Saccharomyces cerevisiae*. *Colloid Surf. B-Biointerfaces* **2010**, *79* (1), 284-290.
111. Pinzon-Arango, P. A.; Nagarajan, R.; Camesano, T. A., Effects of L-Alanine and Inosine Germinants on the Elasticity of *Bacillus anthracis* Spores. *Langmuir* **2010**, *26* (9), 6535-6541.
112. Fang, T.-H.; Kang, S.-H.; Hong, Z.-H.; Wu, C.-D., Elasticity and nanomechanical response of *Aspergillus niger* spores using atomic force microscopy. *Micron* **2012**, *43* (2-3), 407-411.
113. Minc, N.; Boudaoud, A.; Chang, F., Mechanical Forces of Fission Yeast Growth. *Curr. Biol.* **2009**, *19* (13), 1096-1101.
114. Stenson, J. D.; Hartley, P.; Wang, C. X.; Thomas, C. R., Determining the Mechanical Properties of Yeast Cell Walls. *Biotechnol. Prog.* **2011**, *27* (2), 505-512.
115. Nakanishi, K.; Kogure, A.; Fujii, T.; Kokawa, R.; Deuchi, K., Development of method for evaluating cell hardness and correlation between bacterial spore hardness and durability. *J. Nanobiotechnology* **2012**, *10*, 22.
116. Shen, Y. J.; Nakajima, M.; Yang, Z.; Tajima, H.; Najdovski, Z.; Homma, M.; Fukuda, T., Single cell stiffness measurement at various humidity conditions by nanomanipulation of a nano-needle. *Nanotechnology* **2013**, *24* (14).
117. Koch, A. L.; Ehrenfel.E, Size and shape of bacteria by light scattering measurements. *Biochim. Biophys. Acta* **1968**, *165* (2), 262-&.
118. Coles, H. J.; Jennings, B. R.; Morris, V. J., Infrared scattering - method for evaluating mass and size of bacteria. *Phys. Med. Biol.* **1975**, *20* (2), 225-234.
119. Mumford, P. M.; Pappelis, A. J., Dry mass of *fusarium roseum* spores before and after germination. *Mycopathologia* **1978**, *64* (1), 63-64.
120. Pappelis, A. J.; Mumford, P. M.; Wu, L. B., Dry mass changes in germinating spores of *diplodia maydis*. *Mycopathologia* **1979**, *67* (2), 111-113.
121. Algie, J. E.; Watt, I. C., Calculation of mass and water-content between the core, cortex, and coat of *bacillus-stearothermophilus* spores. *Curr Microbiol* **1984**, *10* (5), 249-253.
122. Koch, A. L.; Robertson, B. R.; Button, D. K., Deduction of the cell volume and mass from forward scatter intensity of bacteria analyzed by flow cytometry. *J. Microbiol. Methods* **1996**, *27* (1), 49-61.

123. Toth, P. P., The “Good Cholesterol”. *Circulation* **2005**, *111* (5), e89-e91.